Downloaded from orbit.dtu.dk on: Apr 29, 2024

DTU Library

Analysis and Design of Wideband Matched Feeds for Reflector Antennas

Palvig, Michael Forum

Publication date:
2017

Document Version
Publisher's PDF, also known as Version of record

Link back to DTU Orbit

Citation (APA):
Palvig, M. F. (2017). *Analysis and Design of Wideband Matched Feeds for Reflector Antennas*. Technical University of Denmark.

General rights
Copyright and moral rights for the publications made accessible in the public portal are retained by the authors and/or other copyright owners and it is a condition of accessing publications that users recognise and abide by the legal requirements associated with these rights.

- Users may download and print one copy of any publication from the public portal for the purpose of private study or research.
- You may not further distribute the material or use it for any profit-making activity or commercial gain
- You may freely distribute the URL identifying the publication in the public portal

If you believe that this document breaches copyright please contact us providing details, and we will remove access to the work immediately and investigate your claim.

Technical University of Denmark

Michael Forum Palvig

Analysis and Design of Wideband Matched Feeds for Reflector Antennas

PhD thesis, November 2017

DTU Electrical Engineering
Department of Electrical Engineering

Analysis and Design of Wideband Matched Feeds for Reflector Antennas

Michael Forum Palvig

PhD Thesis, November 2017

DTU

TICRA

Innovation Fund Denmark

Thesis title:
Analysis and Design of Wideband Matched Feeds for Reflector Antennas

PhD Student:
Michael Forum Palvig
michael@forumpalvig.dk
mfp@ticra.com

Supervisors:
Olav Breinbjerg[1]
Peter Meincke[2]
Erik Jørgensen[2]

[1] **Electromagnetic Systems**
DTU Electrical Engineering
Ørsteds Plads, building 348
DK-2800 Kgs. Lyngby
www.ems.elektro.dtu.dk
ob@elektro.dtu.dk

[2] **TICRA**
Landemærket 29, 5.
DK-1119 Copenhagen K
www.ticra.com
ticra@ticra.com

Submission date:
14 November 2017

Remarks:
The present version was adapted for printing after the thesis defence. A few typos were corrected.

© 2017 Michael Forum Palvig

Abstract

Analysis and Design of Wideband Matched Feeds for Reflector Antennas

The offset single reflector antenna enables simple, high efficiency, high gain systems, but suffers from high cross polarization. The cross polarization can be reduced by matched feeds, but these suffer from being narrowband. In this thesis, insights on the reasons for the inherent bandwidth limitation of matched feeds are presented and methods to overcome it are proposed and demonstrated.

A thorough account of the working principles of conventional matched feeds is first presented, including an alternative, effective method for determining the required waveguide modes and their excitations. In this process it is discovered that TE_{01} and TM_{01} modes can be used in matched feeds instead of the TE_{21} modes reported in the literature thus far. A matched feed design using TM_{01} is presented as a demonstration.

A design procedure for conventional matched feeds is proposed. The procedure involves use of optimization in several stages of the design including direct far-field optimization. With an axially corrugated horn, a 7 dB improvement of cross polarization is achieved across a 13 % bandwidth for dual polarizations.

By surrounding a circular waveguide with a coaxial one, the modal phase dispersion which arises in conventional matched feeds, can be eliminated. This property is used to present a design method for a new type of mode launcher combining techniques from directional coupler theory and analytical mode coupling models. Designs featuring excellent performance over a 30 % bandwidth for both polarizations are presented. A dual-polarized matched feed using this kind of mode launcher is demonstrated in a subset of the band.

It is shown that elimination of phase dispersion between modes can also be achieved using impedance surface waveguides. Horns made of a specific range of anisotropic impedance surfaces provide far superior conditions for wideband matched feed design than smooth or corrugated metal horns.

With the analysis framework and the innovations presented in this thesis, matched feeds are several steps closer to becoming the standard for offset reflector antennas.

Resumé (in Danish)

Analyse og design af bredbåndede, krydspolarisationskompenserende fødehorn til reflektorantenner

Forskudte (offset) enkeltreflektorantenner er simple og gør det muligt at opnå høj effektivitet og direktivitet, men de lider under forhøjet krydspolarisation. Krydspolarisationen kan reduceres med krydspolarisationskompenserende fødehorn (matched feeds), men disse har en begrænset båndbredde. Denne afhandling præsenterer indblik i årsagerne til båndbreddebegrænsningen, og demonstrerer metoder til at afhjælpe den.

Først præsenteres en grundig gennemgang af virkemåden for krydspolarisationskompenserende fødehorn inklusiv en alternativ, effektiv metode til at bestemme de nødvendige modes i bølgelederen og deres excitationer. Det opdages i denne proces at bølgeledermodes TE_{01} og TM_{01} kan bruges til krydspolarisationskompenserende fødehorn i stedet for TE_{21}, som hidtil er rapporteret i litteraturen. Som demonstration af dette præsenteres et design, som kun bruger TM_{01} til krydspolarisationskompensering.

En designmetode til konventionelle krydspolarisationskompenserende fødehorn præsenteres. Proceduren involverer optimering i flere trin af designet, inklusive direkte optimering i fjernfeltet. Med et aksialt korrugeret horn opnås en 7 dB undertrykkelse af krydspolarisation over en båndbredde på 13 % i begge polarisationer.

Ved at omslutte en cirkulær bølgeleder med en koaksial kan fase-dispersionen, som opstår i konventionelle krydspolarisationskompenserende fødehorn, elimineres. Denne egenskab bruges til at præsentere en designmetode til en ny type modetransformator, som kombinerer teknikker fra bølgelederkobler-teorien og analytiske modeller for kobling mellem bølgeledermodes. Der præsenteres prototyper som har fremragende ydeevne i en 30 % båndbredde for begge polarisationer. Et dobbeltpolariseret krydspolarisationskompenserende fødehorn, som bruger en sådan modetransformator, præsenteres.

Det vises endvidere, at fase-dispersionen mellem modes også kan elimineres ved brug af bølgeledere lavet af impedansoverflader. Horn lavet med nogle specifikke impedansoverflader giver langt overlegne forhold for design af bredbåndede krydspolarisationskompenserende fødehorn sammenlignet med perfekt ledende horn med glat overflade eller korrugerede horn.

Med analysemetoderne og innovationerne præsenteret i denne afhandling er krydspolarisationskompenserende fødehorn flere skridt tættere på at blive standarden for forskudte reflektorantenner.

Preface

The work presented in this thesis was carried out by the author at the Electrical Engineering department of the Technical University of Denmark (DTU) and at the company TICRA between November 2014 and November 2017. It is submitted as a requirement for obtaining the PhD degree from the Technical University of Denmark.

The study is funded by TICRA with support from Innovation Fund Denmark within the framework of the Industrial Researcher Programme.

Acknowledgements

I would like to thank my supervisors Olav Breinbjerg, Peter Meincke, and Erik Jørgensen for their guidance through this project. Without their initiative, immense knowledge, assistance, and encouragement, this work would not have been possible.

My sincere thanks to Professor Bhattacharjee for welcoming me to India and to the Indian Institute of Technology in Guwahati. Thank you for your personal hospitality and for sharing your vast knowledge on antenna theory as well as on the history of India. I would also like to thank all of the many people who assisted me in navigating an unfamiliar, but interesting culture. A special thanks to my wonderful lab-mate Shivanshu, who helped me and kept me company through thick and thin.

Thank you Dr. Rajib Jana, for welcoming me to the National Institute of Technology in beautiful Arunachal Pradesh. Our discussions on matched feeds were very fruitful for me. I was moved by the exceptional warmth and hospitality that you and your fantastic colleagues showed me.

I am very grateful to Dr. Pour for arranging my visit to the University of Alabama in Huntsville. Thank you so much for making me feel welcome and for sharing your knowledge and experience with me in many discussions. It was a privilege to be able to give a presentation at the IEEE EMC Society meeting — an excellent forum of very nice and engaging people.

With the help of my colleagues at DTU and TICRA, I managed to keep most of my sanity (I think). Thank you for being a joy to be around and for never hesitating to help me in any way you could. A monumental thanks to Piotr Marek Kaminski and Paula Irina Muntianu for proofreading the entire thesis. It was a *huge* help.

To my nearest family: thank you for your love, wisdom, and delicious food. I owe you everything.

Michael Forum Palvig
November 2017

Contents

Abstract **i**

Resumé (in Danish) **iii**

Preface **v**

Contents **vii**

List of Publications **ix**

1 Introduction **1**

2 Reflector Antenna Cross Polarization and Matched Feeds **5**
2.1 The Focusing Properties of Ellipsoids and Paraboloids 5
2.2 Cross Polarization of the Symmetric Reflector Antenna 6
2.3 Cross Polarization of the Offset Reflector Antenna 7
2.4 The Matched Feed Concept 12
2.5 Bandwidth Limitations of Matched Feeds 14
2.6 Literature Survey of Matched Feeds 16
2.7 Summary 19

3 Determination of Compensating Waveguide Modes **21**
3.1 Focal Region Field Approach 21
3.2 Optimizing Reflector Aperture Field 23
3.3 Summary 29

4 Mode Conversion **31**
4.1 Need for Asymmetry 31
4.2 Mode Excitation from Currents 32
4.3 Waveguide Inclusions Modeled by Currents 33
4.4 Excitation of Currents by Incident Mode 36
4.5 Validation by Simulation 36
4.6 Frequency Characteristics of Mode Launchers 40
4.7 Summary 40

5 Directional Waveguide Couplers for Matched Feeds **43**
5.1 Discrete Directional Couplers 43
5.2 Coaxial Coupler Design 45
5.3 Performance Evaluation of Coaxial Couplers 50
5.4 Feed Design with Axially Corrugated Horn 52
5.5 Summary 59

6 Impedance Surface Waveguides for Matched Feeds **61**
6.1 Impedance-Surface Waveguides in the Literature 61
6.2 Dispersion Diagrams 62
6.3 Simultaneous HE_1 and HE_2 propagation 63
6.4 Capacitive X_z and Inductive X_ϕ 64
6.5 Impedance Surface Matched Feed Design 65
6.6 Summary 66

7 Conclusion **69**

A TM_{01} Matched Feed **71**

B Waveguide Modal Analysis **75**

C Papers **87**

Bibliography **113**

List of Publications

The conference papers [P1–P3] and the Journal paper [P4] have been prepared during this study. They are included in Appendix C as part of this thesis.

[P1] M. F. Palvig, E. Jørgensen, P. Meincke, and O. Breinbjerg. “Optimization Procedure for Wideband Matched Feed Design”. In: *The 10th European Conference on Antennas and Propagation (EuCAP 2016).* Davos, Switzerland, Apr. 2016.

[P2] M. F. Palvig, O. Breinbjerg, P. Meincke, and E. Jørgensen. “Analytical Modelling of Waveguide Mode Launchers for Matched Feed Reflector Systems”. In: *IEEE Antennas and Propagation Society International Symposium (AP-S 2016).* Puerto Rico, June 2016.

[P3] M. F. Palvig, E. Jørgensen, P. Meincke, and O. Breinbjerg. “Metasurface Waveguides Applied to Matched Feeds for Reflector Antennas”. In: *The 11th European Conference on Antennas and Propagation (EUCAP 2017).* Paris, France, Mar. 2017, pp. 3636–3638.

[P4] M. F. Palvig, P. Meincke, E. Jørgensen, and O. Breinbjerg. “A Design Method for Mode-Selective Waveguide Couplers in Dual-Polarized Wideband Matched-Feed Antennas”. In: *IEEE Transactions on Antennas and Propagation* 66.2 (Feb. 2018), pp. 990–995.

CHAPTER 1

Introduction

The reflector antenna has a long heritage, dating at least back to Newton's, Gregory's, and Cassegrain's first reflecting telescopes in the 17th century. To this day, reflector antennas are the preferred choice for high gain applications, especially where a wide bandwidth is required. This makes them widespread in the space industry where signals have to be broadcast over large distances at demanding data rates [1]. As well as in the fields of radio and radar astronomy which use many frequency bands and require a high sensitivity [2].

Reflector antennas can be characterized by the number of reflecting surfaces that makes up the antenna. Both single and double reflector systems are very common. Systems with more than two reflectors also exist, e.g. in beam waveguide fed antennas. Another important characteristic of a reflector antenna system is if it is symmetric or offset. In a symmetric antenna system, the antenna structure is rotationally symmetric around the axis of radiation, which is not the case in an offset system. The motivation for offsetting the elements of the antenna system is to thereby avoid that the elements are blocking each other's radiation.

The reduced blockage in the offset reflector antenna system is a compelling advantage for several reasons: among others, enhanced efficiency, lower side-lobe levels, and reduced coupling. However, from the offset geometry, a major drawback arises: increased cross polarization for linear polarization[1] [3]. Cross polarization is an obvious disadvantage in systems where two polarizations are used independently, e.g. in polarimetric radars and radiometers, and in communication satellites that employ frequency reuse. Increased cross polarization is a serious problem which translates directly into disturbance in the signal of the other polarization channel. In dual (or more) offset reflector systems, cross polarization may be compensated by letting the combined reflector system satisfy the Mizuguchi condition [4, 5].

Despite the increased cross polarization, offset single reflector antennas are still used extensively due to their other desirable properties, especially within satellite broadcast and communication. The cross polarization enters into the link budget of the system engineer and can be somewhat limited by choosing relatively long focal lengths. There is, however, a limit to how long the focal length can be made in a practical system, especially on a satellite body. An alternative solution was proposed by Rudge and Adatia [6] in 1975. It involves radiating cross polarization from the feed antenna in such a way that it compensates the cross polarization introduced by the offset geometry. The original design method involved matching the aperture field of the feed to fields of a received plane wave, which gave rise to a commonly used term *matched feeds*. The horn field is matched to the received field by introducing higher order waveguide modes in the horn. The present work is concerned with feed horns employing this concept.

---

[1] For circular polarization, this translates to a beam squint instead as will be explained in Chapter 2. Unless otherwise stated, cross polarization will refer to linear cross polarization.

Despite the apparent attractiveness of getting the advantages of both the symmetric and offset reflectors, only a moderate amount of research on matched feeds was conducted in the years after the invention, including but not limited to [7–10]. In recent years, the interest in matched feeds has been revived, and feed designs with circular [11–14], rectangular [15, 16], corrugated [17–21], and other geometries [22, 23] have been presented. Examining the existing literature shows that the primary challenge of the matched-feed technique is to achieve a decent bandwidth[2], which is essential for the use of this technology in communication applications. This difficulty stems mainly from two factors: 1) that mode conversion is often based on near-resonant structures and 2) that the fundamental and higher-order modes have different cutoff frequencies, resulting in phase dispersion. For the feed to be able to compensate cross polarization, the higher order mode must be in specific amplitude and phase relationships with the main radiating modes at the aperture. This condition is challenging to maintain over a large bandwidth because the modes inside the horn propagate at different speeds and the difference in speed varies with frequency. On top of this difficulty, the amplitude and phase responses of the mode conversion components change rapidly with frequency when they are near resonance.

The working bandwidth of a matched feed may be defined as the frequency range within which it reduces the cross polarization by a certain amount, say by 10 dB relative to the case of a perfectly co-polarized, non-matched feed. Watson, Rudge, and Adatia [8] were first to introduce this bandwidth measure, and they achieved a 10 dB reduction over a 4 % fractional bandwidth with a dual polarized matched feed. Most other references in the literature feature even narrower bandwidth, or the obtained bandwidth is not provided at all. In a recent work, Dey et al. [19, 24] have presented designs with a wider bandwidth. They report a 10 dB cross polarization reduction over a 8 % bandwidth for a single polarization using a new kind of mode launching concept followed by a corrugated horn.

Good cross polarization discrimination is often motivated by frequency reuse: if the two polarizations do not interfere, two distinct signals can be transmitted and received at the same frequency, thus doubling the data rate. Dual polarization may also help to reduce interference between closely spaced beams in multi-beam satellite systems. If both of the data channels are to be available in a system which has only one antenna, the antenna must be able to operate in dual polarizations. Satellite earth terminals are often required to transmit and receive in opposite polarizations, with polarizations depending on coverage area and specific satellite [25–27]. Hence, a feed for a reflector antenna will likely be required to work in two polarizations, however, the literature on matched feeds deals almost exclusively with single polarized designs. The matched feed effect for two simultaneous polarizations is possible as demonstrated already in 1978 [8]. To my knowledge, there are in fact only three additional published examples of matched feeds which work in dual polarization and these are a very sparsely described corrugated horn [28] and two patents which are almost identical [20, 21]. In the present work all designs are dual polarized[3].

Drastically reducing the cross polarization of offset reflector systems without compromising other design goals or significantly increasing the size or cost of the feed sys-

---

[2] "Decent" is a bit vague, but it is hard to be more concrete without locking onto a specific application.

[3] Except the demonstrator TM_{01} design in Appendix A

tem would be immensely valuable to the satellite industry — for both the space and earth segments. Published works on the matched-feed concept have not yet obtained satisfactory results. Reducing cross polarization for a narrow frequency band has been proven many times over, but doing so in dual polarizations across a bandwidth suitable for high data rate communication, is still to be shown and therein lies the justification of this thesis.

The purpose of this study is to investigate the inherent bandwidth limitation of matched-feed antennas and develop methods to overcome it. A framework of simple analytical and semi-analytical models is set up in order to gain insight into the physical mechanisms. This knowledge will form a basis for improving existing design methods. By properly understanding the workings of the mode launchers, it is possible to design more advanced kinds which work in both polarizations and suppress the generation of unwanted modes at the same time.

Eliminating the phase dispersion between waveguide modes is key to achieving a wide bandwidth in matched feed antennas. Two promising methods for doing so have been investigated: circular to coaxial waveguide coupling and impedance surface waveguides. For the former, a comprehensive design procedure for a wideband mode launcher is developed. Extensive use of numerical optimization is used on the analytical models as well as on full wave simulations of prospective designs. The analysis and the designs presented are based on horn antennas of circular aperture, but the theory and methods may be applied to any waveguide shape.

Reading Guide

Chapter 2 is an introduction to reflector antennas and their cross polarization as well as a brief description of the matched feed concept. Chapter 3 goes on to definitively account for the modal requirements of a matched feed before Chapter 4 gives physical insight into the way these modes may be generated. Chapter 5 presents a novel way in which to achieve broadband mode conversion using coupled circular and coaxial waveguides as well as a matched feed design using this. Finally, an investigation of horns with anisotropic impedance walls as an alternative way to solve the matched feed bandwidth problem is presented in Chapter 6.

All field and current quantities in this thesis are given in phasor notation with the time factor, $e^{j\omega t}$, suppressed. Unless otherwise stated, results presented here are related to systems where the reflector is offset in the y-direction.

CHAPTER 2

Reflector Antenna Cross Polarization and Matched Feeds

This chapter will set the scene of the core problem: cross polarization in reflector antennas. There are many ways to explain or derive polarization properties of symmetric and offset single reflector antennas. The following is based on examining the reflector aperture field calculated by Geometrical Optics. This method is basically the simplest way of analyzing a reflector, but it nicely illustrates the cross polarization arising from the offset system. More accurate techniques will be used whenever the reflector far fields need to be evaluated, but introducing them here would only serve to clutter the conclusions.

After the problem has been concisely described, the matched feed technique will be introduced. The basic workings of the invention will be explained and some remarks on the bandwidth problem will be given. Finally, there will be a comprehensive literature survey of the research within the field.

2.1 The Focusing Properties of Ellipsoids and Paraboloids

Ellipses as the one shown in Figure 2.1(a) have two associated foci (F_1 and F_2). An interesting property of the elliptical curve is that rays originating from one focus will pass through the other focus after just one reflection (assuming angle of incidence equal to angle of reflection). An ellipse can therefore move radiation from one point to another. Often it is of interest to move radiation from a localized source to somewhere far away in a specific direction. If we place one of the foci of the ellipse at infinity in a certain direction, a parabola is formed. Radiation from the focus of a parabola will thus be reflected in parallel rays as illustrated in Figure 2.1(b). Conversely, all rays entering the parabola from this direction will reflect into the focus.

If the ellipse or parabola is rotated around the axis containing the two foci, the focusing properties are retained for the entire resulting surface. These surfaces are called ellipsoids[1] and paraboloids, respectively.

Because of their focusing property, paraboloids are used in many technologies such as search lights, optical telescopes, and microwave antennas. The simple ray-optical

---

[1] More precisely, they are prolate spheroids, since not all ellipsoids have two point foci.

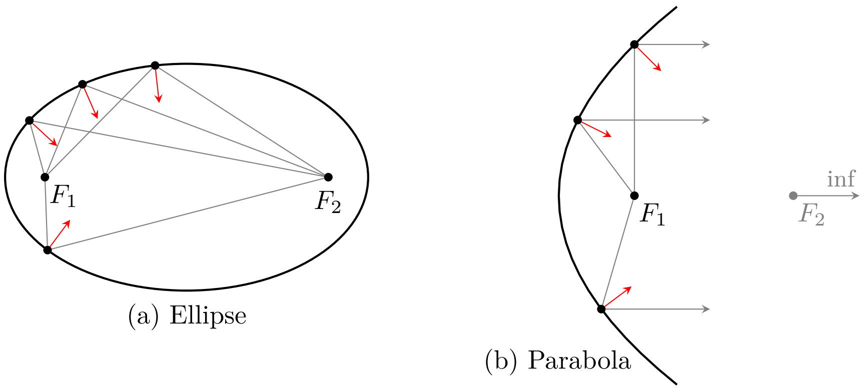

(a) Ellipse

(b) Parabola

Figure 2.1: Focusing properties of ellipses and parabolas. The parabola is a special case of the ellipse, where one of the foci is in infinity, and it is therefore well suited for sending radio signals *far away*. Red arrows indicate normal vectors.

reflection assumption is only an approximation at microwave frequencies, but even still, paraboloids are the workhorses of high gain microwave antennas. Ellipsoidal, as well as hyperboloidal surfaces, are frequently used as intermediate *subreflectors* in antenna systems, but this work will "focus" on antennas with a single paraboloid reflector.

2.2 Cross Polarization of the Symmetric Reflector Antenna

A symmetric reflector antenna illuminated by a purely co-polarized feed will radiate very little cross polarization. This antenna consists of a paraboloidal reflecting surface and a feed antenna in the focus, pointed towards the vertex (tip) of the paraboloid as shown in Figure 2.2.

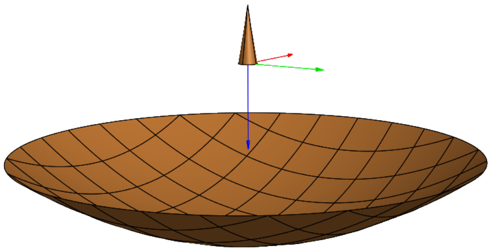

Figure 2.2: Simplest rotationally symmetric reflector antenna system: paraboloidal reflector and feed pointed toward vertex. A real antenna would require support structures for the feed.

The reason for this very low cross polarization may be realized by analyzing the system using just Geometrical Optics (GO), which is an approximation valid in the high frequency limit. Electromagnetic power is assumed to be TEM waves propagating in ray tubes, or bundles, and reflect of surfaces like simple mirror reflection, i.e. the reflected ray makes the same angle with the surface normal as the incident ray, and all three vectors are in the same plane. The GO formula for the reflected field may be derived assuming an infinite PEC plane at the reflection point, and is given

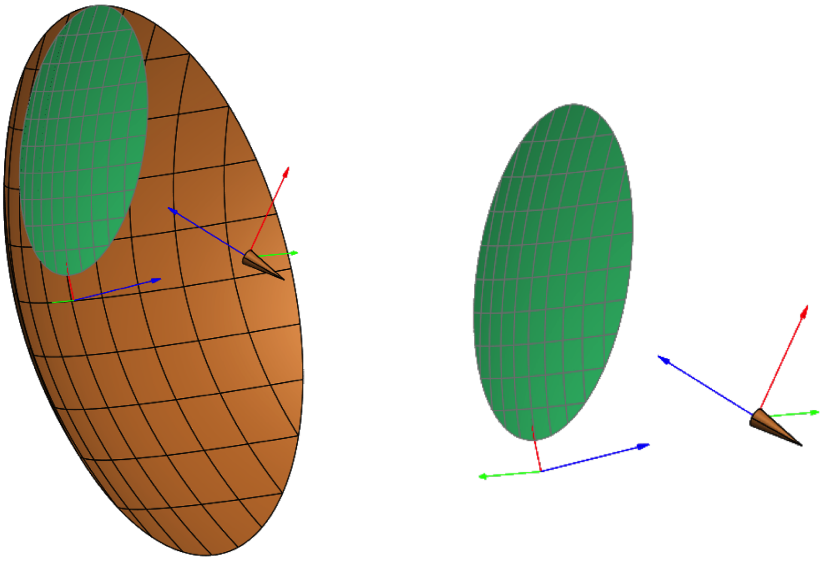

Figure 2.3: An offset reflector antenna as constructed from a parent paraboloid surface.

by:

$$\mathbf{E}_r = 2(\hat{\boldsymbol{n}} \cdot \mathbf{E}_i)\hat{\boldsymbol{n}} - \mathbf{E}_i \tag{2.1}$$

in which $\hat{\boldsymbol{n}}$ is the surface normal, and $\mathbf{E}_i$ and $\mathbf{E}_r$ are the incident and reflected fields, respectively. The formula also provides information on the polarization of the reflected wave.

We may use Equation (2.1) to find the aperture field of the reflector in Figure 2.2. It turns out that if the feed has no cross polarization by Ludwig's 3$^{\text{rd}}$ definition [29], the aperture field will be parallel everywhere. Indeed, this was one of the arguments put forth by Ludwig, in favor of using his 3$^{\text{rd}}$ definition of cross polarization for radiated fields.

As we have already assumed TEM waves, the H-field will also be parallel in the aperture and perpendicular to the electric field. More importantly, the plane wave relation between the two ensures that the equivalent electric and magnetic currents represent Huygens sources everywhere in the aperture. A single Huygens source is perfectly co-polarized by Ludwig's 3$^{\text{rd}}$ definition, and by linearity, so is a sheet of parallel Huygens sources. Therefore, a symmetrical reflector will not introduce any cross polarization — in the GO assumption — it will only propagate cross polarization already present in the feed field.

In a more sophisticated model, z-directed currents and edge diffracted fields will contribute a small amount of cross polarization. However, even when using Physical Optics (PO) with Physical Theory of Diffraction (PTD) or Integral Equation solvers of GRASP [30], the cross polarization of a typical reflected field (with no strut or feed blockage) is in the order of 50 dB to 60 dB below peak directivity.

2.3 Cross Polarization of the Offset Reflector Antenna

An undesirable effect in a practical symmetrical reflector system is that the feed — or a subreflector — and the structure suspending it will block the field of view of the reflected rays. Feed and strut blockage deteriorates efficiency, sidelobe levels, and return loss. Also, it is more complicated to predict the exact performance of the antenna system, when the feed, reflector, and struts couple strongly. Feed blockage can be avoided by cutting out an section of the parent paraboloid and tilting the feed toward this section. The configuration — an offset parabolic reflector antenna — is illustrated in Figure 2.3.

Offset parabolic reflectors also have one major drawback: high cross-polarization in lobes that are near the maximum radiation direction of the antenna. This is true even when the feed is ideal and has no cross polarization of its own. One may think that cross polarization arises from the asymmetry of the reflector surface itself, but it is in fact introduced when the feed is tilted away from the vertex towards the cutout section of the paraboloid. If the feed had been unrotated, the observations about parallel aperture field which we made for the symmetric antenna would still hold.

Consider a feed which is strictly co-polarized by Ludwig's 3rd definition illuminating a paraboloid reflector from the focus at an angle of θ_f as in Figure 2.3. The aperture co and cross polarized components ($\hat{\boldsymbol{x}}$ and $\hat{\boldsymbol{y}}$) were calculated by Chu and Turrin [3]. The formulas are reproduced here (but for a y-offset reflector instead of x-offset as in [3]):

$$\begin{aligned} E_{\text{co}} = \frac{F(\theta',\phi')}{tr} & \left[\sin\theta' \sin\theta_f \sin\phi' \right. \\ & \left. - \cos^2\phi' \left(\cos\theta_f + \cos\theta'\right) - \sin^2\phi' \left(1 + \cos\theta_f \cos\theta'\right)\right] \end{aligned} \tag{2.2a}$$

$$E_{\text{cr}} = \frac{F(\theta',\phi')}{tr} \cos\phi' \left[\sin\phi' \left(1-\cos\theta_f\right)\left(1-\cos\theta'\right) - \sin\theta' \sin\theta_f\right] \tag{2.2b}$$

where primes indicate coordinates that are relative to the (tilted) feed. F is the feed amplitude pattern, r is the distance from the focus to the point on the reflector, and

$$t = 1 + \cos\theta_f \cos\theta' - \sin\theta_f \sin\theta' \sin\phi'.$$

The feed may be either horizontally polarized ($E_{\text{co}} = E_x$ and $E_{\text{cr}} = E_y$) or vertically polarized ($E_{\text{co}} = E_y$ and $E_{\text{cr}} = -E_x$). The cross polarization component is identical in both cases. It may also be observed that, by virtue of $\cos\phi'$, the aperture cross polarization is of opposite signs on either side of the symmetry plane. And as expected, if $\theta_f = 0$, the cross polarization vanishes everywhere in the aperture, symmetric reflector or not.

So why tilt the feed if this causes cross polarization? Much of the radiation from an untilted feed would shoot past the reflector, causing very poor spillover efficiency, but also increased edge illumination and poor aperture efficiency. In a practical system, the feed will have to be pointed upwards to some degree, thus inducing the cross polarization. The concept has been illustrated in Figure 2.4 by plotting the aperture fields due to Equations (2.2) of three configurations: (a) a symmetrical antenna, (b) an offset antenna with no feed tilt, and (c) an offset antenna with a tilted feed. Electric field lines of the reflector aperture are shown for horizontally and vertically polarized feeds. It is evident, that aperture fields of the offset reflector with an untilted feed in Figure 2.4(b) are parallel, though the utilization of the aperture area is very poor. For the tilted the feed in Figure 2.4(c), the equivalent currents in the aperture are still Huygens sources, but as they are not parallel, there will be cross polarization in the far field.

An alternative perspective on the subject is given by Jacobsen [7]: the cross polarization of an offset reflector system may be regarded as the cross polarization of the feed when the polarization of the tilted feed is referenced to an untilted coordinate system. Since the polarization vectors of Ludwig's 3rd definition change with direction, even a perfectly polarized feed will generate cross polarization when tilted. In this way, the generated cross polarization is always just that of the feed, as with the symmetrical reflector system.

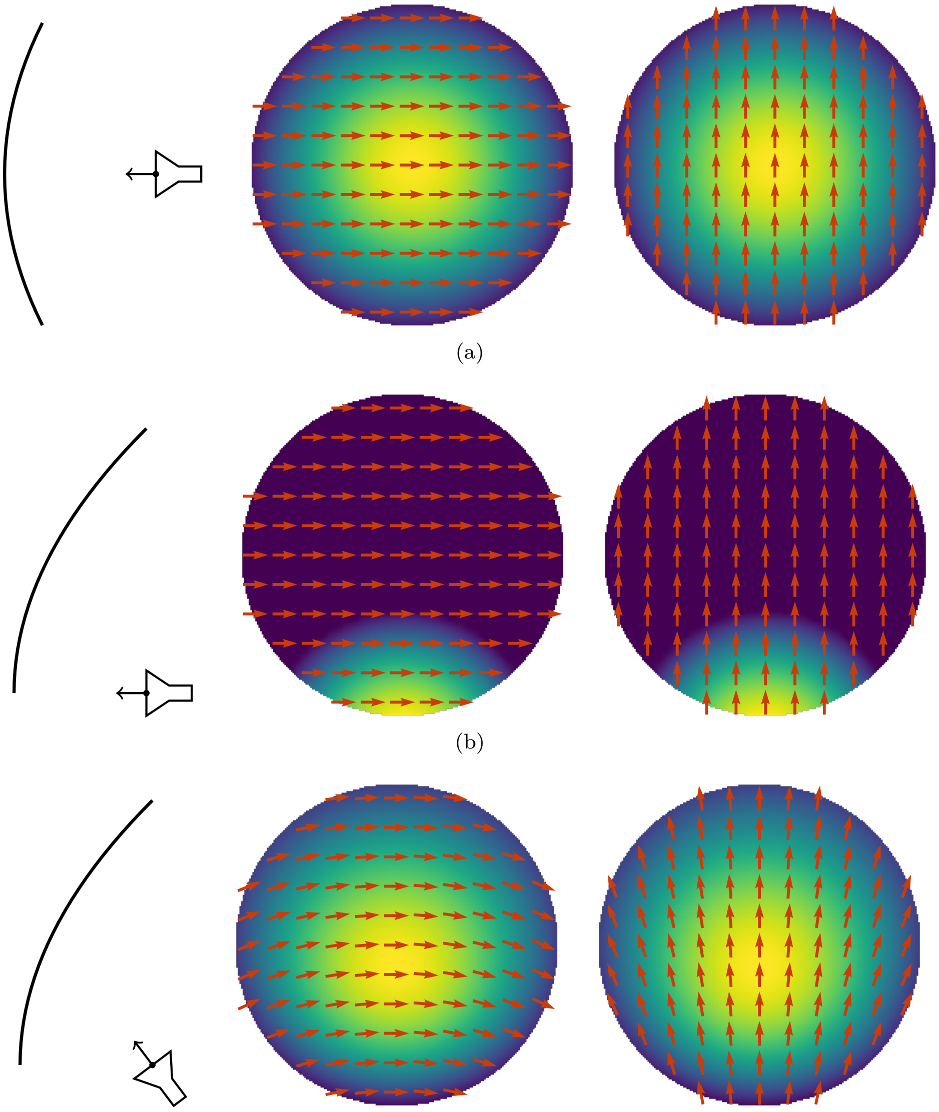

(a)

(b)

(c)

Figure 2.4: Symmetric and offset reflectors illuminated by Gaussian beam feeds with no cross polarization. Horizontally and vertically polarized reflector aperture fields are plotted for symmetric (a), offset with no feed tilt (b), and offset with feed tilt (c). The reflector $f/D = 0.5$ in all three cases and the feed tilt is 62° in (c). It is evident that the cross polarization arises from the feed tilt.

In the plane of symmetry, vertical in Figure 2.4(c), the cross polarization cancels out in the far field, but in other planes, the curved aperture field lines result in cross polarization. The cross polarization is most severe in the plane perpendicular to the symmetry plane, denoted here as the asymmetry plane. As an example of cross polarization in the far field, the antenna treated in [3] will be recalculated here. The antenna is an offset reflector system with $f/D = 0.5$. Additional parameters are summarized in Table 2.1. Figure 2.5 shows the antenna far-field cuts calculated with GRASP in the asymmetry and diagonal planes. The maximum cross-polar radiation is high: only 18.5 dB below the main beam peak. Note that the cross polarization lobes are in phase quadrature with the co-polar radiation and opposite phase on each side of the symmetry plane. The phase relationships between co- and cross-polar radiation will be detailed in the following section.

	Symbol	Value
Frequency	-	18.5 GHz
Focal length	f	6 in
Aperture diameter	D	12 in
Clearance	D'	0 in
f over D	f/D	0.5
Feed tilt	θ_f	53°
Cone tilt	θ_0	45°
Subtended half angle	θ^*	45°

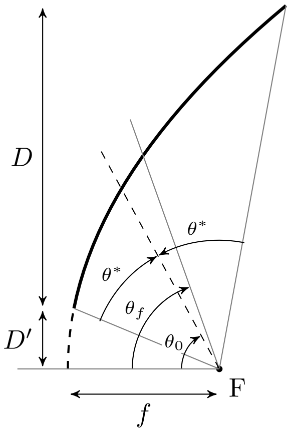

Table 2.1: Parameters of the antenna measured in [3].

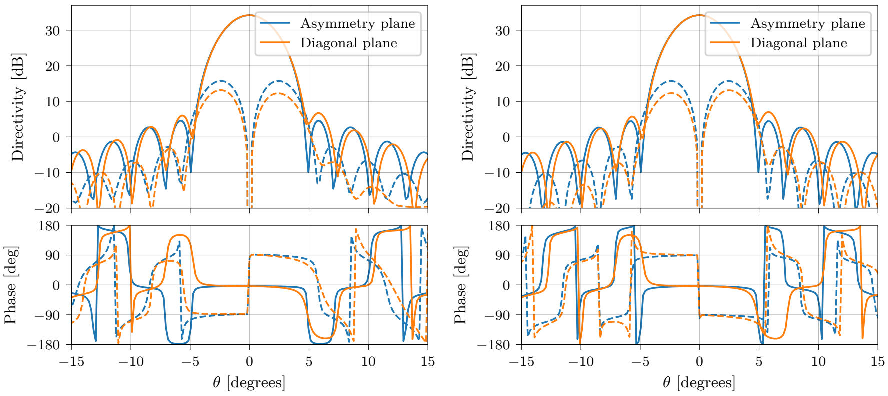

(a) Polarized in symmetry plane

(b) Polarized in asymmetry plane

Figure 2.5: Radiation pattern of offset reflector antenna defined in Table 2.1 [3] illuminated by a purely co-polarized Gaussian beam feed. Cuts in the asymmetry and diagonal planes are shown, there is no cross polarization in the symmetry plane. Cross polarization patterns are drawn with dashed lines. Reflector scattering is calculated with PO+PTD in GRASP.

2.3.1 Phase of Cross Polarization

There is some confusion in the literature as to the phase relationship between co- and cross-polar components in an offset reflector system and especially in a matched feed

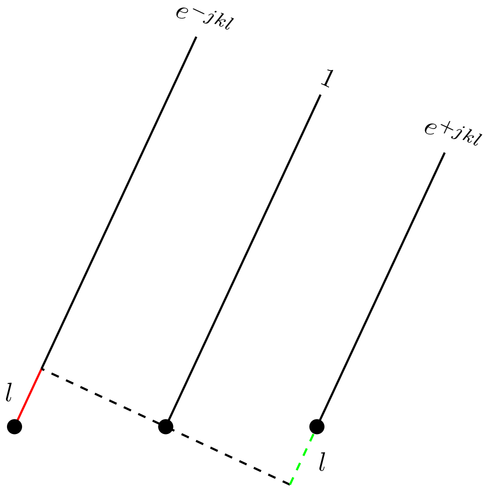

Contribution from outer sources if in-phase:

$$e^{+jkl} + e^{-jkl} = 2\cos kl$$

or if in anti-phase:

$$e^{+jkl} - e^{-jkl} = 2\jmath \sin kl$$

Figure 2.6: Radiation from displaced sources. If the outer elements are in phase with the middle element, their contribution will be in phase with the middle one's and maximum at boresight. If one of the outer elements is in phase with the middle element and the other in anti-phase, their contribution will be in phase quadrature with the middle one's and maximum when $kl = \frac{\pi}{2}$.

system. There is a lot of mention of phase quadrature and/or 90° phase offsets. The root of it all is in fact very simple, though one has to be a little careful to specify *where* we are examining the fields. From Figure 2.5 it is evident that the far-field cross-polar lobes are ±90° out of phase with the co-polar main lobe — plus or minus on either side of the symmetry plane.

The cross polarization arising from the feed tilt is not in phase quadrature — see [7, Fig. 5]. On one side of the symmetry plane, it is along (in phase with) and on the other side opposite (in anti-phase with) the co-polar component. The GO translation to the reflector aperture plane does not change this — see Figure 2.4. The phase quadrature of the far field cross-polar lobes arises from the radiation of the equivalent currents in the aperture. The cross-polar directed sources are displaced on either side of the symmetry plane and in opposite directions, i.e. they are in anti-phase with each other. These sources will radiate cross-polar lobes in phase quadrature with the co-polar sources which are centered in the middle of the aperture. A simplified example is depicted in Figure 2.6: three sources are horizontally displaced. We let the middle one radiate co-polar field and the outer ones cross-polar. If one of the outer sources is in-phase with and the other in anti-phase with the middle source, their total contribution in the far field will be in phase quadrature with the middle component. This is exactly the case with the equivalent sources of the offset reflector aperture in Figure 2.4(c) resulting in far-fields like the ones in Figure 2.5. In the boresight direction, the anti-phase displaced sources cancel out, and there is therefore no cross polarization exactly on axis.

Conversely, in order to compensate the in-phase/anti-phase cross-polar components in the reflector aperture, the feed must radiate cross-polar lobes which are *not* in phase quadrature with the co-polar part. In order to do so displaced cross-polar sources in the feed region must be 90° and −90° out of phase with the co-polar part, respectively.

In summary, offset reflector antennas exhibit high cross polarization in the far field. The cross polarization is in phase quadrature with the co-polar part because it stems from cross polarization in the reflector aperture which is *in-phase* (and anti-phase) with the co-polar component. To compensate it, cross-polar components in the feed aperture must be in phase quadrature with co-polar components.

2.3.2 Beam Squint for Circular Polarization

If the offset reflector system is circularly polarized, the feed tilt does not induce cross polarization (axial ratio degradation), but a depointing — squinting — of the main beam. The squint is in opposite directions for opposite hands of polarization. The main focus of this thesis is on linear polarization, so the effect will only briefly be explained here. For further reference on the subject see e.g. [3, 31–33].

We may understand the beam-squinting effect by inspecting Figure 2.4(c) again. The field is rotated towards the edges of the aperture: counter-clockwise in the left and clockwise in the right side. The direction and amount of rotation is the same for both horizontal and vertical feed polarization, which means that the field lines are still perpendicular to each other in the entire aperture[2]. In consequence, the polarization is still circular, but slightly rotated. The rotation is equivalent to either a delay or advance in time/phase. The increasing phase delay across the aperture results in a scanning of the beam in the plane of asymmetry. Inverting the hand of polarization turns delay into advance and vice-versa, meaning that squinting will be in opposite directions for opposite hands of circular polarization.

Adatia and Rudge [31] present an approximate formula for the amount of beam squint as a function of feed tilt angle and electrical focal length:

$$\psi_s = \mp \frac{\lambda \sin\theta_f}{4\pi f}. \tag{2.3}$$

For the reflector given in Table 2.1, the expected beam squint is

$$\psi_s = \mp 0.39^\circ \tag{2.4}$$

which fits well with simulated results and the results presented in [3].

According to Equation (2.3) the following can be observed about circular polarization beam squint in offset reflector systems:

- Higher frequency will cause *less* beam squint. (But narrower beam.)
- For fixed f/D and θ_f, a larger antenna will cause *less* beam squint.
- For a fixed f, larger D and/or D' will cause *more* beam squint.

2.4 The Matched Feed Concept

As explained in the preceding sections, the cross polarization of offset reflector antennas arises from the tilted feed. An ideal feed would have a tilted beam, but low cross polarization referenced to the untilted coordinate system. A theoretical way of implementing this is to have an array of untilted feeds which are phased such that the beam is scanned upwards as proposed by Jacobsen [7]. Another way would be to have a single feed which is not perfectly polarized, but radiates cross polarization which cancels the cross polarization from the tilt.

---

[2] This can also be realized from the fact that the rotation of the feed and the reflection are both conformal mappings (locally angle-preserving transformations) [5]. In fact, since any combination of N elliptical/parabolic reflectors can be reduced to an equivalent bilinear conformal transformation, circular polarization will always be preserved, but possibly squinted.

In their 1975 paper Rudge and Adatia [6] propose to generate this desired cross polarization by exciting higher order modes in the feed. For circular horns, they propose the use of the TE_{21} mode. It is later clarified in [32] that each of the two degenerate TE_{21} modes can be used for two polarization operations of the antenna. The need for TE_{21} modes is determined by observing the focal region field of the antenna when it is in receiving mode. An analysis of this method and an alternative method for determining compensating modes are given in Chapter 3.

The different horn sections of an example matched feed are depicted in Figure 2.7. Since the TE_{21} mode has a different angular variation ($m = 2$) than the fundamental TE_{11} mode, a waveguide component without rotational symmetry is required to excite it — see Chapter 4 for a detailed analysis. The prototype feed presented in [6, 34] featured two pins with 90° separation inserted near a step in the waveguide diameter. Following the step, the waveguide is large enough to support propagation of the TE_{21} mode, but not TM_{11}. After the next step in diameter, the TM_{11} mode is also supported. The length of the waveguide sections (l_1 and l_2) can be used to independently tune the phase of the TE_{21} and TM_{11} modes relative to TE_{11}. Given the correct relationships in the aperture, the TM_{11} mode will compensate cross polarization of the TE_{11} mode (Potter horn [35]) and the TE_{21} mode will compensate cross polarization from the feed tilt. This is the basic operating principle of most matched feeds in the literature.

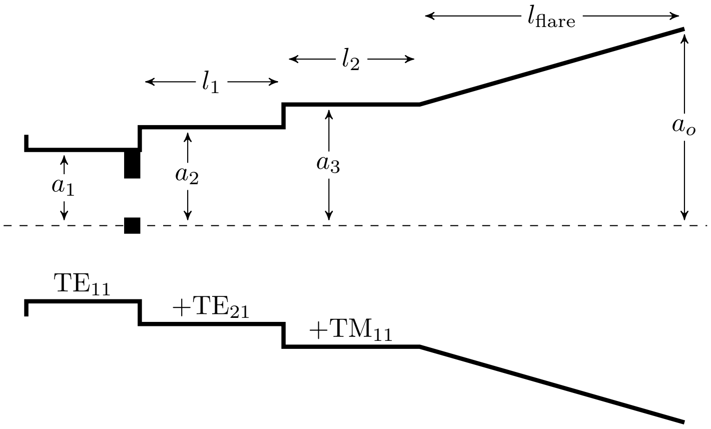

Figure 2.7: Topology of the matched feed horn presented by Rudge and Adatia [6] and most other designs in the literature. Only TE_{11} can propagate where the radius is a_1, TE_{21} and TM_{11} are excited in subsequent sections. The inclusions at the a_1 to a_2 step represent the asymmetric mode launcher.

Another way to realize that the TE_{21} modes are suitable for cross polarization compensation, is by inspecting the modal fields and remembering the discussion on displaced sources in Section 2.3.1. The modal fields of the TE_{11} and TE_{21} modes are illustrated in Figure 2.8. To radiate the required cross polar lobes which are anti-symmetric in the symmetry plane, we need cross-polar sources which are also anti-symmetric in the symmetry plane. The two TE_{21} modes satisfy this requirement — one for each polarization of the primary field. These regions in the waveguide fields are highlighted in the figure. In order to cancel the in-phase (and anti-phase) cross-polar components induced by the feed tilt, the TE_{21} modes will have to be in phase quadrature with the TE_{11} mode as discussed in Section 2.3.1.

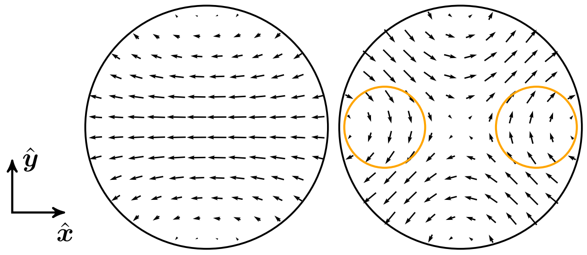

(a) Horizontal polarization: TE$_{11}^{1}$ and TE$_{21}^{2}$

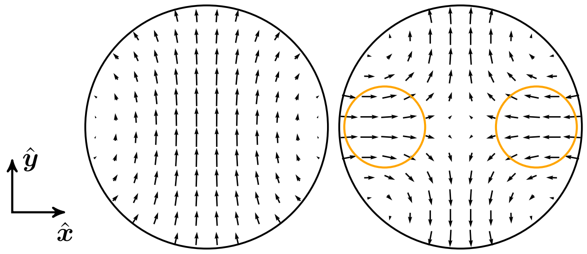

(b) Vertical polarization: TE$_{11}^{2}$ and TE$_{21}^{1}$

Figure 2.8: Transverse fields of the TE$_{21}$ modes needed for matched feed operation shown together with the corresponding TE$_{11}$ mode for each polarization. The desired regions of cross-polar field are highlighted. A y-offset reflector is assumed. The TM$_{11}$ modes are omitted here.

2.4.1 Beam Squint Compensation with Matched Feeds

With the explanation given in Section 2.3.2, it is straight forward to realize, that if a matched feed compensates the aperture cross polarization for both horizontal and vertical inputs, then the beam squint is also eliminated when the feed is excited with circular polarization. Unfortunately, there is a catch. If both polarizations are not compensated to the same degree, we introduce a degradation of the axial ratio, which was otherwise perfect.

In a practical matched feed design, it is unrealistic to maintain the exact same level of compensation for both polarizations over a wide frequency bandwidth. The feed presented in [P1] *does* compensate beam squint when excited by circular polarization, but also degrades axial ratio.

In reference [36], the authors demonstrate beam squint compensation by use of a matched feed. The matched feed is single polarized[3] and therefore quite severe axial ratio degradation must be expected, but this is not considered in the paper.

2.5 Bandwidth Limitations of Matched Feeds

It has previously been mentioned that the matched feed concept is challenged with respect to bandwidth. Indeed the purpose of this work is to clarify and overcome this challenge. Two main factors limit the bandwidth of matched feed designs in the literature: modal phase dispersion and resonance effects. These topics are touched upon several times in this thesis and in the attached papers, but shall be briefly explained now.

---

[3] Can be deduced from the pin configuration; higher order modes will not be in correct phase relationship for dual polarization. See Chapters 3 and 4.

2.5.1 Modal Phase Dispersion

The relative phase between the fundamental and compensating TE_{21} mode is very important for the proper operation of a matched feed. As previously mentioned and as shall be detailed further in Chapter 3, the compensating mode must be in phase quadrature with the fundamental ones. The TE_{21} mode should either lag or lead in phase (plus or minus 90°) depending on the sign convention of the waveguide mode fields used. If it is one or the other is not so important for this discussion.

To illustrate the difficulty in maintaining phase quadrature relationship at the aperture of the horn, dispersion curves for selected waveguide modes are plotted in Figure 2.9. In it, we can read the phase constant as a function of frequency of the three principal waveguide modes used in Rudge and Adatia's matched feed horn [6] — see again Figure 2.7. The modes have significantly different cutoff wavenumbers/frequencies. To be exact: the cutoff frequency of TE_{21} is 1.66 times larger than that of TE_{11}. In consequence, the phase constants are different, and the difference changes with frequency.

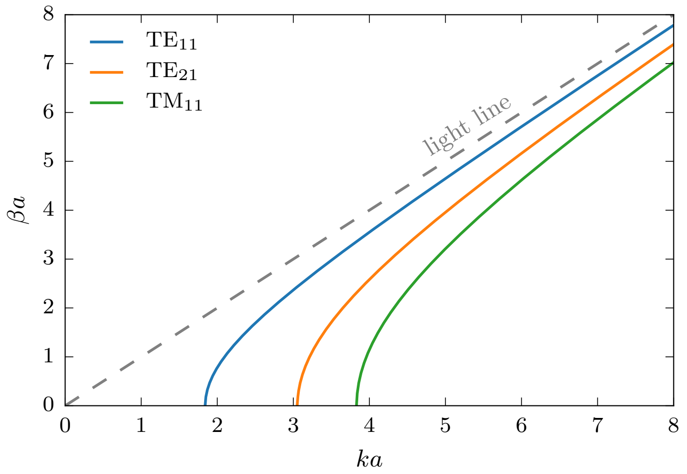

Figure 2.9: Dispersion plot of selected modes in a circular waveguide. $k = \frac{2\pi f}{c}$ is the free space wavenumber. $\beta = \sqrt{k^2 - k_c^2}$ is the propagation constant of the mode, with k_c being the smallest wavenumber at which the mode can propagate. a is the radius of the waveguide.

The relative phase between two modes travelling in a waveguide is the length travelled times the difference in phase constant:

$$\Delta\phi = l\,(\beta_1 - \beta_2)\,. \tag{2.5}$$

It is clear from Figure 2.9 that this quantity will change with frequency, since the distances between the curves change. Herein lies one of the fundamental bandwidth limitations of matched feeds: the phasing lengths of the horn in Figure 2.7 can only be tuned for a single frequency.

To limit the phase dispersion effect of Equation (2.5), one must either minimize l, the distance travelled, or stabilize the difference in phase constant. For a smooth walled circular PEC waveguide, the latter can only be accomplished by choosing a relatively large waveguide. However doing so is seldom very practical.

Equal cutoffs of fundamental and compensating higher order modes *is* possible if the modes travel in different waveguides, which will be explored in Chapter 5, or if the waveguides are made from certain anisotropic surfaces, which will be investigated in Chapter 6.

2.5.2 Resonance Effects

The mode launcher of a matched feed is typically made from one or more *inclusions* in the waveguide, e.g. a pin/rod. A certain amount of higher order mode must be excited by this inclusion and this amount increases with increasing compactness of the system (see Chapter 3). The desired amount can be obtained by tuning the size of the inclusions.

Often, the inclusions reach a size close to their resonance in order to generate a sufficient amount of higher-order mode. This is bad news for the frequency bandwidth of the matched feed. The magnitude and phase of the currents on the waveguide inclusion change rapidly with frequency in the range around the resonance. It is well known from circuit theory that the response looking into e.g. a canonical series RLC circuit, changes from capacitive to inductive when crossing the resonance frequency.

This large phase and magnitude gradient with respect to frequency adds to the difficulty of getting a matched feed to work at more than a very narrow frequency range. Creating conditions which enable us to use many sub-resonance instead of few near-resonance inclusions is discussed in Chapters 5 and 6.

2.6 Literature Survey of Matched Feeds

The invention of matched feeds, namely that the cross polarization arising in offset reflector antennas can be compensated by asymmetrical waveguide modes in the feed, is attributed to Rudge and Adatia [6]. In their first paper on the subject, they explain the necessity of an asymmetrical mode by considering the focal plane fields when the antenna is in receive mode from a distant source at boresight. These focal plane fields had been derived analytically some years earlier by Bem [37]. Rudge and Adatia state that this field can be approximately matched by the addition of the TE_{21} mode in a circular feed, the HE_{21} in a radially corrugated feed, or the TE_{11} mode in a rectangular feed. Additionally, the inherent cross polarization of the circular TE_{11} mode must also be compensated by the TM_{11} mode, as proposed by Potter [35]. They go on to present the practical design of a smooth conical Potter horn with a *mode launcher* attached at the throat. The mode launcher is responsible for generating the asymmetrical TE_{21} waveguide mode. The device consists of two pins inserted into the waveguide at a 90° angle from each other. The feed illuminates a reflector with $f/D = 0.8$ at 30 GHz. Both calculated and measured patterns are presented, but the calculation method is not given. In [34], the authors also consider the method applied to a monopulse radar configuration and simulated results show a successful reduction in *boresight jitter*. Boresight jitter reduction is further investigated in [38]. A more thorough explanation, including the analytical expressions of Bem [37] and how they relate to the waveguide modes, is given by the authors in [32], which is a review paper on offset reflector antennas. Jacobsen [7] also presents an example rectangular matched feed in his treatment of offset reflector cross polarization in 1977.

In [8], the technique is extended to dual polarized operation with shorted rectangular waveguide stubs around the circumference of a waveguide acting as the TE_{21} mode launcher. The mode launcher is still attached to a Potter-type horn and illuminates the same reflector as in [6, 34]. The authors now take up the question of operation bandwidth and state that this configuration has a theoretically achievable bandwidth of 5 % and they obtain 4 % in measured results. They define bandwidth as the band within which the cross-polar discrimination is 10 dB better than a conventional Potter horn feed. Different authors have used different bandwidth definitions, but in the following, the given bandwidths will be related to this measure if possible.

The same authors were granted a patent [39] for the invention in 1978 in which both rectangular, smooth circular, and radially corrugated circular horns are described. Each of the horn types have different mode launching mechanisms. The mechanism in the rectangular horn consists of two slightly different wedge inserts. The wedge material is not given. The smooth circular horn is identical to the horn given in [6, 34] with pins as mode launcher. The corrugated horn incorporates the HE_{21} mode generation by letting one of the corrugation rings have a non-circular shape. Thus, in effect, the "pins" are projected onto one of the corrugations. The authors state that a larger bandwidth is possible with the corrugated feed. Indeed, a dual polarized corrugated feed is reported in [28], but no details or design drawings are given.

Aboul-Atta and Shafai [9] consider a method of efficiently computing the fields from offset reflector antennas illuminated by matched feed using the so-called modified stationary phase method. Zaghloul and Shafai [40] study the effect of feed displacement on the cross polar performance of a reflector system with a matched feed. They use two methods for calculating the field, namely the scalar aperture method and the vector current method, where the scalar aperture method will always yield lower cross polarization. The scalar method refers to the approximation that the feed amplitude pattern on the reflector surface is the same when the feed is displaced in the focal plane and only the phase term is modified.

Tun and Clarricoats [41] consider a feed array of seven circular feeds. Instead of matching the focal plane fields with higher order modes in each horn, they introduce orthogonally polarized fundamental modes (TE_{11}) in two feeds next to the excited one with the right phasing and amplitude. The method achieves larger bandwidth than the conventional matched feeds, but requires a bulky feed array and additional feed network components. A similar technique is used by Foged et al. [42, 43] for cross-polarization reduction in the quiet zone of a compact range by matching the focal plane asymmetric field with two additional horns and a feeding network. And also by Zamanifekri and Smolders [44], who use excitation of adjacent array elements to compensate beam squint for circular polarization. These array techniques, where several discrete radiators are used to obtain cross polarization reduction, will not be treated further in this thesis.

In a 1980 paper on general offset reflector antennas Jamnejad-Dailami and Rahmat-Samii [45] conclude that in most cases, a feed tilt in the direction of the center of the projected aperture produces " ...a better overall antenna pattern." than a tilt towards the center of the generating cone. Prasad and Shafai [10] perform a similar study, but with matched feeds and come to basically the same conclusion: Though cross polarization performance deteriorates with larger feed tilt, pattern symmetry and sidelobe level are improved by directing the feed towards the center of the projected aperture. This is especially true for larger feed tapers ($-20\,\mathrm{dB}$ in the article). The study uses the analytical model for waveguide mode radiation [46], and they note that the larger the feed tilt, the larger the amount of TE_{21} mode is needed. It can also be seen from the results that with more feed taper, in effect meaning a larger feed aperture, *less* of the TE_{21} mode is needed.

Nearly ten years pass before Shee and Smith [47] publish a paper on matched feeds in 1997. This time employed on a seven element hexagonal feed array. The feed elements are circular and presumably, analytical mode radiation patterns have been used, but no mention of this is made. The mode content for each of the seven feeds is optimized using a numerical minimization procedure. The objective function is an average of cross polarization levels in a number of discrete far-field points. The radiation from each mode in each feed in these FF points is precomputed and used during the optimization. Good reduction in maximum cross polar levels are obtained, but no real horn designs or bandwidth data are given.

The next major contribution to the matched feed technology is a European patent filed by Eutelsat in 2001 and granted in 2005 [20]. In it, an axially corrugated elliptical matched feed is described employing a mode launcher with three axial slits. The slits and corrugations are made such that the whole feed can be manufactured by die casting. It is stated that at least 5 % of bandwidth can be obtained, but no results are presented. An American patent of a very similar structure was filed by Raven in 2007 and granted in 2010 [21].

In a conference paper Bahadori and Rahmat-Samii [48] design a matched feed for an offset back-to-back reflector system described in [11]. The same feed design is published in a later paper [12]. The authors apply a global minimization algorithm, Particle Swarm Optimization (PSO), to first find the required mode coefficients based on analytical radiation formulas [46]. A feed which approximately produces these modes in the aperture is subsequently designed in HFSS. The feed axis has a large offset angle of 90°. Cross-polar reduction is good at midband, but the -25 dB (9 dB improvement) bandwidth is only 2.5 % and the pin configuration will only work in one polarization.

Meanwhile, Sharma, Pujara, Dey, and colleagues have published several papers on matched feeds [16, 17, 36, 49–56] from 2008 to 2016. They have treated both smooth circular horns [36, 49, 54, 56], corrugated waveguides [17, 51, 55], and pyramidal horns [16, 53]. Also a numerical technique for extracting scattering parameters of waveguide sections with posts has been presented [56–58]. The technique is based on Method of Moments (MoM), but with waveguide Green's functions. Several of the papers concern an $f/D = 0.82$ reflector. Most of the papers do not mention the bandwidth of the cross polarization reduction. However, they were the first to publish measured results of a corrugated matched feed [55]. In this publication three arc-shaped septums are employed instead of pins, which reportedly gives a better return loss.

Pour and Shafai have also published work on matched feeds in this period [14, 22, 59–65]. They introduce a novel way of exciting the asymmetric mode, namely, in a coaxial choke around the main feed [22, 59]. The advantages of exciting the higher order mode in a separate waveguide is an improved impedance bandwidth and the ability to independently control the cutoffs of the modes. The authors also introduce a variation on the well known mode launcher with two pins in the waveguide. They place the pins right at the radiation aperture of the waveguide feed [59, 62]. This is done in order to minimize the bandwidth limitation introduced by the different phase velocities of the modes in waveguide sections. Owing to this, they obtain a cross polar level 30 dB below peak over a 7.5 % bandwidth corresponding to a 10 dB improvement bandwidth of approximately 4.5 %. However, unwanted non-propagating higher order modes can potentially radiate, since there is no section of waveguide to suppress them.

Yang et al. [18, 66, 67] apply the concept of matched feeds to a tri-reflector compact range. The motivation is to improve the cross-polar discrimination in the quiet zone. They use a similar design method as Rudge and Adatia used for a single reflector, namely conjugate matching the focal plane field when the main reflector is illuminated by a plane wave. As in the single reflector case, they arrive at an asymmetrical cross-polar component in the focal region which can be matched with HE_{21} hybrid mode. They design a corrugated horn with a mode launcher before the corrugated section. The achieved bandwidth is less than 1 % at a frequency of 119 GHz.

In three recent papers, Jana, Anoop, and Bhattacharjee consider circular [68] and rectangular [15, 69] matched feeds. The -30 dB cross-polar discrimination bandwidth of the circular feed is 2.7 %. Power normalized versions of analytical circular waveguide modes are presented. The rectangular matched feed in [15] employs the higher order TM_{11} instead of the TE_{11} proposed in [34]. In [23], Jana and Bhattacharjee introduce a novel horn cross section shape which puts the cutoffs of the higher order waveguide modes closer to that of the fundamental mode. The cross section shape is an intersection between a circle and a rectangle and the eigensolutions are found with a 2D finite element method. The same authors have also presented work on numerical techniques to treat matched-feed systems [70–72].

The largest 10 dB improvement bandwidth is, to the author's knowledge, achieved by Dey et al. [24] by exciting the TE_{21} mode in a series of irises with displaced centres. They obtain a bandwidth of 10 % for one polarization in two cases: an f/D of 0.5 and 0.8. However, since the feed has no flaring after the mode launcher, it is basically an open ended waveguide, the pattern would be too broad for most practical reflector systems. Also, the omission of a horn after the mode launcher would most likely result in significant cross polarization in the 45° plane, which is not mentioned. In a later paper, Dey [19] has combined the displaced iris mode launcher with a corrugated horn section and demonstrates that the concept also works for a more realistic feed. He obtains 8 % 10 dB and 9.5 % 7 dB improvement bandwidth for one polarization. The considered reflector system has a severe offset angle of 90°.

2.7 Summary

The preceding sections have given the reader an introduction to cross polarization in offset reflector antennas and matched feeds. Basic concepts regarding reflector antennas, particularly of the offset kind, have been refreshed.

The problem and precise nature of the cross polarization arising in offset reflector antennas has been described, which leads naturally to the introduction of matched feeds. The idea behind the matched feeds is explained and fundamental difficulties in making them wideband are examined.

We have taken a look at the existing literature on the subject, with special interest in how other authors address the bandwidth problem. A satisfactory solution has yet to be published. Also virtually absent in the literature are: 1) dual polarized designs and 2) proper explanation of how mode launching devices work.

CHAPTER 3

Determination of Compensating Waveguide Modes

Compensating the cross polarization in an offset single reflector system requires cross polarization to be radiated by the feed with specific pattern and phase. In this chapter, we shall concern ourselves with determining combinations of waveguide modes which can achieve this desired radiation. A review of the most commonly used method, the focal field approach, is given. Then an alternative method based on direct optimization of a set of waveguide modes based on the reflector aperture field is presented. A parametric study using this method is carried out.

3.1 Focal Region Field Approach

The fields in the focal plane[1] of an offset parabolic reflector antenna were investigated by Bem [37] in 1969. The focal plane field is computed given a plane wave incident from boresight of the antenna. PO currents are calculated followed by the fields near the focal point of the paraboloid. Bem subsequently makes some approximations assuming a large f/D ratio which simplifies the fields in the focal plane to

$$\frac{E_x}{E_0} = 2\frac{J_1(u)}{u} + j\frac{D}{f}\tan\frac{\theta_f}{2}\frac{J_2(u)}{u}\cos\phi \tag{3.1a}$$

$$\frac{E_y}{E_0} = -j\frac{D}{f}\tan\frac{\theta_f}{2}\frac{J_2(u)}{u}\sin\phi \tag{3.1b}$$

$$\frac{E_z}{E_0} = -j\frac{D}{f}\frac{J_2(u)}{u}\cos\phi, \tag{3.1c}$$

where $u = \frac{D}{2f}k\rho$, in which k is the free space propagation constant and ρ represents the radial distance to the observation point in the focal plane. This case is for a reflector which is offset in the xz-plane and with the incident plane wave polarized in the x direction. The expressions for an incident wave polarized along y are obtained by interchanging x and y components and negating ϕ in Equation (3.1)[2] resulting in:

---

[1] In this context the focal plane is a plane which contains the focal point and is perpendicular to the axis of the cone generating the offset reflector, i.e. where the feed horn aperture would be.

[2] There seems to be a typo in [37] where it states that ϕ should be replaced by $\phi + \pi/2$.

$$\frac{E_x}{E_0} = j\frac{D}{f}\tan\frac{\theta_f}{2}\frac{J_2(u)}{u}\sin\phi \tag{3.2a}$$

$$\frac{E_y}{E_0} = 2\frac{J_1(u)}{u} + j\frac{D}{f}\tan\frac{\theta_f}{2}\frac{J_2(u)}{u}\cos\phi \tag{3.2b}$$

$$\frac{E_z}{E_0} = -j\frac{D}{f}\frac{J_2(u)}{u}\cos\phi. \tag{3.2c}$$

Several things are worth noting from these equations:

- The cross-polar field in the focal plane disappears in the case of no feed tilt ($\theta_f = 0$). This is in line with the discussions of Sections 2.2 and 2.3.
- The cross-polar (and the second term in the co-polar) component are in phase quadrature with the principal co-polar term.
- The z-component of the electric field is larger than the cross-polar component (for $\theta_f < 90°$) and unaffected by the offset angle.

Rudge and Adatia [6, 32, 34] use the above to justify the use of higher order waveguide modes for cross polarization compensation. The idea is that, by reciprocity, conjugately matching the incident fields will yield an antenna which radiates the same as the incident wave, but in the reverse direction. Thus if a feed horn can be made which generates the complex conjugate of the field given in (3.1), a linearly polarized plane wave will be generated in the aperture of the reflector.

The authors propose that this is accomplished by overmoding the feed horn of the reflector to match the desired field. Specifically, they propose the addition of the TE_{21} mode in a circular horn. Field configurations of circular waveguide modes are given in Appendix B.3. Setting $m = 2$ and choosing the top line (first of two degenerate sets) in Equation (B.42b), we obtain the transverse E-field of the TE^1_{21} mode. Evaluating the field along the two paths $\phi = 0$ and $\phi = \pi/2$ yields

$$E_x(u', 0) \propto \frac{J_2(u')}{u'} \tag{3.3a}$$

$$E_y(u', 0) = E_x(u', \pi/2) = 0 \tag{3.3b}$$

$$E_y(u', \pi/2) \propto \frac{J_2(u')}{u'}, \tag{3.3c}$$

where $J_2(x)$ is the second order Bessel function and $u' = \frac{\chi'_{21}\rho}{a}$, in which χ'_{21} is the first root of the derivative of the second order Bessel function, and a is the radius of the waveguide. Looking in the same two cuts of Equation (3.1) ($\phi = 0$ and $\phi = \frac{\pi}{2}$), we see that given the right constants and the correct waveguide radius such that $u = u'$, the TE^1_{21} mode can be matched with the x component and the second term of the y component of the focal plane field. Now choosing the bottom line in Equation (B.42b) and evaluating along the same two paths, we obtain the TE^2_{21} (second degenerate set) mode fields

$$E_y(u', 0) \propto J'_2(u') \tag{3.4a}$$

$$E_x(u', 0) = E_y(u', \pi/2) = 0 \tag{3.4b}$$

$$E_x(u', \pi/2) \propto J'_2(u'). \tag{3.4c}$$

These must satisfy the cross terms in Equation (3.2). The fit between $J'_2(u')$ and $J_2(u')/u'$ is not perfect, but it is argued in [32] that a good approximate match can be obtained since the functions are similar.

The above constitutes the focal plane matching method which justifies the use of the two orthogonal TE_{21} modes for compensating cross polarization in offset reflector antennas. The analysis provides valuable insights, and by careful bookkeeping, even the required amount of the higher order modes can be approximated with this method. However, there are several issues:

1. Equations (3.1) and (3.2) are approximations for large f/D. Bem [37] states that the approximation is good for $f/D \geq 1$, but matched feeds would typically be desirable to implement for reflectors with smaller f/D.
2. Only boresight incidence is considered.
3. Rudge and Adatia only demonstrate a match in the two principal planes as reproduced above. The rest of the focal plane field cannot be matched perfectly with the TE_{21} modes alone. What is the implication of this?
4. Feed tapering is not included in the model, and thus, we are trying to match an unrealistic focal plane field, which may have an effect on the optimal excitation coefficients.
5. The considerable amount of z-directed field is not addressed.

Most of the problems above may be solved or partly solved by augmenting the method. Valentino and Toulios [73] have presented results which could be used to address issues two and four. They have generalized Bem's work to include other angles of incidence, and they present radiation patterns where they indirectly take the feed taper into account. Issue number one can be accounted for by using the full formulas given in [37] or [73]. Since the focal plane field and waveguide fields are known in the whole focal plane, one could also find the best match with TE_{21} and/or other modes over the whole aperture, thus addressing issues three and five.

Implementing all these solutions would be quite tedious. Therefore, a simpler, more direct approach which does not suffer from the above issues shall be presented below.

3.2 Optimizing Reflector Aperture Field

To mitigate the drawbacks of the focal field matching method described in the previous section, we employ a more direct method. The procedure is based on the conjecture that a nicely polarized reflector aperture field will produce a nicely polarized far-field. Indeed, since the aperture fields of the paraboloid are everywhere locally plane waves according to the GO approximation, the equivalent currents constitute Huygens sources, as explained in Section 2.2. A single Huygens source radiates no cross polarization, so if the aperture field is parallel everywhere, the equivalent Huygens sources will radiate no cross polarization.

A combination of radiating waveguide modes in the aperture of a circular feed are optimized to approximate the above condition as well as additional conditions given below. The resulting excitation coefficients will be the mode combination needed for matched feed operation.

3.2.1 Optimal Excitation Coefficients

In order to find the optimal combination of modes in the horn aperture we must first define what the desired reflector aperture is. In other words, we need a suitable objective function.

While minimizing the cross polarization of the antenna, the directivity must not be degraded. A good measure of the maximum directivity of an antenna is the combined spillover and aperture efficiency. The aperture efficiency (η_A) of an antenna as defined in [74, Sec. 4.6] takes illumination efficiency (η_i), cross polarization efficiency (η_x), and phase-error efficiency (η_p) into account:

$$\eta_A = \eta_x \eta_p \eta_i \tag{3.5}$$

$$= \frac{\left| \iint_A E_{co}(\rho, \phi) dA \right|^2}{A \iint_A (|E_{co}|^2 + |E_{cr}|^2) dA}, \tag{3.6}$$

where A denotes the aperture. The spillover efficiency, η_s, measures how well the radiation of the feed is confined within the reflector surface:

$$\eta_s = \frac{P_{\text{aperture}}}{P_{\text{feed}}} \tag{3.7}$$

where P_{feed} is the total power radiated by the feed, and P_{aperture} is the power incident on the reflector. In the GO approximation, this is the same as the power flow of the reflected field passing through the aperture. The product of aperture- and spillover efficiencies, $\eta_A \eta_s$, is a measure of the co-polar on-axis gain of the antenna. However, maximum co-polar gain does not ensure low cross polarization, which is the goal of this study. Therefore, we define the cross-polar aperture error, $\mathcal{E}_{cr}$

$$\mathcal{E}_{cr} = \frac{\iint_A |E_{cr}|^2 \, dA}{\iint_A (|E_{co}|^2 + |E_{cr}|^2) dA}, \tag{3.8}$$

which measures the cross-polar power relative to total power in the aperture.

We now solve the optimization problem

$$\max_{C} \quad \eta_A \eta_s - K_{cr} \mathcal{E}_{cr}, \tag{3.9}$$

where C represents the unknowns to be found: the mode excitation coefficients, the feed tilt, and horn aperture size. K_{cr} is a constant which weighs the importance of our two objectives. It means that the on-axis gain of the antenna is maximized with an additional penalty for high cross polarization controlled by K_{cr}. An *L-BFGS-B* algorithm of MINPACK [75] is used to solve the problem, where the integrals over the aperture are evaluated numerically at each iteration.

As this is a dual-objective optimization problem, choosing the weighting constant, K_{cr}, is critical. We want the cross polarization as low as possible, but on the other hand, putting excessive weight on $\mathcal{E}_{cr}$ will result in some very bad antennas with e.g. nulls in the aperture field. By analyzing both objectives for several values of K_{cr}, a good compromise is found to be $K_{cr} = 50$, for which nearly optimal aperture efficiency can be obtained with very negligible cross polarization.

3.2.2 Calculation Method

An evaluation of the objective function involves the following procedure. The reflector aperture field is evaluated in a list of points which lends themselves well to numerical surface integration. For each xy point in the reflector aperture the following procedure is applied

1. Calculate z-coordinate on reflector surface.

2. Transform xyz-point on reflector to $r'\theta'\phi'$ in feed coordinates.

3. Evaluate feed field for given $\theta'\phi'$ direction by summing the radiation from each mode in the aperture. The radiated field from a waveguide mode is calculated from formulas in [76] (reproduced in B.3.3).

4. Find reflected aperture field by applying Geometrical Optics, Equation (2.2) [3].

The three elements of the objective function (3.9), the aperture efficiency, the spillover efficiency, and the cross-polar aperture error are evaluated by numerical integration.

3.2.3 Results

The optimization described above has been carried out for a range of reflector geometries. Namely the reflector f/D has been varied from 1 to 0.3, keeping the aperture size and clearance constant. This results in increasing offset angles. For each geometry, the mode excitation coefficients, feed tilt, and feed size have been optimized according to Equation (3.9). The resulting mode coefficients can be used in the initial design of a matched feed for the given geometry.

In Figure 3.1 only the modes which have previously been mentioned in the literature are included in the optimization: TE_{21} modes for compensation of the tilt-induced cross polarization and TM_{11} modes for compensation of the cross polarization of TE_{11}. For each polarization, specific degenerate versions of TE_{11}, TE_{21}, and TM_{11} modes are needed[3] (denoted with superscripts) — see also [32].

As expected, the amount of needed TE_{21} content increases with decreasing f/D (increasing offset angles). The requirement for the two different TE_{21} modes is almost equal for horizontal and vertical polarization. On the other hand, the optimal TM_{11} amplitude increases with offset angle for horizontal polarization and decreases for vertical. It may also be noted that the need for phase quadrature of the TE_{21} modes is confirmed. The required phase is 90° for horizontal and $-90°$ for vertical. This is a consequence of yz-offset, but is also dependent on the sign conventions of mode definitions. The sign of the compensating modes is not of importance for the discussion, but of course it must be correct in a design.

Below the respective mode coefficient plots for horizontal and vertical polarization in Figure 3.1, the resulting aperture field is plotted for an f/D of 0.5. No cross polarization is visible with the naked eye, which is a preliminary validation of the method. The aperture fields may be compared to the ones in Figure 2.4(c), which represent the same geometry, but with a conventional feed.

In the literature, only TE_{21} modes are mentioned in relation to smooth circular horns. However, we have found that including the zero-order modes TE_{01} and TM_{01} can enhance the performance and even replace the TE_{21} modes[4]. Figure 3.3 shows optimum mode content when the zero order modes are included with the TE_{21} modes. TE_{01} is included for horizontal polarization and TM_{01} for vertical polarization. This may be easily understood by looking at the zero order mode fields in Figure 3.2 and comparing with Figure 2.8. The modes have regions of cross polarization which are equivalent to the TE_{21} modes'.

Figure 3.4 shows the results when TE_{21} modes are excluded and only the zero-order modes compensate the cross polarization. As is evident from the aperture field plots, the cross polarization is adequately suppressed. To the author's knowledge,

---

[3] Note that the specific TE_{21} mode needed for each polarization depends on if the reflector is offset in the x- or y-direction. In this analysis, the offset is in the y-direction, which means that TE_{21}^2 (set 2) is needed to compensate the fundamental mode TE_{11}^1 (set 1). Would the reflector be offset in the x-direction instead, TE_{21} and TE_{11} would be of the same set.

[4] The zero order modes were included in the mode optimization by suggestion from Dr. Stig Busk Sørensen, TICRA.

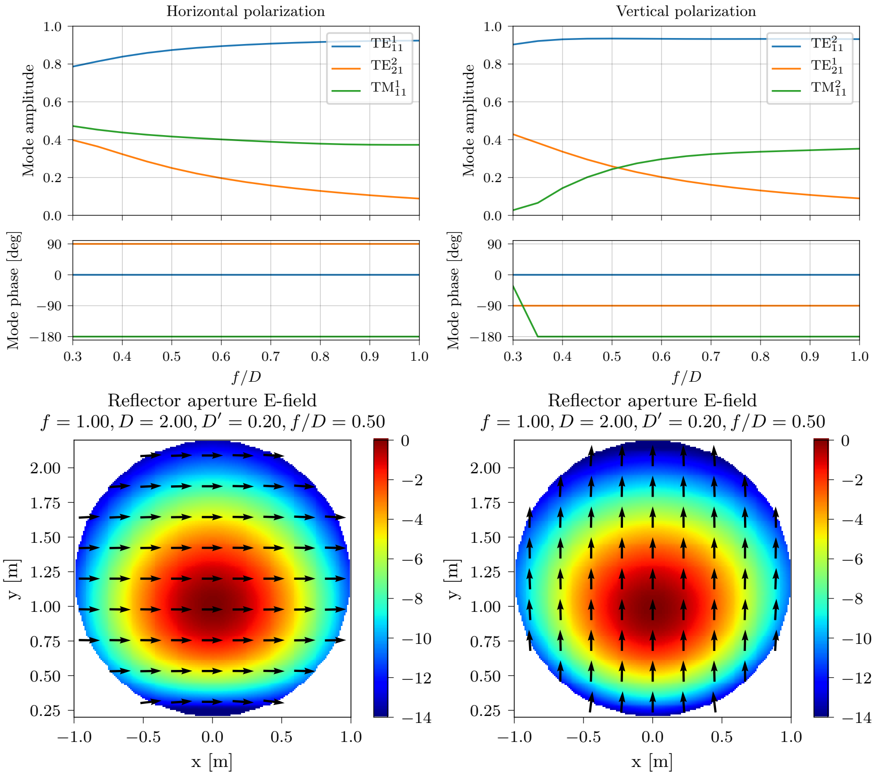

Figure 3.1: Optimized mode excitation coefficients for f/D values between 0.3 and 1. Zero-order modes have been excluded. Resulting reflector aperture fields for $f/D = 0.5$ are shown. $K_{cr} = 50$.

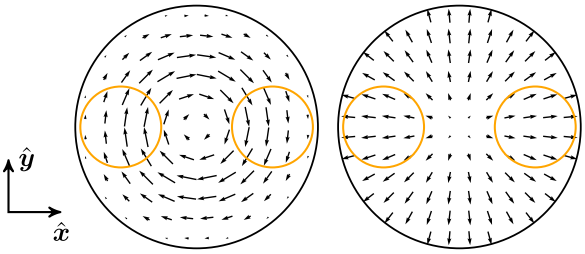

(a) TE^2_{01} (b) TM^1_{01}

Figure 3.2: Transverse fields of the zero order modes. Regions of cross polarization equivalent to those of the TE_{21} modes are highlighted.

the use of TE_{01} and TM_{01} modes for matched feed design had not been mentioned in the literature before [P1]. In order to validate the claim, a full matched feed design employing only TM_{01} for matching, is presented in Appendix A.

Including the zero order modes produces slightly better results, but all the aperture plots in Figures 3.1, 3.3, and 3.4 are satisfactory. Therefore, in a design situation, compensating modes should be chosen based on convenience: ease of generation and possibility of sustaining across a large bandwidth. An advantage of the TM_{01} mode is that its cutoff is closer to TE_{11} than the cutoff of TE_{21} is. This advantage is, however, only applicable in single polarized designs, since TE_{01} or TE^2_{21} is needed

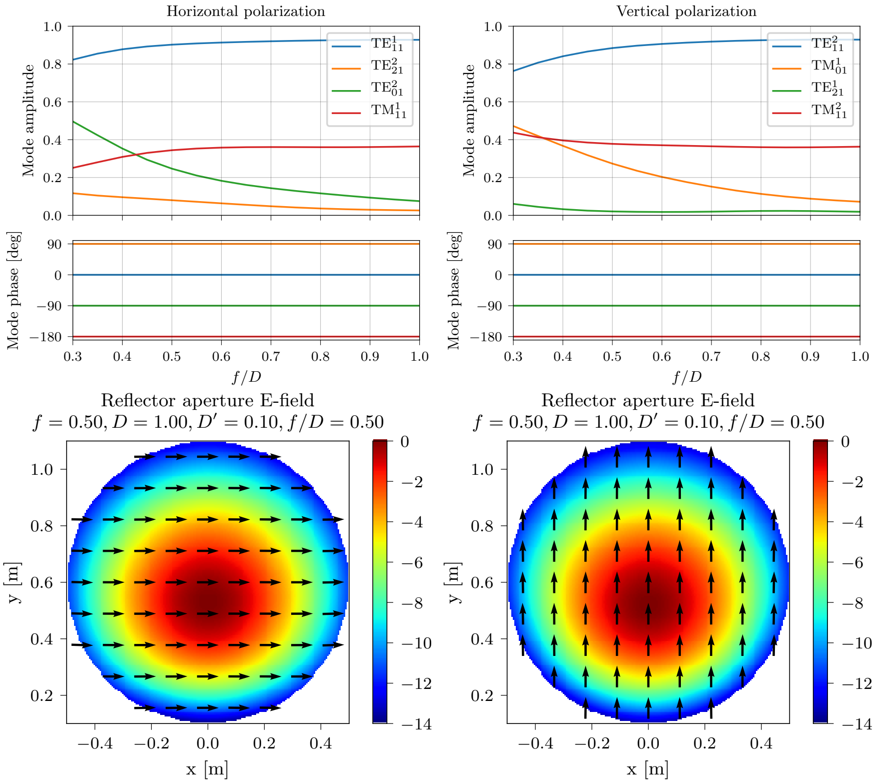

Figure 3.3: Optimized mode excitation coefficients for f/D values between 0.3 and 1. Horizontal (left column) and vertical (right column) polarization. Resulting reflector aperture fields for $f/D = 0.5$ are shown. $K_{cr} = 50$.

for the other polarization. For dual polarized designs, it is most convenient to use the two degenerate TE_{21} modes, as they have equal cutoff frequencies and therefore phase constants.

Does the optimization of the reflector aperture field actually result in good far-fields? An example reflector with $f = 0.5\,\mathrm{m}$, $D = 1\,\mathrm{m}$, and clearance $D' = 0.1\,\mathrm{m}$ is analyzed in GRASP at 13 GHz. Illuminated by a co-polarized feed, the very compact reflector system radiates severe amounts of cross polarization as shown in Figure 3.5(a). Next the reflector is illuminated by an open ended waveguide excited by TE_{11}^{2}, TM_{01}^{1}, TE_{21}^{1}, and TM_{11}^{2} in phase and magnitude as dictated by the top right plot of Figure 3.3. The resulting far-field pattern of the reflector system in Figure 3.5(b) exhibits significantly lower, basically negligible cross polarization. The field from the feed is calculated as a full waveguide-excited method of moments analysis and not by the Risser formulas [76] used during optimization.

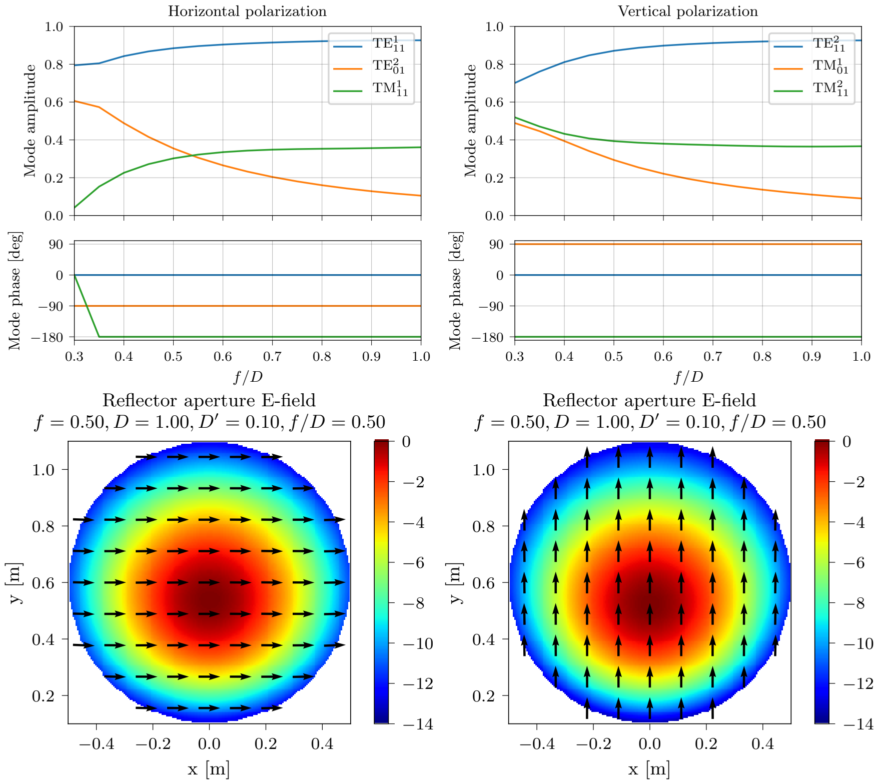

Figure 3.4: Optimized mode excitation coefficients for f/D values between 0.3 and 1. TE_{21} modes have been excluded. Resulting reflector aperture fields for $f/D = 0.5$ are shown. $K_{cr} = 50$.

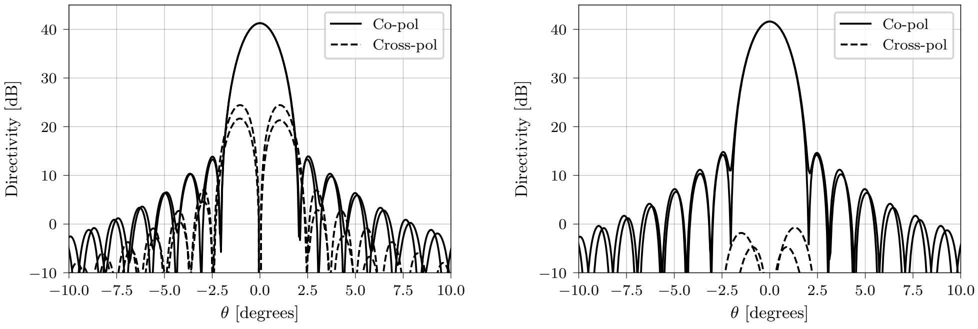

(a) Gaussian beam feed

(b) Optimized modes

Figure 3.5: Validation of the aperture field optimization procedure. Secondary patterns of an $f/D = 0.5$ reflector illuminated by modes dictated by the upper right plot of Figure 3.3 (PO+PTD calculation). The secondary pattern when the same reflector is illuminated by a perfectly co-polarized Gaussian beam is shown for reference. Asymmetry and diagonal plane cuts are plotted.

3.3 Summary

A review of the focal plane matching method was given; the method originally used to justify the use of TE_{21} mode for matched feed design. Examining the focal plane fields around the focus provides good insight into the problem at hand, however for a quantitative analysis, it has several drawbacks. Therefore, a direct optimization of mode coefficients given an objective function in the reflector aperture was presented. This method is simple enough to retain physical insight of the problem, but sophisticated enough to provide concrete modal excitation coefficients which result in high quality secondary patterns.

A parametric study of the required mode combinations for different system configurations was conducted. The reflector f/D was varied and optimal modal combinations were acquired for both modes of linear polarization. In the process it was discovered that TE_{01} and TM_{01} modes can be used together with or instead of the TE_{21} modes.

CHAPTER 4

Mode Conversion

In this Chapter, possible ways to generate the desired waveguide modes found in Chapter 3 shall be discussed. Usually, the input of a feed is a waveguide supporting only the fundamental mode, possibly in two polarizations. In order to get the desired combination of modes, some of the energy propagating in the incident mode must be coupled to higher order modes. The component of the feed which achieves this, is the previously mentioned *mode launcher* or *mode converter*.

A simple analytical framework is presented to analyse how inclusions in the waveguide excite higher order modes. Currents or equivalent currents are induced on the inclusion and these currents subsequently radiate waveguide modes depending on their position and orientation. The method is very simple and it effectively predicts the behavior of common mode converters in excellent agreement with simulations. The simple nature of the model paves the way for conception of new, more advanced mode converters, as will become clear in Chapter 5. The essential results of this chapter have been published in [P2].

4.1 Need for Asymmetry

The desired higher order modes in a circular waveguide are: the TE_{21}, TE_{01}, TM_{01}, and TM_{11} modes. For all modes $m \neq 0$ there exists two orthogonal versions corresponding to $\cos m\phi$ and $\sin m\phi$ azimuthal variations, respectively. TE_{01} and TM_{01} have only one version each. We need both orthogonal TE_{21} and TM_{11} versions — one for each operating polarization. The two versions are denoted as part of the first and second *set* (see Section B.3) and this number is placed in superscript, e.g. TE_{21}^{2} is the TE_{21} mode, second set.

Usually we are interested in converting power from the fundamental mode, TE_{11}, into these other modes. The fundamental mode also has two orthogonal versions, corresponding to two linear polarizations. Power cannot be coupled between different azimuthal indexes and different sets in circular symmetric waveguides and horns (e.g. smooth conical, radially corrugated, axially corrugated, and Potter horns). One way to realize this, is by setting up the mode matching equations from the boundary conditions of the electric field [77]. Terms in the mode matching equations are integrals of products between waveguide modes at either side of the junction. Each component of each circular waveguide mode contains factors of $\sin m\phi$ or $\cos m\phi$, corresponding to the set (cos or sin) and the azimuthal index (m). If the two factors are not the same, that integral will be zero. This is a consequence of the full period orthogonality of the sine and cosine functions. Namely, letting m and m' be two integers then

$$\int_0^{2\pi} \sin(m\phi)\cos(m'\phi)d\phi = 0 \quad \text{for all } m, m', \tag{4.1}$$

accounts for the orthogonality between set 1 and set 2 and

$$\begin{aligned} &\int_0^{2\pi} \sin(m\phi)\sin(m'\phi)d\phi \\ &= \int_0^{2\pi} \cos(m\phi)\cos(m'\phi)d\phi \\ &= \begin{cases} 0 & \text{for } m \neq m' \\ \pi & \text{for } m = m' \end{cases} \end{aligned} \tag{4.2}$$

accounts for orthogonality between different azimuthal indexes.

Thus, the TM_{11} (in the same set as the incident mode) mode can be generated by circular symmetric structures, but the other desired modes must be generated in circularly asymmetric parts of the feed.

4.2 Mode Excitation from Currents

Consider a waveguide of arbitrary cross-section. In a region of the waveguide, electric and magnetic source currents exist, as shown in Figure 4.1. The fields due to the source currents can be expanded in waveguide modes travelling along the waveguide in both directions. The excitation amplitude of these modes can be found by applying the Lorentz reciprocity theorem with each waveguide mode as the secondary field as in done in e.g. [78, 79].

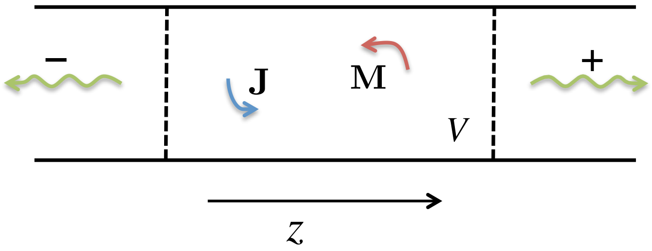

Figure 4.1: Electric and magnetic currents, **J** and **M**, exciting modes in a waveguide.

Assuming that all the waveguide modes are power normalized as in [80], the excitation coefficient of the ith mode due to the currents is

$$V_i^{\pm} = \frac{Z_i}{2} \iiint_V \left(-\mathbf{E}_i^{\mp} \cdot \mathbf{J} + \mathbf{H}_i^{\mp} \cdot \mathbf{M}\right) dv, \tag{4.3}$$

where Z_i is the wave impedance of the mode and plus or minus signs in the superscript refer to waves travelling in the positive or negative z-direction, respectively. In short, the excitation coefficient of a mode due to a current can be found by simply projecting the current onto the field of the same mode travelling in the opposite direction.

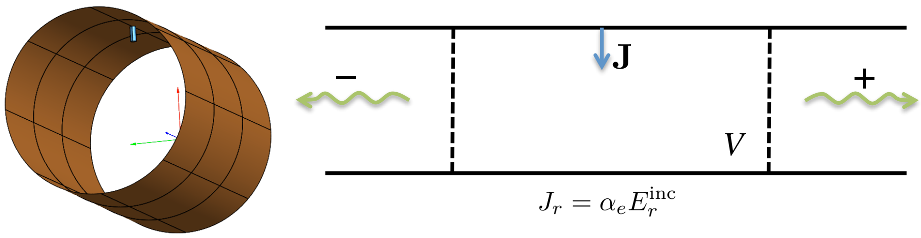

(a) Radial pin model

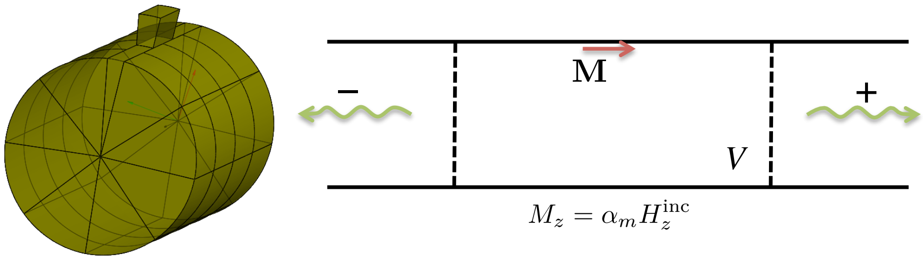

(b) Longitudinal stub model

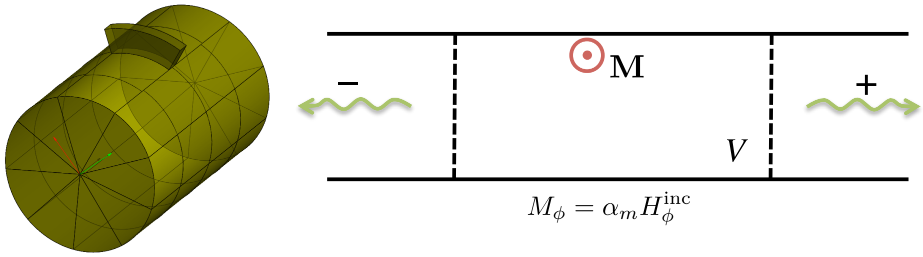

(c) Azimuthal stub model

Figure 4.2: MoM meshes of three types of mode launchers and their analytical current representations. Blue arrows represent electric current and red arrows represent magnetic current.

4.3 Waveguide Inclusions Modeled by Currents

Nearly all matched-feed mode launchers in the literature can be represented by a combination of current filaments, electric or magnetic. An overview can be seen in Figure 4.2.

Pin type mode launchers are especially popular (e.g. [6, 12, 36]). These can be effectively modeled using electric currents, see Figure 4.2(a). Let us assume that a current element in the ρ direction represents a metallic post

$$\mathbf{J}_e = \hat{\boldsymbol{\rho}} I_0 \delta(\mathbf{R} - \mathbf{R}'). \tag{4.4}$$

We initially disregard how this current might be excited on the post and look only at the consequences. Inserting (4.4) into (4.3) together with mode fields of circular waveguide modes, we obtain the coupling coefficient of each mode. Dropping some constants we can write

$$V_{mn}^{\mathrm{TE}} \propto \pm \frac{m}{\rho'} J_m(\mu\rho') \begin{matrix}\cos\\ \sin\end{matrix}\ m\phi' \tag{4.5}$$

$$V_{mn}^{\mathrm{TM}} \propto \frac{jk_\lambda}{k} J_m'(\lambda\rho') \begin{matrix}\cos\\ \sin\end{matrix}\ m\phi', \tag{4.6}$$

where the top and bottom choices correspond to coupling to the first and second set, respectively. The factor of m for V_{mn}^{TE} means that the desired TE$_{01}$ cannot be excited by a radial current, which is because the mode has no E-field in the ρ-direction. Conversely, the desirable TM$_{01}$ mode is excited equally well independent of the azimuthal position of the current. Considering the generation of the TE$_{21}$ mode excited by a current at a position near the edge of the waveguide, the dependence on azimuthal position is

$$V_{21}^{TE} \propto \begin{matrix}\cos\\ \sin\end{matrix}\, 2\phi'. \tag{4.7}$$

This function has four extrema around the waveguide, two positive and two negative. Thus, if more than one radial current is present they need to be in the correct phase depending on position. Figure 4.3 shows the direction of currents placed at the maximum positions such that they all couple constructively to the two degenerate TE$_{21}$ modes.

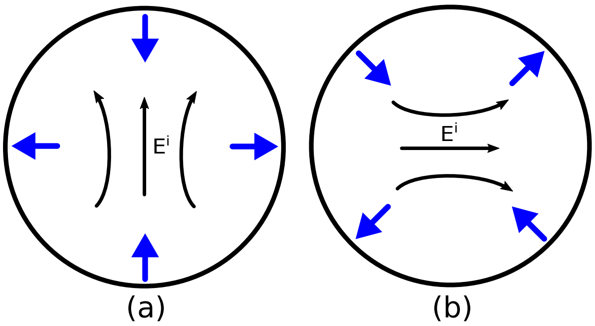

Figure 4.3: Azimuthal positions of radial currents to excite maximum TE$_{21}$ mode of (a): set 1, and (b): set 2. Arrows indicate the mutual directions the currents must have to add constructively to the TE$_{21}$ modes. Blue arrows indicate electric current. The incident TE$_{11}$ modes from which the currents need to be excited are indicated with black arrows.

Another class of mode converters are based on *stubs*, rectangular waveguide attached perpendicular to the guide wall. The first of these was presented by Watson et al. [8] in which sliders could tune the depth of the stubs. A similar concept is that of grooves placed at a step in the radius of the waveguide like in [20, 21]. In fact there are also examples of TE$_{21}$ and TE$_{01}$ mode converters where the circular waveguide is fed directly from rectangular waveguides around the circular waveguide wall [81–83], but not for matched feed applications.

For conceptual understanding, we shall again start by disregarding the excitation of the stubs and assume a rectangular waveguide fundamental mode in their apertures. For simplicity we model this as a magnetic current element along the length of the opening (transverse to the electric field lines) — see Figures 4.2(b) and 4.2(c). Let us first consider a z-directed magnetic current corresponding to stubs like the ones in [8]:

$$\mathbf{J}_m = \hat{z} I_0 \delta(\mathbf{R} - \mathbf{R}'), \tag{4.8}$$

where the current is placed at the waveguide wall, $\rho = a$. Inserting into Equa-

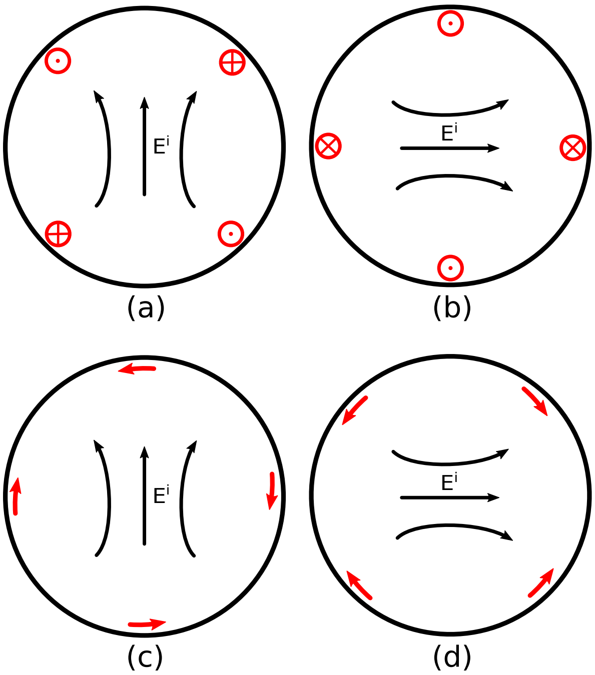

(a) (b)

(c) (d)

Figure 4.4: Azimuthal positions of magnetic currents to excite maximum TE_{21} mode of (a) and (c): set 1, (b) and (d) : set 2. Arrows indicate the mutual directions the currents must have to add constructively to the TE_{21} modes. Red arrows indicate magnetic current. The incident TE_{11} mode from which the currents need to be excited in each case is indicated with black arrows.

tion (4.3), we obtain coupling coefficients to TE and TM modes as follows

$$V_{mn}^{\mathrm{TE}} \propto \begin{matrix}\sin\\ \cos\end{matrix}\; m\phi' \tag{4.9}$$

$$V_{mn}^{\mathrm{TM}} = 0. \tag{4.10}$$

Note that a z-directed magnetic current does not couple to the TM modes, because the z-directed H-fields are zero. The positions of maximum coupling to the TE modes are 90° shifted compared to the case with radial electric currents (Equation (4.5)).

We can also consider a stub which has the leading dimension in the azimuthal direction, thus giving rise to a ϕ-directed magnetic current:

$$\mathbf{J}_m = \hat{\boldsymbol{\phi}} I_0 \delta(\mathbf{R} - \mathbf{R}'). \tag{4.11}$$

Again inserting into Equation (4.3), the coupling coefficients to the waveguide modes from a ϕ-directed magnetic current element is obtained:

$$V_{mn}^{\mathrm{TE}} \propto \mp m \begin{matrix}\cos\\ \sin\end{matrix}\; m\phi' \tag{4.12}$$

$$V_{mn}^{\mathrm{TM}} \propto \begin{matrix}\cos\\ \sin\end{matrix}\; m\phi'. \tag{4.13}$$

The positions exciting a maximum of $\mathrm{TE}_{21}^{1/2}$ are shown in Figure 4.4 for both z- and ϕ-directed magnetic currents. The incident electric field lines of the TE_{11} mode which we wish to couple from are also shown.

4.4 Excitation of Currents by Incident Mode

Next task is to relate the incident field, and the type and position of waveguide inclusions to the generated currents, electric and magnetic. A rigorous implementation of this would require an integral equation formulation. Here, we shall use a simpler formulation based on the perturbation principle. Namely that the incident mode will directly induce a current in the inclusion without itself being perturbed.

An inclusion is represented by a dipole, electric or magnetic. The dipole is oriented in the direction given by the unit vector, $\hat{\boldsymbol{c}}$. The currents are then determined from the incident fields, $\mathbf{E}^{\text{inc}}$ and $\mathbf{H}^{\text{inc}}$ as

$$\mathbf{J} = \alpha_e(\mathbf{E}^{\text{inc}} \cdot \hat{\boldsymbol{c}})\hat{\boldsymbol{c}} \tag{4.14a}$$

$$\mathbf{M} = \alpha_m(\mathbf{H}^{\text{inc}} \cdot \hat{\boldsymbol{c}})\hat{\boldsymbol{c}}, \tag{4.14b}$$

where α_e and α_m are the electric and magnetic polarizabilities, respectively[1]. The polarizabilities are unknown quantities which depend on the inclusion shape and the frequency. Even without knowing the specific polarizability, useful knowledge can be gained from the remaining part of (4.14): the incident field projected onto the inclusion determines the sign and magnitude of the excited current.

In a more general case, we could have included polarizabilities linking electric field and *magnetic* current and vice versa and/or dyadic polarizabilities (coupling fields to differently oriented currents), but the scalar polarizabilities work well with the simple inclusions treated here.

4.5 Validation by Simulation

In order to confirm the analysis of Section 4.3 and 4.4, we perform a series of simulation experiments. A piece of waveguide which supports higher order modes is excited at one end with the fundamental mode. Midway on the waveguide we insert an asymmetrical component in the form of a radial pin, a longitudinal stub, or an azimuthal stub. The configurations are the ones shown in Figure 4.2. We proceed to find the coupling from the fundamental modes to the higher order modes at the output for different ϕ-positions of the asymmetrical component. The simulation is carried out with the full wave method of moments (MoM) solver of GRASP [30].

Equations (4.3) and (4.14) are used to compute the same coupling quantities. The absolute polarizabilities of the inclusions are not known. Therefore, the analytical results are scaled by a constant complex factor to bring them to the level of the MoM results, but it is the same number for all modes and for all ϕ-positions. The comparisons between the analytical model and MoM are shown in Figures 4.5, 4.6, and 4.7 for longitudinal stubs, radial pins, and azimuthal stubs, respectively. The full lines are calculated with the analytical model and the stars of the same color are MoM simulations.

The correspondence between the simple analytical model and full wave simulations is excellent considering how crude the model appears. The case of the longitudinal stub shows especially good correspondence. Note that the phase relationship between modes as well as amplitude is well captured[2].

From these figures, it is easy to devise mode launchers with several inclusions around the circumference, which couple to desired modes and in which contributions to unwanted modes cancel out. The simple two- or three-inclusion mode launchers in the literature may be understood by manual inspection of the curves. More advanced mode launchers may be derived from the same theory by automatic methods, as will be demonstrated in the next chapter.

---

[1] Polarizabilities are often used as the ratio between dipole moment and field, and not as here, current and field. The difference is merely a time derivative.

[2] Different phase delays of the modes travelling in the length of waveguide after the inclusion are taken into account in the analytical model.

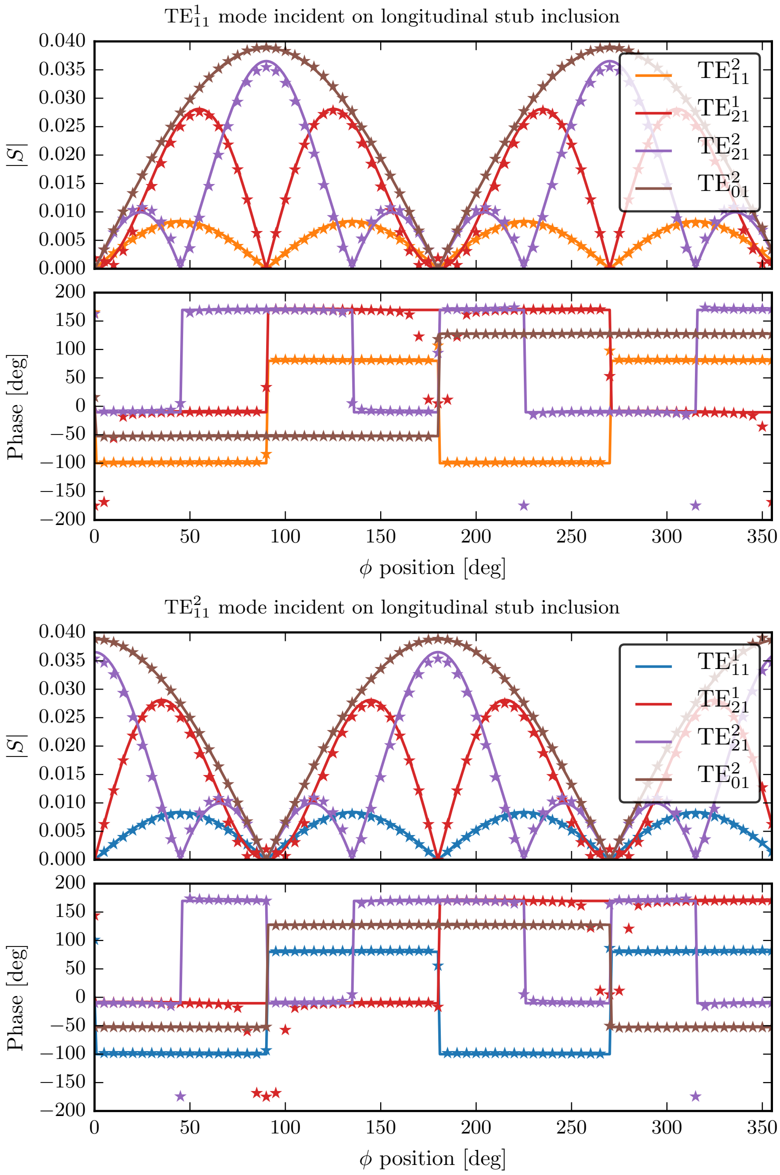

Figure 4.5: Mode generation from a longitudinal stub as function of stub ϕ-position around the waveguide wall. The incident mode is the TE_{11} mode of set 1 (top) and set 2 (bottom). Full lines are the analytical model and stars are from MoM simulations in GRASP.

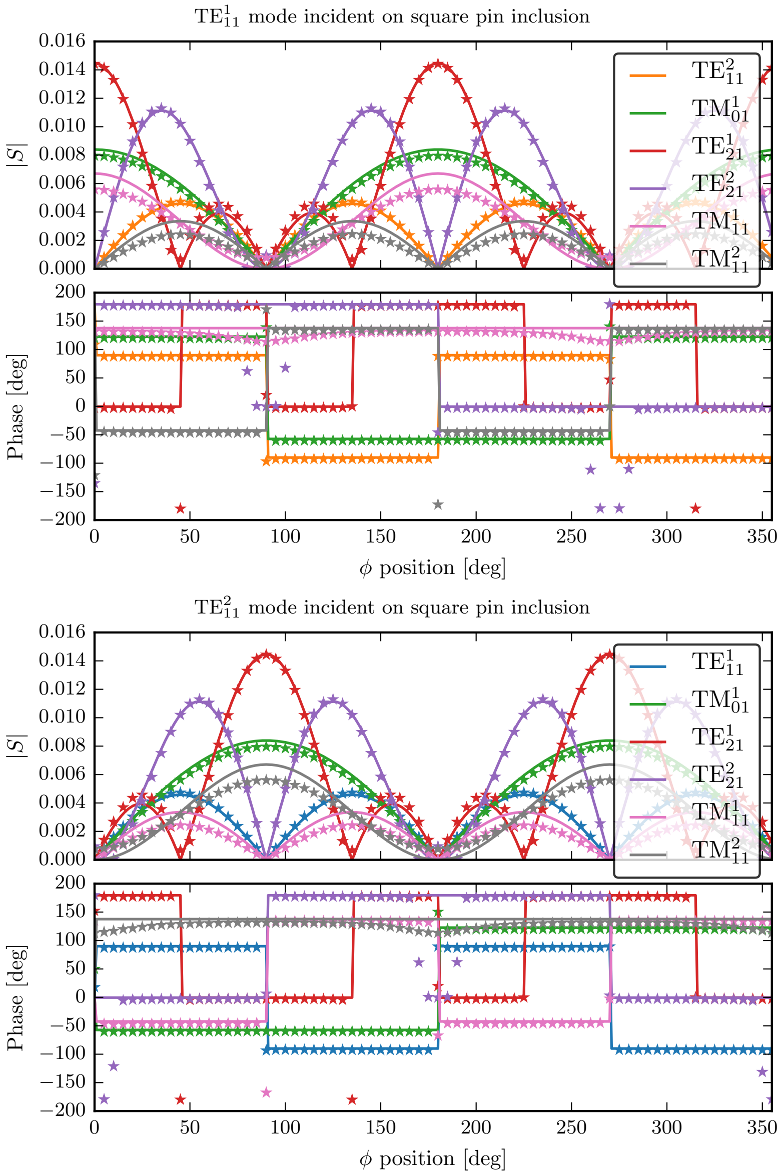

Figure 4.6: Mode generation from radial pin as function of pin ϕ-position around the waveguide wall. The incident mode is the TE$_{11}$ mode of set 1 (top) and set 2 (bottom). Full lines are the analytical model and stars are from MoM simulations in GRASP.

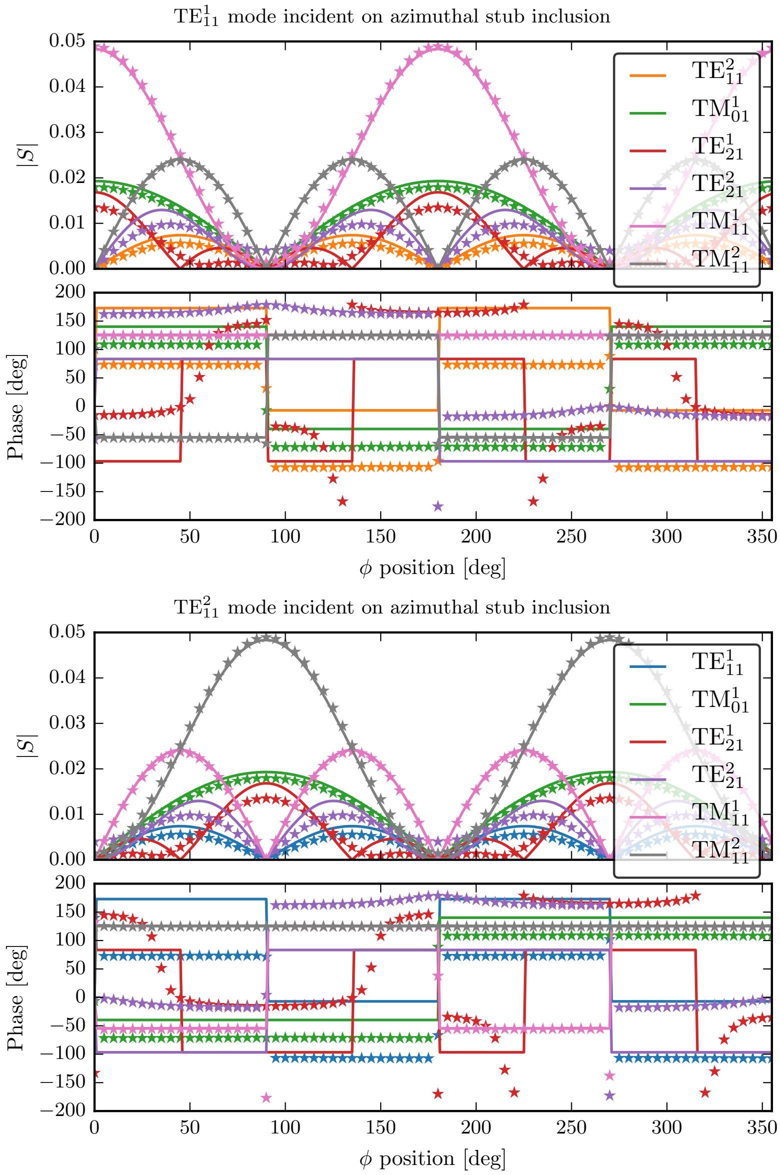

Figure 4.7: Mode generation from azimuthal stub as function of stub ϕ-position around the waveguide wall. The incident mode is the TE_{11} mode of set 1 (top) and set 2 (bottom). Full lines are the analytical model and stars are from MoM simulations in GRASP.

4.6 Frequency Characteristics of Mode Launchers

As mentioned in Section 4.4, the polarizability of the waveguide inclusions depend on frequency, thus making the mode launcher frequency dependent. In this section we shall examine the frequency dependence of an example mode launcher from the previous sections.

Consider the simplest possible mode launcher, namely a waveguide with one or more of the inclusions shown in Figure 4.2. This specific design has not been used in the literature, since the generated modes can, and will, propagate in both directions away from the inclusion. Therefore the asymmetric inclusions are often placed in conjunction with a step in waveguide radius which allows higher order modes to propagate only after the step (See e.g. [6]). The following observations also apply to this kind of mode launchers.

The simulations here are made with a waveguide of radius $a = 6.3\,\text{mm}$. Cutoff frequencies for the first seven modes of this waveguide are listed in Table 4.1.

TE_{11}	TM_{01}	TE_{21}	TE_{01}	TM_{11}	TE_{31}	TM_{21}
13.94	18.21	23.13	29.02	29.02	31.82	38.89

Table 4.1: Cutoff frequency in GHz of waveguide modes in a circular waveguide of radius $a = 6.3\,\text{mm}$

Figure 4.8(a) shows frequency dependent generation of several modes when a radial pin is placed at $\phi = 90°$ and illuminated by the TE_{11}^2 mode. From Figure 4.6 we know that illumination with TE_{11}^1 (first set) would not have excited any modes, because the incident ρ-directed field is zero at $\phi = 90°$. TE_{21}^1 output rises to a peak when it hits the cutoff frequency at around 23 GHz. At approximately 32 GHz there is another large peak in mode generation corresponding to the cutoff frequency of the TE_{31} mode. The softer peak around 37 GHz corresponds to the resonance of the pin.

The same configuration as just described, but with a longitudinal stub instead of a pin, can be seen in Figure 4.8(b). Similar behaviour as that of the pin is observed, but other modes are excited. TM modes do not get excited by longitudinal magnetic currents, but on the other hand, the TE_{01} gets excited here. Again, the last peak in all three curves results from a resonance of the stub.

It is clear that when a mode hits cutoff, it wildly disturbs the excitation of the other modes. It is critical that this issue is properly handled in a matched feed design. Unwanted modes must either be kept below cutoff, or their excitation should be heavily suppressed. The latter approach shall be demonstrated in connection with the coaxial coupler design in Section 5.2, where the cutoff of the coaxial TE_{31} mode is within the design band.

4.7 Summary

This chapter provides a framework for understanding and designing mode converters for matched feeds. Though all the concepts are well known, the presentation of them in this context has been missing in the literature. Despite the simplicity of the models, excellent agreement with full wave simulations is demonstrated.

Lastly, the frequency responses of selected mode launchers are examined substantiating the conclusions on the bandwidth limitations of matched feeds given in Section 2.5.

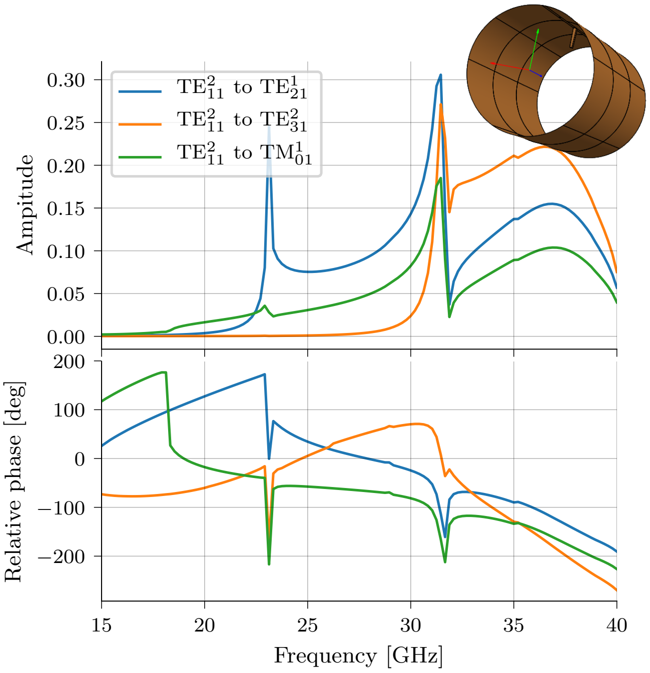

(a) radial pin at $\phi = 90°$

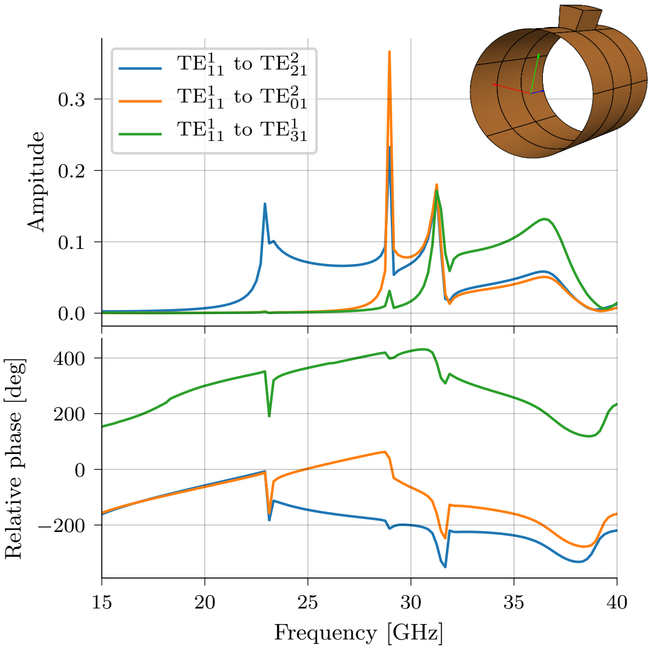

(b) longitudinal stub at $\phi = 90°$

Figure 4.8: Selected scattering parameters of a piece of waveguide with a) a radial pin and b) a longitudinal stub. The radius of the waveguide is 6.3 mm, cutoff frequencies listed in Table 4.1. The pin is 1.8 mm long. The stub is 6.5 mm long, 2 mm deep, and 10° wide.

CHAPTER 5

Directional Waveguide Couplers for Matched Feeds

As discussed in Section 2.5, our main challenges with regard to widening the bandwidth of matched feeds are

1. phase dispersion due to unequal cutoff frequencies of modes,
2. resonances of the pin, slot, or other inclusion of the mode launcher.

If the first problem can be fixed, we can also fix the second problem. The reason is that if the phase velocity of the generated mode is close to that of the incident mode, we can allow the coupling to take place at several points along the guide, thus avoiding the need for large resonant inclusions. This is the technique used in waveguide directional couplers.

In this chapter a fix to the cutoff problem, inspired by Pour and Shafai [22], is presented. The compensating TE_{21} mode is coupled to a coaxial waveguide surrounding the circular one. The cutoff nature of the coaxial and circular guides allows the dimensions to be tuned such that the TE_{21} mode in the coaxial section has the same cutoff frequency as the TE_{11} mode in the circular section. The phase dispersion can thus be eliminated at the cost of separating the two modes. The implementation is inspired by Choung et al. [84, 85], where selected higher order modes in a circular waveguide are coupled to rectangular waveguides.

The synthesis procedure for a specialized directional coupler will be presented in this chapter. The coupler is able to couple a specified fraction of the incident TE_{11} modes in a circular waveguide to specific TE_{21} modes in a coaxial guide, effectively suppressing unwanted couplings. This design procedure is documented in publication [P4].

The higher order modes generated by the coupler are intended for a matched feed horn — but it is not as simple as Plug-and-Play. Difficulties arise from the extended length of the coupler when the modes need to be radiated. These challenges will be discussed and an example matched feed design demonstrated.

5.1 Discrete Directional Couplers

Coupling between two transmission lines at discrete points is quite simple and is briefly derived in [P4]. This method disregards more complex mutual interactions

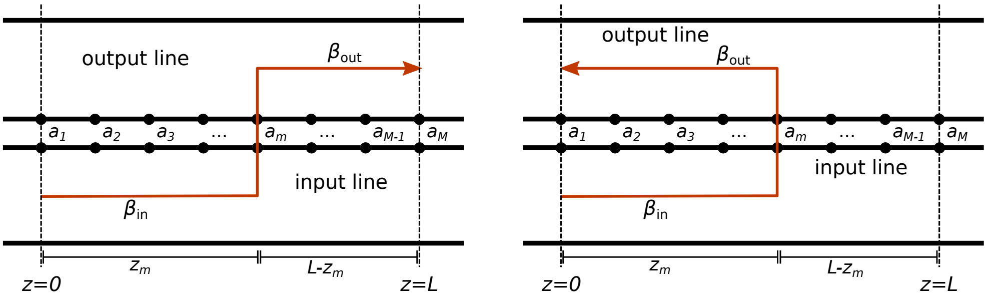

(a) Forward coupling (b) Backward coupling

Figure 5.1: Coupling between two transmission lines at discrete coupling points. The two lines can represent two waveguides or two modes in the same waveguide. β_{in} and β_{out} are the phase constants of the input and output mode, respectively. $a_1, a_2, \ldots, a_M$ are coupling coefficients at M evenly spaced coupling points. L is the length of the coupler and z_m is the z-position of the mth coupling point.

between primary and coupled transmission lines, but is effective in our case because only a fraction of the incident field needs to be coupled. The characteristics of the coupler are completely described from the length of the coupling section, phase velocities of the transmission lines, and the discrete coupling coefficients. The concept is illustrated in Figure 5.1 for forward and backward coupled waves. Refer to [86] for a detailed description — here just the result is shown for forward and backward coupling, respectively:

$$I_f = e^{-j\beta_{\text{out}}L} \sum_{m=1}^{M} a_m e^{-jz_m(\beta_{in}-\beta_{\text{out}})} \tag{5.1}$$

$$I_b = \sum_{m=1}^{M} a_m e^{-jz_m(\beta_{\text{in}}+\beta_{\text{out}})}. \tag{5.2}$$

Quantities are defined in Figure 5.1. Note that both the backward and forward coupled waves can be evaluated from the function

$$F(\theta) = \sum_{m=1}^{M} a_m e^{-jz_m\theta}, \tag{5.3}$$

if $\theta = \beta_{\text{in}} - \beta_{\text{out}}$ for forward coupling, and $\theta = \beta_{\text{in}} + \beta_{\text{out}}$ for backward coupling[1]. $F(\theta)$ is a Fourier transform of the coupling distribution in the spectral variable θ, transforming the coupling coefficients to the θ-*domain*.

The phase velocities, β_{in} and β_{out}, are those of the waveguide modes which are coupled from and to, respectively. For metallic waveguides, they are calculated from the cutoff wavenumber, k_c, as

$$\beta = \sqrt{k^2 - k_c^2}, \tag{5.4}$$

and thus, they vary with frequency.

---

[1] This is a slightly different definition of θ than the one in [86].

5.1.1 Relative Phase

Relative phase is of great importance in multimode feed design. The phase difference between the input mode and the coupled mode as they leave the coupler are dependent on the length of the coupler and the difference in propagation constant. If the coupling coefficients have a phase different from zero, this will naturally induce an additional phase shift.

The difference due to propagation constants can be derived as follows. We will assume that the coupling coefficients have the same phase, $\angle a$. The input mode has a simple phase delay through the coupler:

$$I_{f_{\text{in}}} \propto e^{-j\beta_{\text{in}} L}. \tag{5.5}$$

The output mode is given by

$$I_f = e^{-j\beta_{\text{out}} L} \sum_{m=1}^{M} a_m e^{-jx_m \theta}, \tag{5.6}$$

where $\theta = \beta_{\text{in}} - \beta_{\text{out}}$. Assuming symmetric filter coefficients, the summation part can be shown to have the phase:

$$\angle \sum_{m=1}^{M} a_m e^{-jx_m \theta} = -\frac{\theta}{2} L + \angle a. \tag{5.7}$$

Evaluating the total phase difference between the output mode and the input mode propagated to the end of the coupler results in

$$\begin{aligned} \Delta\phi &= \angle I_f - \angle I_{f_{\text{in}}} \\ &= \left(-\beta_{\text{out}} L - \frac{\theta}{2} L + \angle a \right) - (-\beta_{\text{in}} L) \\ &= \angle a + \frac{L}{2}\theta. \end{aligned} \tag{5.8}$$

Thus, the phase drift is half of the phase drift of the two modes just propagating for the length L. The factor of one half is only valid for symmetric coupling distributions. Keeping coupling structures (holes, pins, slots) small compared to the wavelength will result in coupling coefficients that are purely reactive: i.e. $\angle a$ close to ±90° as desired.

5.2 Coaxial Coupler Design

Most of the contents of this section is presented in [P4] and concerns the design of the coupler itself. The device is in a sense designed like any other directional coupler, but many special challenges have to be taken into account for this specialized application.

5.2.1 Optimal Coupling Coefficients

The coupler is first designed on a conceptual level, where the coupling coefficients a_m are sought before we decide how to implement them. The dimensions have first to be defined such that we know the cutoff frequency of input and output modes as well as undesired modes.

We take advantage of the fact that there exists a discrete Fourier mapping between the coefficients and the coupling at specific θ values as a consequence of Equation (5.3). This makes the choice of coupling coefficients precisely equivalent to the design of a finite impulse response filter (FIR) on a discrete signal. The equivalent of the theta domain is the frequency response of the FIR filter. We just need to set up the requirements for the design in the θ-domain, and methods for FIR filter design can be used to find the desired coupling coefficients. The procedure is illustrated by an example given below. Physical synthesis of the coupling coefficients will be treated in Section 5.2.3.

Example Design

An example design is summarized in Figure 5.2 for a coaxial coupler to be working in the full K_u band. The table contains the information relevant for coupler design: length of coupler, number of holes, and cutoff frequencies of desired and undesired modes. This information is used to evaluate the θ-values for the modes in question over the band of interest in Figure 5.2(b). Pass- and stopbands are defined as the theta ranges we want to enhance and suppress, respectively.

The stopband and passband are used together with the length and number of holes to find an optimal discrete coupling distribution. The length and number of holes translate to the sampling frequency and filter length in FIR filter design. The coupling of the desired mode in this case is 0.13 corresponding to $-18\,\mathrm{dB}$ in a θ-range close to zero. The coupling in θ-ranges of the undesired modes should ideally be zero. An algorithm which finds coupling coefficients that minimize the maximum deviation from these goals is described in [87, 88] and implemented as a part of SciPy [89].

Figures 5.2(c) and 5.2(d) show the coefficients and θ-response of the resulting coupler, respectively. The stop- and passbands are indicated in the θ-response. As an additional design parameter, the cutoff of the coaxial TE_{31} mode is positioned in a null of the coupler by tuning the length. This technique is employed to counteract the general effect that modes couple strongly around the frequency of their cutoff as illustrated in Section 4.6.

5.2.2 Azimuthal Hole Distribution for Unwanted Mode Discrimination

Now that the desired amount of coupling at discrete z-positions has been determined, we must find out how to most effectively transfer this energy from the input to output modes. Many directional couplers work by simply drilling a hole of a specific size at each coupling point. The same approach shall be taken here — however, single holes are out of the question. The reason is that we do not have the luxury of single mode propagation in either waveguide. By the coupler design given above, we can suppress the TE_{31} mode as well as backward travelling TE_{21} modes because they result in different θ-values than the desired couplings. The two unwanted TE_{21} couplings, however, result in the same θ values as the desired ones. The hole distribution must therefore be designed to suppress unwanted TE_{21} coupling.

The azimuthal placement of waveguide inclusions can be analysed by the mode coupling theory presented in Sections 4.3 and 4.4. In Chapter 4, the inclusions were pins or stubs in a single waveguide: a dipole is excited in the inclusion which then radiates in the form of waveguide modes. The same principle applies for a hole coupling between two distinct waveguides: dipoles are excited in the hole which then radiate modes in both waveguides.

Though determining the exact coupling caused by a hole is not trivial [90–92], the variation with azimuthal position and the inter-mode relationships are in excellent agreement with the simple model as verified in Section 4.5. This variation between the input and output modes reduces to a simple product between two sinusoidal

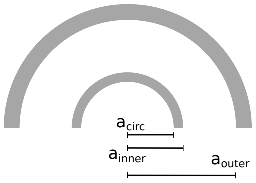

a_{circ}	11.0 mm
a_{inner}	11.1 mm
a_{outer}	13.6 mm
Coupler length	96 mm
N° coupling points	23
Circ TE_{11} cutoff	8.0 GHz
Coax TE_{21} cutoff	7.7 GHz
Coax TE_{31} cutoff	11.6 GHz
Circ TE_{21} cutoff	13.2 GHz

(a) Dimensions

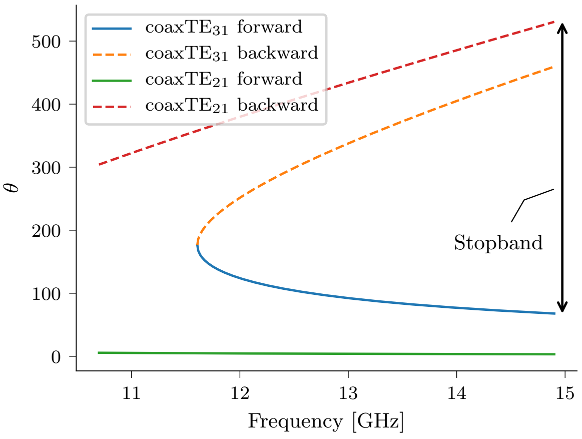

(b) θ-domain mapping

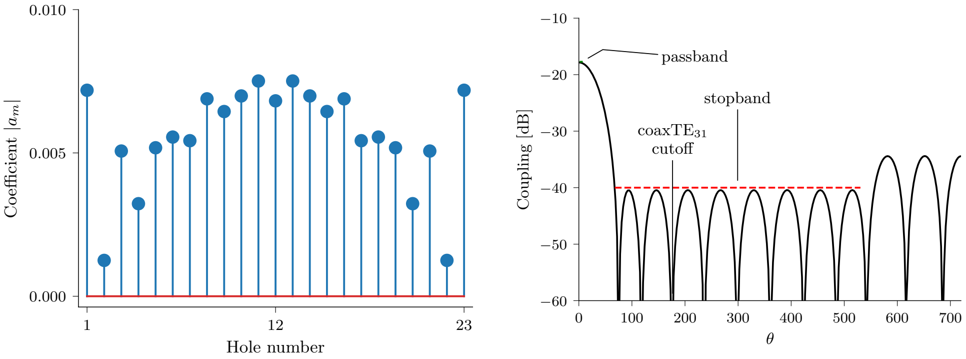

(c) Coupling coefficients

(d) θ-domain response

Figure 5.2: Design of directional coupler based on wanted and unwanted mode cutoffs (a). Phase constants are mapped to the θ-domain (b) and optimal filter coefficients are found (c). The resulting response of the coupler is shown in (d).

functions in the azimuthal variable ϕ. A summary of desired and undesired mode couplings for the coaxial coupler is given in Table 5.1.

Very few of the matched feed designs in the literature are designed for dual polarization. The ones that are [8, 20, 21] employ the azimuthal distribution of inclusions 45°, 90°, and 135°. Figure 5.3(a) illustrates how this distribution of holes/stubs/pins excites desired modes in the correct phase, but none of the undesired TE_{21} modes. Note that the desired couplings do not have equal strength, one is 40 % higher, meaning almost twice the power. This is a significant drawback, since the optimal amount of TE_{21} mode is approximately the same for both polarizations (see Figure 3.1 in Section 3.2.3). It can be analytically derived that moving the two outer inclusions to 50° and 130° instead, will equalize the coupling. Figure 5.3(b) illustrates these slightly enhanced inclusion positions and shows that the coupling to desired TE_{21} modes is now the same and unwanted modes still cancel out.

Both of the above three-inclusion configurations couple significantly to one of the TE_{31} modes. Though the TE_{31} couplings are also suppressed by the longitudinal distribution of the coupler, their behaviour at cutoff (Section 4.6) makes it advantageous to suppress them as much as possible.

Coupling	ϕ-dependence
Desired	
$\mathrm{TE}_{11}^{1} \rightarrow \mathrm{TE}_{21}^{2}$	$\cos\phi\sin 2\phi$
$\mathrm{TE}_{11}^{2} \rightarrow -\mathrm{TE}_{21}^{1}$	$-\sin\phi\cos 2\phi$
Undesired	
$\mathrm{TE}_{11}^{1} \rightarrow \mathrm{TE}_{21}^{1}$	$\cos\phi\cos 2\phi$
$\mathrm{TE}_{11}^{2} \rightarrow \mathrm{TE}_{21}^{2}$	$\sin\phi\sin 2\phi$
$\mathrm{TE}_{11}^{x} \rightarrow \mathrm{TE}_{31}^{x}$	$\cos\phi\cos 3\phi$
	$\cos\phi\sin 3\phi$
	$\sin\phi\sin 3\phi$
	$\sin\phi\cos 3\phi$

Table 5.1: Summary of desired and undesired mode couplings.

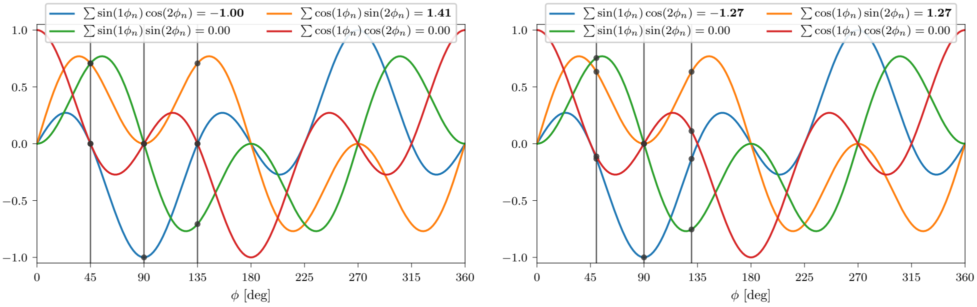

(a) inclusions at 45°, 90°, and 135°

(b) inclusions at 50°, 90°, and 130°

Figure 5.3: TE_{11} to TE_{21} mode coupling in circular or coaxial waveguide geometries. Each line represents the coupling from one of the input mode polarizations to an output mode. Each inclusion is represented by a vertical line and can contribute coupling to several modes (dots). The total coupling of the input-output mode pairs is summed and shown in the legend.

When more than the four couplings in Figure 5.3 need to be analyzed, it becomes too cumbersome to do by hand, especially as the number of holes is increased. Therefore, the determination of azimuthal inclusion placement is optimized in a more systematic manner. The ratio of undesired to desired modes in Table 5.1 is minimized by a numerical optimization routine (fminimax of Matlab in this case). Constraints are given to the optimization to ensure that the inclusions are spaced a certain minimum distance from each other, and that the strength of the two desired coupling are the same.

The optimal result will vary depending on how constraints and weighting between objectives are chosen. The azimuthal distribution used in designs presented in this thesis, is illustrated in Figure 5.4. The strength of desired couplings is almost equal and has been increased from 1.3 to 2.1. TE_{31} couplings are suppressed at the expense of a small amount of undesired TE_{21} modes. The hole positions are also indicated in orange on the cross section illustration in Figure 5.5.

This method of optimizing azimuthal placement of inclusions based on the theory in Chapter 4 is not only applicable to the coaxial coupler. It is also not limited to circularly symmetric waveguide structures, as the field configurations can be replaced by those of any waveguide shape.

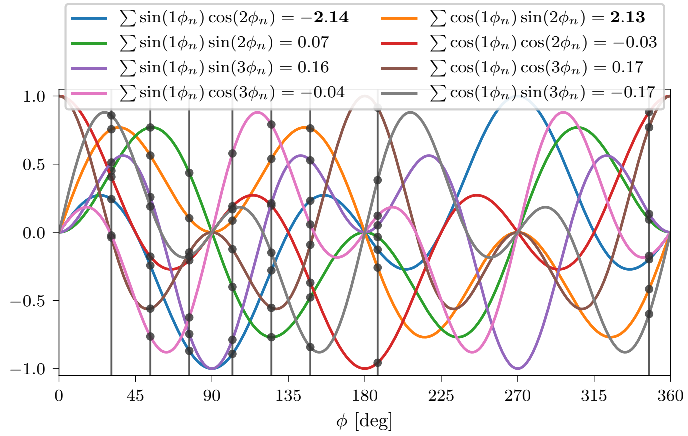

Figure 5.4: TE_{11} to TE_{21} and TE_{31} mode coupling in circular or coaxial waveguide geometries. Each line represents the coupling from one of the input mode polarizations to an output mode. Each inclusion is represented by a vertical line and can contribute coupling to several modes (dots). The total coupling of the input-output mode pairs is summed and shown in the legend.

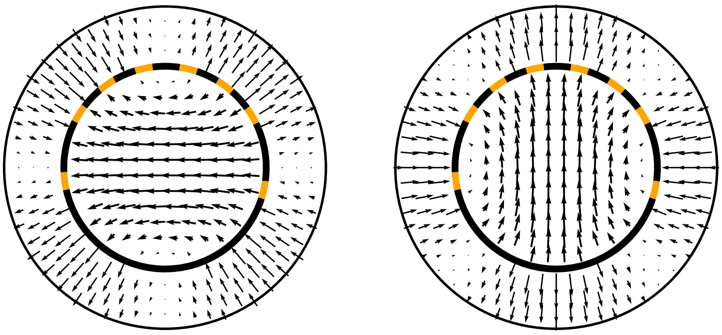

(a) (b)

Figure 5.5: Modal E-fields of the incident circular and desired coaxial modes for the two polarizations: (a) TE_{11}^1 to TE_{21}^2 and (b) TE_{11}^2 to TE_{21}^1. The azimuthal positions of the coupling holes are indicated in orange: $\phi = \{30.9°, 53.8°, 76.7°, 102.1°, 125.0°, 147.9°, 187.6°, 347.4°\}$.

5.2.3 Hole Shape and Coefficient-to-Size Mapping

The frequency dependence of the coupling is dependent on the shape of the hole in the waveguides. A hole with the leading dimension in the z-direction, a longitudinal hole, will exhibit decreasing coupling with increasing frequency. This is because the z-directed magnetic field of the input and coupled modes decreases in magnitude with increasing frequency, as with any TE mode. The opposite applies for ϕ-oriented, transverse holes, whose coupling *increases* with increasing frequency. Riblet and Saad [93] demonstrate that the frequency dependence can be stabilized by placing one longitudinal and one transverse hole at each z position. In the designs presented here, we have chosen to use square holes, which essentially accomplishes the same thing with a single hole, providing very stable coupling as a function of frequency. The concept may be further enhanced by letting the length to width ratio of each hole be slightly dependent on the hole size.

The coupling coefficients determined in Section 5.2.1 must be translated into actual hole sizes. The task is achieved by carrying out a few simulations with just a single slice of the coupler. This slice has the holes distributed around the circumference of the circular guide as detailed in the previous section. The method is described in [P4] and will not be further elaborated on here. However, the coefficient-to-hole mapping corresponding to the waveguide dimensions of the example design listed in Figure 5.2(a) with the azimuthal hole distribution of Figures 5.4 and 5.5 is given in Figure 5.6.

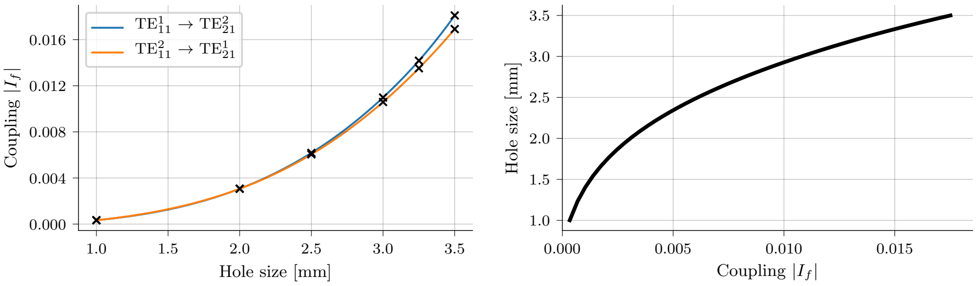

(a) (b)

Figure 5.6: Coupling of desired modes in a single coaxial slice with the azimuthal hole distribution shown in Figure 5.5. The waveguide dimensions are listed in Figure 5.2(a). (a) Shows the relationship between hole size and coupling values. The markers show simulated hole sizes and cubic splines interpolate between. The coupling value for each size is an average over the design frequency band. (b) Shows the inverse of the average of the two curves in (a).

5.3 Performance Evaluation of Coaxial Couplers

The coupler design outlined in Figure 5.2 is just a list of 23 (12 unique) coupling coefficients and a length specification. By the very simple mapping procedure described in [P4], the coefficients are translated to specific hole sizes arranged in z according to the coupler design and in azimuth according to the procedure described in Section 5.2.2. Nothing more is required to define the geometry of the coupler. Obviously some initial design decisions are made regarding dimensions of the coaxial geometry, which mostly concerns the cutoff frequencies of different modes in the two regions.

Now let the coupler design in Figure 5.2 be translated to an actual geometry by using the mapping in Figure 5.6(b). A electromagnetic model (mesh) of the geometry is assembled (shown on the right in Figure 5.7). The coupler is a waveguide device with four ports: a circular and a coaxial waveguide port at each end. The field entering and leaving each port is expanded in a number of waveguide modes. The generalized scattering parameters describe how outgoing power is divided between all modes on all ports when power enters on a specific port and mode.

Several scattering parameters of the simulated coupler are shown in Figure 5.7 as a function of frequency. The plotted scattering parameters — or couplings — are the ones resulting from excitation of the TE$^1_{11}$ and TE$^2_{11}$ modes on one of the circular ports, e.g. coming from an orthomode transducer. The desired couplings are close to the design value of −18 dB and all undesired couplings are suppressed below −40 dB. The phase of the two desired couplings relative to the phase of TE$_{11}$ straight through the circular section is also shown with the expected result from Equation (5.8) as reference.

It is uncanny how well this design procedure works — no parameters have been tuned after the full model is assembled and simulated. The azimuthal hole distribution alone is responsible for the near identical desired TE$_{21}$ couplings as well as suppression the undesired ones below −48 dB in the whole band. The simple coupling to size mapping effectively achieves the correct coupling value. Even the phase is as predicted by the simple theory. Each of the coupling holes radiate modes forwards and backwards in both waveguides, but by virtue of the suppression achieved in the θ-domain, the contributions cancel out except for the desired modes in the forward direction. Note that the lobes in the undesired couplings are direct consequences of the lobes in the discrete Fourier transform of the coupling coefficients shown in Figure 5.2(d), i.e. the θ-domain.

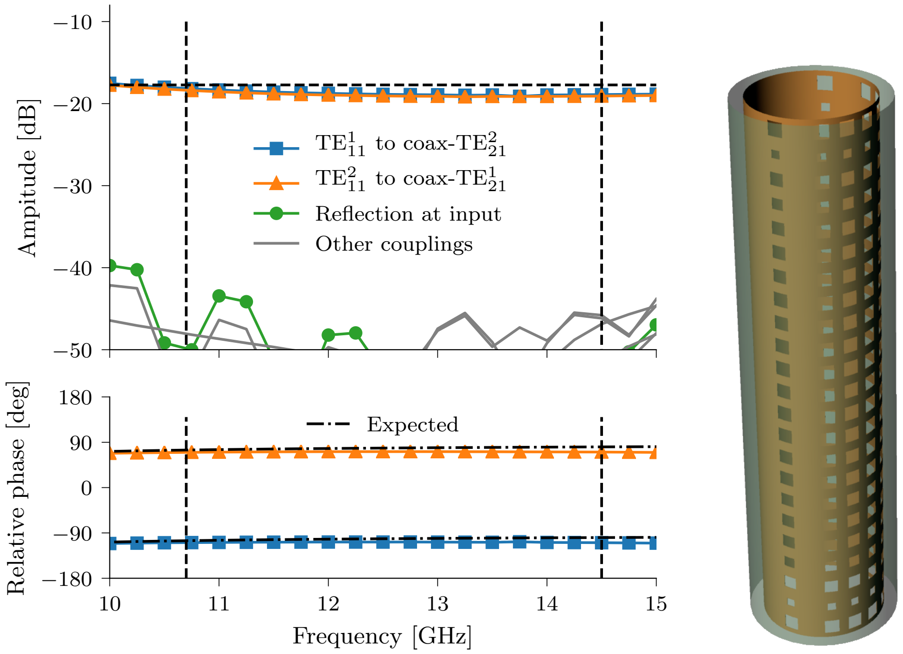

Figure 5.7: Coupling from the two input modes in the circular waveguide to several modes in the coaxial guide. The two desired couplings are colored as well as the most critical undesired coupling: the maximum reflection at the input circular port. The horizontal dashed line in the amplitude plot indicates the desired coupling level −18 dB. Vertical dashed lines delimit the frequency range of interest. The phases of desired modes are plotted relative to the phase of TE$_{11}$ propagation through the circular waveguide (bottom). A CAD model of the coupler is shown on the right.

5.3.1 Validation of the Solver

In an effort to validate the results presented here, one of the coupler designs has been simulated with another commercial solver. The coupler geometry is the one presented in [P4], and not the same as the one just discussed. The alternative simulation is carried out in HFSS [94] by transferring the geometry via CAD file export/import. A comparison of selected scattering parameters computed with the two softwares is given in Figure 5.8. Desired couplings are nearly indistinguishable between the two calculations. Even for undesired coupling lower than $-50\,\mathrm{dB}$, the two methods agree. The solution methods used in the two softwares are very different and the agreement shown here is a testament to the reliability of both.

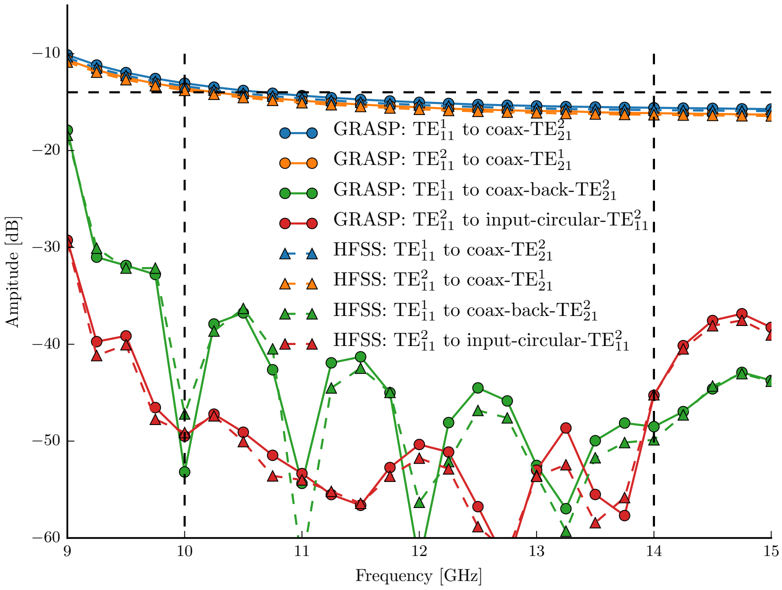

Figure 5.8: Computed scattering parameters compared with HFSS [94]. HFSS uses a volumetric finite element solver as opposed to the surface integral equation solver of GRASP. Markers indicate evaluated frequency points. Results calculated with GRASP are shown with full lines and circular markers, corresponding results calculated with HFSS have the same colors, but are shown with dashed lines and triangular markers.

5.4 Feed Design with Axially Corrugated Horn

The coaxial directional coupler described above successfully generates a prescribed amount of TE_{21} modes from input modes in two polarizations, over a large bandwidth. A fundamental task remains: radiating the modes onto the reflector in suitable manner. Additional modes may also need to be added to compensate the inherent cross polarization of the TE_{11} mode.

The stable amplitude and phase of the coaxial coupler comes at the price of added complexity in this task of radiation. The fact that the fundamental and compensating modes are separated in two distinct regions has turned out to be a significant challenge to overcome. The following accounts for considerations and difficulties with regard to radiating the waveguide modes. Finally, a dual polarized matched feed design is demonstrated, though not in the full operating frequency range of the coupler. These result are not covered by [P4].

5.4.1 Horn Topology

The topology that we are going to use is based on the axially corrugated horn, see e.g. [95]. This kind of feed is widely used in the industry for single beam symmetrical as well as offset reflectors. It can be optimized for very good radiation characteristics, but is simpler and easier to manufacture than the *radially* corrugated horns. As explained in [P1], axially corrugated horns are well suited for matched feeds because they are short and have a wide flare — see also Section 2.5 on modal phase dispersion. The motivation for adding a horn section to the coupler is to raise the directivity of the antenna, minimize reflection, and minimize cross polarization arising from $m = 1$ modes.

To accommodate the coaxial coupler, we let the first axial corrugation of the horn be very deep. The holes of the coupler perforate the wall between this corrugation and the input waveguide. The configuration is illustrated in Figure 5.9. Holes in the inner waveguide may be etched on a thin sheet of metal before it is rolled into a cylinder.

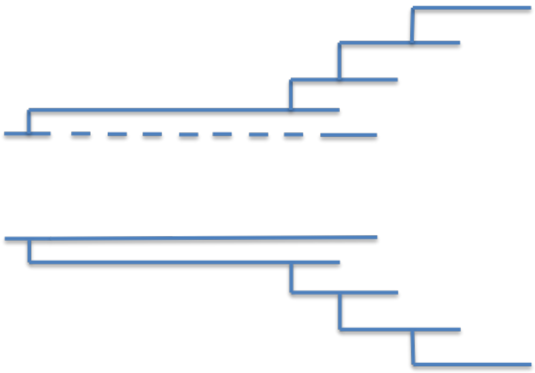

Figure 5.9: Geometry of the axially corrugated horn assembled with the coaxial coupler. The first corrugation of the horn accommodates the coupler.

5.4.2 Requirements

The requirements to the feed depend on the geometry of the reflector configuration. The main parameter is the beamwidth, which should be narrow enough to avoid excessive spillover and wide enough to allow a decent reflector aperture efficiency. Obviously, the total reflector system should radiate less cross polarization than if it was illuminated by a conventional feed.

The feed is initially analyzed *without* the coaxial coupler, where an unperforated section is inserted in its place. Without the coupler, the whole feed structure is circularly symmetric, and can thus be analyzed using Mode Matching or Body of Revolution MoM (BoR MoM), depending on the exact geometry. These methods *drastically* reduce computation time compared to general 3D methods, and are thus well suited for optimization. Intermediate goals are defined which serve to estimate the desired properties of the final feed.

Other than beamwidth and return loss, the circular symmetric feed is optimized for two objectives: 1) Low cross polarization and 2) small reflection into the coaxial guide. The first objective is added because cross polarization can easily arise in the 45° plane from circular symmetric structures. This cross polarization will be transformed to the far field and cannot be compensated by the TE_{21} radiation. The second objective serves to ensure that the TE_{21} modes generated by the coupler can get out of the coaxial waveguide, so they can be radiated by the horn. A transition into another waveguide geometry or free space gives rise to reflections which must be kept low. Otherwise, the TE_{21} modes are reflected back and forth in the coaxial section, destroying the phase relationship with TE_{11} mode in the circular guide.

5.4.3 Reflection From Coaxial Guide

The couplers designed using the above method have a relatively narrow coaxial region. This is a consequence of the aim to match the cutoff frequencies of TE_{11} and TE_{21} in the circular and coaxial guide, respectively. A narrow coaxial waveguide like this is not a good radiator [96, 97]. The blue curve in Figure 5.10 plots the reflection of a coaxial waveguide port excited by the TE_{21} coaxial mode. The dimensions used are the ones from the coupler design in Section 5.3. More than half of the power is reflected back into the coaxial waveguide in the entire band of interest, which is useless in practice.

The reflection can be mitigated by flaring the coaxial waveguide towards the aperture. The orange curve in Figure 5.10 plots the reflection of the same coaxial mode when a simple linear flare is added. Reflection below −10 dB is obtained by optimizing the dimensions of the linear flare[2]. Better results are possible with a more advanced spline flare, but the linear flare illustrates the point well enough.

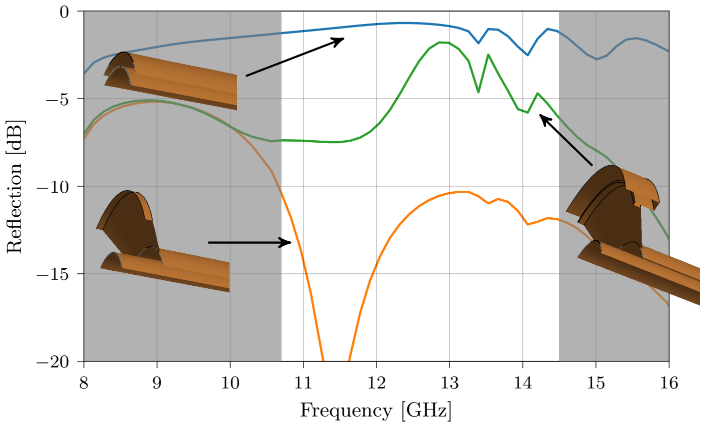

Figure 5.10: Reflections of a coaxial waveguide: with no alterations (blue), with a simple flare (orange), and with a flare and an axial corrugation (green). The inset figures show a quarter of the rotationally symmetric devices. The inner coaxial radius is 11.1 mm and the outer is 13.6 mm. The unshaded area is the frequency interval of interest.

The last curve of Figure 5.10 (green) is the reflection when a typical axial corrugation is added outside the flare. The corrugation severely deteriorates the performance.

---

[2] The resulting dimensions are: a flaring of 10 mm over a length of 5.0 mm followed by a straight section 1.5 mm long.

The reason for this can be regarded as too sharp a transition in the surface impedance seen by the coaxial mode. The same is true in radially corrugated horns, where the transition from smooth to corrugated regions is performed gradually. A common way to do this is to start the corrugations at half a wavelength and decrease to a quarter over a few corrugations, see e.g. [98] or [99, Sec. 3.6][3].

It is possible to optimize the geometry to obtain good reflection characteristics from the coaxial region, while sticking to the axially corrugated horn topology. An example is given in Figure 5.11, where by a combination of smooth flare, steps, and tuning of corrugation depths, a reflection performance around −25 dB is achieved across the entire band. Irises in the coaxial region can also be used as matching elements [96, 100, 101], though since the waveguide is very narrow here, some flaring would be necessary.

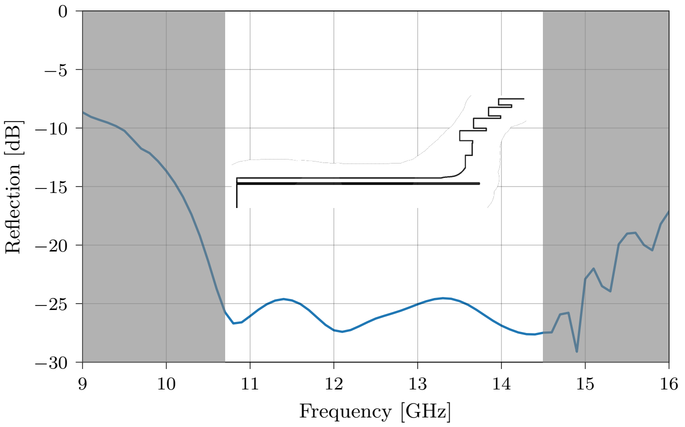

Figure 5.11: Reflection from the coaxial input with an axially corrugated horn. Transition and first corrugations optimized for low reflection. The unshaded area is the frequency interval of interest. The generating curve of the circular symmetric horn is shown in the inset.

5.4.4 Co-Polar Radiation Radiation Characteristics

Let us consider what the efforts to achieve low coaxial reflections did to the co-polar radiation pattern. The optimized geometry shown in Figure 5.11 is now excited from the circular input port instead of the coaxial, and the coaxial guide/corrugation is terminated at the bottom with PEC. The radiation patterns at selected frequencies within the range of interest are plotted in Figure 5.12. Needless to say, these are very unsatisfactory. The cross polarization is high, the patterns are too broad, and exhibit varying dip in the boresight direction.

The variation effect that we observe in the beam, is due to TE_{11} mode being coupled into the long corrugation, reflected at the back, and radiating. The long electrical length of the corrugation results in wildly varying phase of this reflected TE_{11} wave at the aperture. At some frequencies it is approximately in phase with the mode in the circular guide (e.g. 14 GHz) and out of phase at others (e.g. 11.5 GHz). It causes peaks or dips in the boresight direction, respectively. When it is out of phase a peak is formed off-axis due to the displacements of the sources (See Figure 2.6 in Chapter 2). In [22], this difficulty does not arise, since the coaxial region is only a quarter wavelength long and therefore works as a standard choke on the circular waveguide opening.

---

[3] The reason that one does not gradually *increase* the depth of the corrugations, is that the surface would represent an inductive longitudinal surface impedance which gives rise to some ugly surface-wave-like field solutions. It is the same phenomenon which makes these types of surfaces undesirable for matched feeds — see Section 6.3.

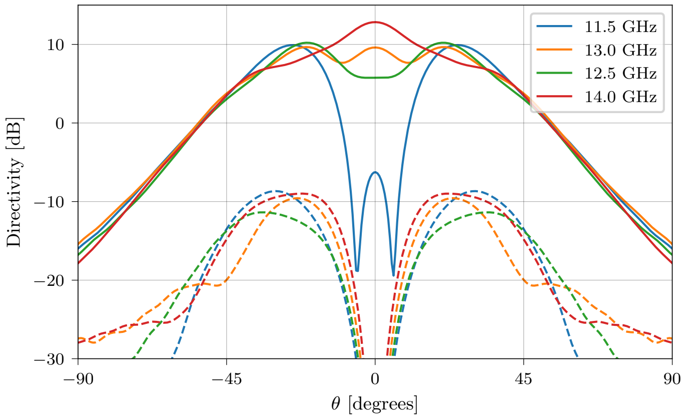

Figure 5.12: Radiation patterns of the horn shown in Figure 5.11 at selected frequencies. Only the 45° plane is shown. Solid lines are co-pol and dashed lines are cross-pol.

The dip in the boresight direction and broad pattern is sometimes sought in symmetrical single reflector antennas with small f/D values, so-called *deep reflectors* [102, Sec. 7.8]. In those geometries the dip in the main beam helps alleviate some of the feed blockage effect. A small dip in the feed beam is not categorically a disadvantage in the case of an offset reflector, but the beamwidth and high cross polarization in these patterns definitely are.

5.4.5 Balancing Objectives

Naturally, optimizing only one of the objectives as above is naive. The two objectives must be optimized together to find the best compromise and hopefully satisfy all the requirements.

Unfortunately, it has proven exeedingly difficult to achieve this with our chosen topology over the full band of the coupler. The objectives are simply pulling the parameters in opposite directions. The goal of low TE_{21} reflection tends to benefit from a large flaring of the first corrugation (the one with the coupler) and a bit longer second corrugation. It also benefits from letting the inner guide protrude into the horn. On the other hand, co-polar pattern suffers from the long corrugations and the protrusion means that the full horn aperture is not used efficiently, thus decreasing the directivity.

It seems that, over a large bandwidth, the long corrugation housing the coupler will always deteriorate the co-polar radiation pattern and in some cases the return loss. The only solution is to somehow isolate the two. In [103] and [104] circular/coaxial horns are presented where the circular and coaxial regions are separate radiators. In the latter, the regions radiate two distinct signals at different frequencies, while the former is more related to the present task with the same signal in both regions.

Performing the same trick in our case would entail flaring the inner circular guide to a spline shaped [105] or corrugated horn of its own. The coaxial region would have to be even wider. This approach poses a serious problem in our case, because the wall of the inner waveguide is thin, and the whole inner structure must carry itself all the way from the start of the coupler. Supporting the inner waveguide by a dielectric rod or pipe could solve this problem at the cost of added complexity and reduced power handling capabilities.

A compromise may be possible by attaching a single small choke between the inner guide and the long coaxial guide similarly to what is done in [106] to separate a circular and coaxial guide. This would also remove the influence of the outer corrugations, thus limiting the achievable directivity. Therefore, the outer corrugations would be dropped and the feed could only be used in very compact systems, where a wide beam is needed.

5.4.6 Matched Feed Design in K_u Uplink Band

The coupler evaluated in Section 5.3 covers the entire K_u downlink and uplink band from 10.7 GHz to 14.5 GHz — a 30 % fractional bandwidth. As outlined above, the horn topology chosen here cannot match this bandwidth. However, in order to validate that the concept works, we shall design a horn which compensates cross polarization in the uplink band only.

The uplink K_u band will here be taken as 13.75 GHz to 14.5 GHz — a 5.3 % fractional bandwidth. An $f/D = 0.8$ reflector system is used: $D = 1\,\text{m}$ aperture, $f = 80\,\text{cm}$ focal length, and $D' = 5\,\text{cm}$ clearance.

At this narrower frequency range, the two aforementioned objectives can both be met with the axially corrugated horn topology. The horn is made to fit the dimensions of the coupler from Section 5.3. When the horn geometry has been optimized, the coupler is attached instead of the dummy unperforated section. Now the secondary pattern of the reflector system is optimized to achieve low cross polarization within the angular region $\theta \in [-1.5°, 1.5°]$. The scattering parameters of the coupler are saved between iterations, such that it does not need to be recalculated when only the outer horn is changed. This drastically reduces the computation time of an iteration, since the coupler must be calculated with a full 3D simulation whereas the rest of the horn is circularly symmetric and calculated with BoR MoM. The geometry resulting from the optimization is shown in Figure 5.13.

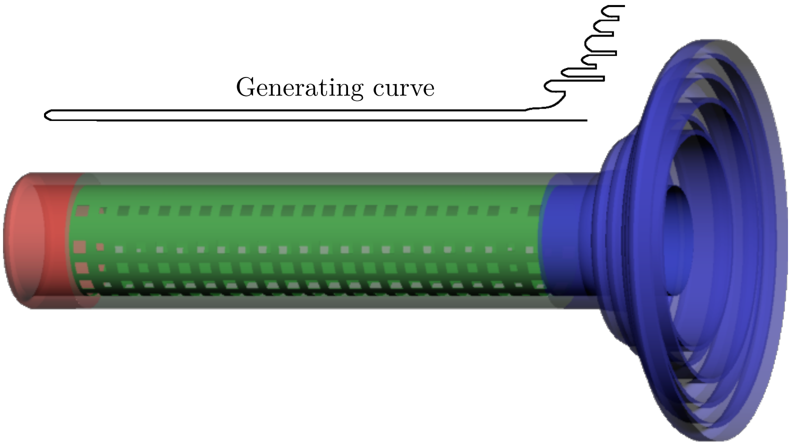

Figure 5.13: Fully assembled matched feed. The coaxial coupler is colored green, the horn section blue, and bottom termination red. The 2D generating curve is shown above the structure.

The bottom of the corrugations have been rounded in order to somewhat suppress resonances in the system arising from specific characteristic dimensions. The performance is represented in Figures 5.14 and 5.15 showing the cross-polar discrimination and patterns, respectively. Over the optimized band, the improvement compared to the same horn without coupler is better than 10.6 dB. Compared to a perfectly polarized Gaussian beam feed, the improvement is better than 9.6 dB everywhere for both polarizations.

As previously discussed, the long first corrugation housing the coupler makes it difficult for the co-polarized input to make use of the full horn aperture. This is also the case for this design: the directivity becomes too low for an f/D of 0.8 and the spillover efficiency suffers. In order to avoid this, the directivity should be improved, or the feed must be used in more compact systems, e.g. $f/D = 0.5$.

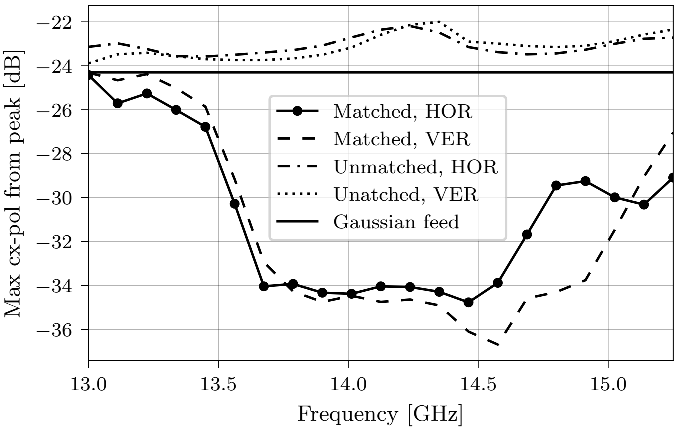

Figure 5.14: Maximum cross polarization within $\theta \in [-1.5°, 1.5°]$ compared to peak co-polar directivity. The values for the horn without coupler and a perfectly polarized Gaussian beam feed are shown for reference.

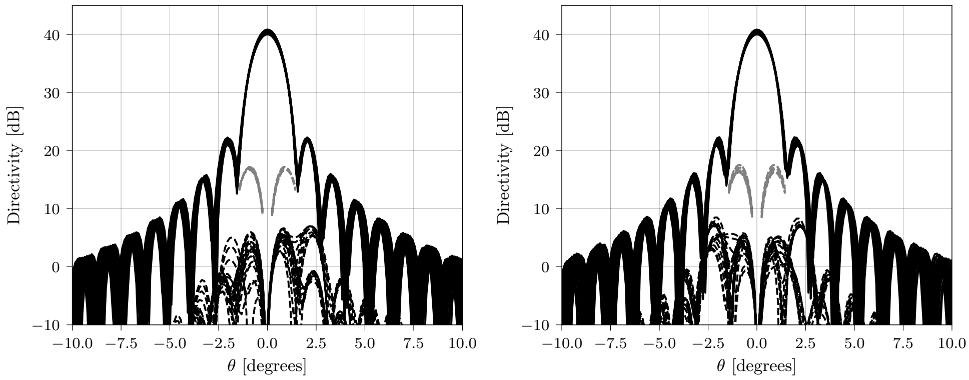

(a) Horizontal polarization

(b) Vertical polarization

Figure 5.15: Secondary patterns of the reflector with the optimized horn. 0°, 45°, and 90° cuts are plotted for nine frequencies across the band 13.75 GHz to 14.5 GHz. Co-polar radiation is in full lines, cross-polar is in dashed lines. The cross polarization of the system with an unmatched feed is indicated in dashed grey within the $\theta \in [-1.5°, 1.5°]$ range.

5.5 Summary

This chapter outlines a novel method for matched feed design. If near-equal cutoff between input and compensating modes can be achieved, distributed directional coupler techniques can be used for wideband, high quality mode conversion.

The condition is achieved by tailoring the dimensions of a circular waveguide surrounded by a coaxial one. In this situation, the TE_{21} mode in the coaxial guide travels at the same phase velocity as the TE_{11} mode in the circular, allowing coupling between the two to happen gradually along the length of the waveguides. A novel technique is presented which by proper placement of coupling holes around the circumference ensures that only desired TE_{21} modes are coupled — in simultaneous dual polarization.

The semi-analytical design procedure is shown to yield excellent results, and be able to couple dual polarization compensating modes with stable amplitude and phase over an unprecedented bandwidth of 30 %.

Substantial challenges in converting the waveguide modes into a radiated field have been discussed. The long coaxial corrugation causes a disturbance of the radiated field from the circular guide, and prevents wideband coupling to an axially corrugated horn section. Intrinsic reflection from an open ended narrow coaxial waveguide must be treated at the same time. In spite of this, a matched feed horn is designed for the K_u uplink band which reduces the cross polarization of the reflector system by 10 dB. It is thereby proven that the coaxial coupler may be used for matched feeds. Widening the bandwidth of the coupler to free space transition is a topic for further development.

CHAPTER 6

Impedance Surface Waveguides for Matched Feeds

As established in the preceding chapter, it is desirable if compensating modes propagate at phase velocities close to that of the input mode. Not only does it eliminate the phase drift toward the horn aperture, but also allows mode conversion to be distributed along the length of the feed.

The motivation behind the work presented in this chapter is therefore the same as the motivation for the coaxial geometry: to control the propagation such that the main and compensating modes have similar dispersion characteristics. This is possible by using anisotropic impedance-surface lined waveguides for the matched-feed horns. The theoretical background for cylindrical waveguides of circular cross-section with impedance wall is summarized in Appendix B.2.

The impedance surfaces we shall deal with in this chapter are characterized by two impedances, which define the ratio of E- and H-fields on the surface. The longitudinal impedance is defined as

$$-\frac{E_z}{H_\phi} = Z_z = R_z + jX_z, \tag{6.1}$$

and the transverse, or ϕ-directed impedance which reads

$$\frac{E_\phi}{H_z} = Z_\phi = R_\phi + jX_\phi, \tag{6.2}$$

where R's and X's are the respective resistance and reactance values. When these boundary condition apply at the walls of the waveguide, the field solution cannot in general be split into TE and TM mode solutions. The solutions which satisfy these conditions and contain both E- and H-fields in the longitudinal direction are termed *hybrid modes.*

6.1 Impedance-Surface Waveguides in the Literature

The early developments of anisotropic impedance-surface waveguide theory is centered around waveguides and horns with radially corrugated walls. This allowed construction of horns with very low cross polarization and symmetric patterns. When the corrugations are at resonance, i.e. one quarter wavelength deep, the longitudinal impedance seen inside the waveguide is infinite while the transverse (ϕ-directed) is still zero. This allows for propagation of hybrid modes under the balanced condition (see Appendix B.2) which exhibit low cross polarization. Early contributions to the analysis of corrugated waveguides and horns include [107–116]. These references culminate in a book by Clarricoats and Olver [99], which is a comprehensive study of the theory and design of corrugated feed horns.

Siblings of the radially corrugated horns are the so-called *hard horns*. A term coined by Kildal [117] along with *soft horns* representing the radially corrugated ones. On the hard surface, the anisotropic impedances are zero longitudinal and infinite transverse impedance, i.e. switched compared to the soft surface. These impedances also support hybrid modes under the balanced condition with low cross polarization. An advantage of the hard horns, is that a TEM mode is supported. The TEM mode has no taper towards the edge of the waveguide and therefore, in principle, the horns can have 100 % aperture efficiency which is useful in focal plane arrays. Other references on hard horns are [118, 119].

Standard metal walled waveguides with losses included are also impedance waveguides. Naturally, the surface impedances are not anisotropic, but in general, hybrid modes are needed to satisfy the boundary conditions when the walls are lossy. Literature treating modes in waveguides with lossy walls include [120, 121], though Dragone [121] also treats anisotropy.

Cylindrical waveguides with arbitrary cross-section and general anisotropic surface impedances were treated in [122]. Unger employs the theory principally for helix waveguides. It is later pointed out in [123], that for noncircular waveguide cross sections, coupling between modes occurs in the impedance waveguide. Other authors Dragone [121], Bernardi [124], Andersen [125], Elsherbeni and Hamid [126], and Elsherbeni et al. [127] also treat various aspects of general impedance waveguides. A good general derivation is also given in Mahmoud [128].

Thomas and Minnett [129] conduct a detailed study on circular cylindrical waveguides with general anisotropic impedance walls. Dispersion diagrams are shown for surface impedance pairs of interest and several observations on limiting cases are made. They also introduce the so-called *hybrid factor*,γ, which measures the ratio of longitudinally directed E- and H-fields. Thomas and Minnett define the HE and EH hybrid modes from the sign of the hybrid factor, a convention which has been carried on in the majority of the literature on impedance and corrugated waveguides. Raveu et al. [130] recently made a similar study also including rectangular waveguides.

As for specific applications utilizing waveguides with impedance walls, there are many works on corrugated horns, academic as well as industrial. However, there are also references on other kinds of anisotropic impedance surface horns. One concept which is of interest, is other combinations of the surface impedances which gives rise to the balanced hybrid condition. Namely the ones which lie between the two extremes of soft and hard horns. Wu et al. have designed several horns based on nonresonant surfaces, which aim at the balanced condition, but not necessarily hard or soft [131–136]. They demonstrate that their surfaces can satisfy the hybrid condition over a large bandwidth. Capet et al. [137] also aim to implement the balanced hybrid condition, but in order to reduce the cutoff size of waveguides.

6.2 Dispersion Diagrams

When dealing with problems that have modal solutions, dispersion diagrams are often used. They link frequency and phase constant for each modal solution. There are a few ways to represent them. In optics, the phase constant is often put on the primary axis and the frequency/free space wavenumber on the secondary axis. In the electrical engineering community, we like the frequency on the primary axis. In the present chapter, we shall represent the dispersion diagrams as follows: the free space wavenumber times waveguide radius on the primary axis (ka) and phase constant times radius secondary axis (βa). The condition that $k = \beta$ is indicated in each plot and denoted the *light line*. Modes below the light line have a phase propagation faster than the speed of light and are therefore denoted *fast waves*. Conversely, modes above the light line are denoted *slow waves* as their phase propagation is slower than the speed of light. The dispersion diagram of a PEC waveguide shown previously in Figure 2.9 has only fast waves which are either TE or TM.

6.3 Simultaneous HE$_1$ and HE$_2$ propagation

For matched-feed applications we are interested in simultaneous propagation of the fundamental mode and a higher order mode to compensate the cross polarization. Already in the first paper by Rudge and Adatia [6], the HE$_{21}$ mode is mentioned for matched feed operation in a corrugated horn. None of the above references include simultaneous propagation of the HE$_{11}$ and HE$_{21}$ modes in general impedance waveguides. In this section, we shall focus only on impedance pairs which satisfy the balanced hybrid condition as detailed in Appendix B.2, namely

$$X_z X_\phi = -Z_0^2, \quad x_z x_\phi = -1, \tag{6.3}$$

or equivalently

$$Z_z Z_\phi = Z_0^2, \quad z_z z_\phi = 1, \tag{6.4}$$

where the uncapitalized quantities are normalized with the free space impedance, e.g. $z_z = Z_z/Z_0$. We fix just one of the surface reactances/impedances, and the other will follow. Figure 6.1 shows dispersion plots for several balanced surfaces. Blue curves are $m = 1$ modes and orange curves are $m = 2$ modes. Dotted lines correspond to balanced EH modes ($\gamma = -1$) and full lines to balanced HE modes ($\gamma = 1$).

The top left plot, Figure 6.1(a), corresponds to the impedance of a corrugated surface at resonance: $X_z = \infty$ and $X_\phi = 0$. This is the surface sometimes referred to as *soft* [138]. For the matched feed application, we are interested in the first HE$_1$ and HE$_2$ modes — the ones which are at cutoff circa $ka = 2$ and $ka = 3$, respectively. The main problem with this configuration is that the difference in phase constant between the two modes of interest changes heavily with frequency, just as in the PEC waveguide.

Figure 6.1(b) represents normalized reactances $(x_z, x_\phi) = (1, -1)$. Slow waves dominate as well as simultaneous HE and EH propagation in the fast region. This configuration is undesirable for horn applications as is also noted by Thomas and Minnett [129] (although they missed the slow waves).

More interesting are the two bottom plots of Figure 6.1. In Figure 6.1(d) a waveguide with the *hard* boundary condition [138] is shown. As mentioned by Kildal [138], this type of waveguide supports a TEM mode with no cutoff and uniform field distribution. This is also true for $m = 2$ modes and they both lie on the light line with the same propagation constant as the free space wavenumber (one hidden by the other). Since the two desired modes have the same phase constant at all frequencies, this configurations seems highly desirable. The problem is that the implementation of infinite transverse reactance is a resonance phenomenon, and therefore narrowband, which is also mentioned in [138]. However, this is not necessarily true for the impedance in the bottom left corner. Figure 6.1(c), which also shows promising propagation

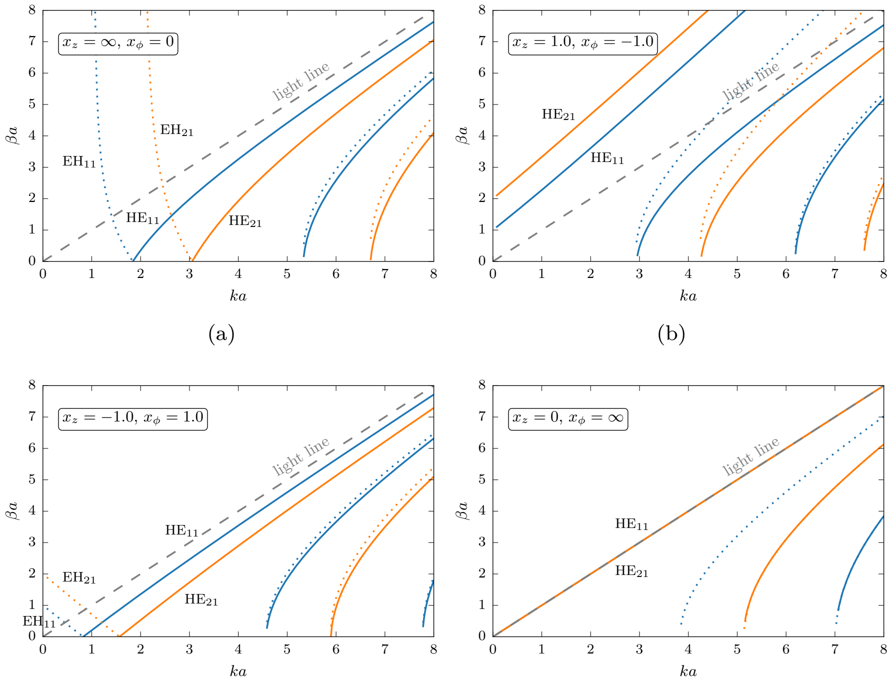

(a) (b)

(c) (d)

Figure 6.1: Dispersion diagrams for different balanced surface impedances, i.e. $x_z x_\phi = -1$. Blue curves are $m = 1$ modes and orange curves are $m = 2$ modes. Dotted lines correspond to balanced EH modes ($\gamma = -1$) and full lines to balanced HE modes ($\gamma = 1$).

characteristics: The difference in HE$_{11}$ and HE$_{21}$ propagation constant changes much less with frequency than for the soft surface. The balanced impedance pairs which lie in the range between the cases in the two bottom plots will be investigated in the following section.

6.4 Capacitive X_z and Inductive X_ϕ

As mentioned in the previous section, it is of interest to look further into the solution space under the balanced hybrid condition between the cases of $(-1, 1)$ and $(0, \infty)$. We let x_z go from -1 toward zero while enforcing the balanced hybrid condition

$$x_z x_\phi = -1. \tag{6.5}$$

Three cases are shown in Figure 6.2. The reactances are capacitive (negative) in the z-direction and inductive (positive) in the ϕ-direction. All the cases exhibit better performance than the soft surface case, i.e. the dispersion lines are more parallel and they are closer. When $x_z = -0.1$ (Figure 6.2(c)), the HE$_{11}$ and HE$_{21}$ curves are practically equal.

These are idealised impedances. A practical (non-PEC) surface would never exhibit the same impedance over such a large frequency band. Luckily that is not required as we only need the surface to be in the ballpark of small capacitive longitudinal impedance and larger inductive transverse impedance, while being approximately balanced. But is this practically realisable? Considering the horns produced

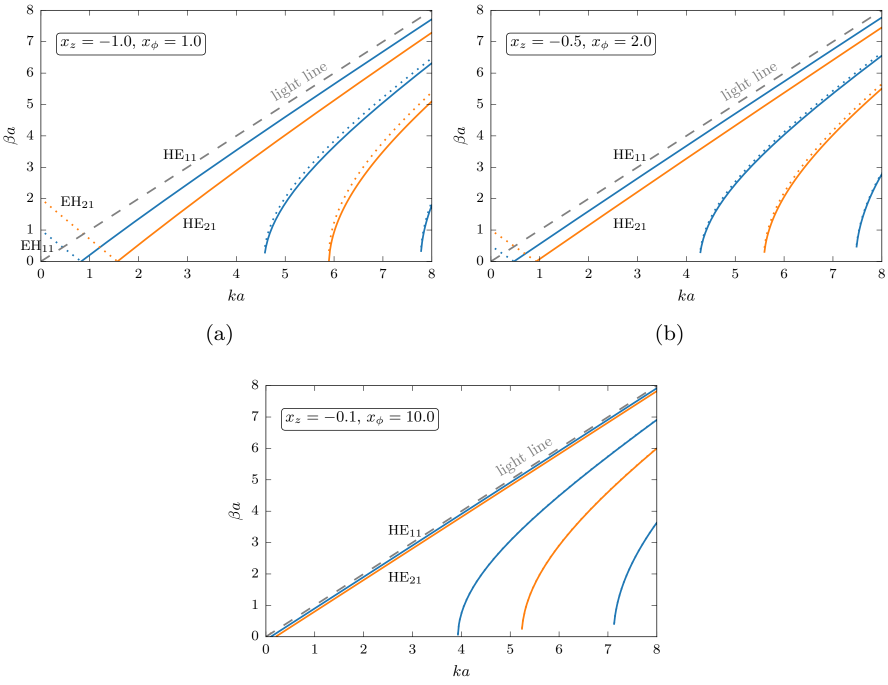

(a)

(b)

(c)

Figure 6.2: Dispersion plots for different balanced surface impedances, i.e. $x_z x_\phi = -1$. All four cases are with a capacitive reactance in the z-direction and thus an inductive reactance in the ϕ-direction. Blue curves are $m = 1$ modes and orange curves are $m = 2$ modes. Dotted lines correspond to balanced EH modes ($\gamma = -1$) and full lines to balanced HE modes ($\gamma = 1$).

by Wu et al. [132–135], the impedances they arrive at are quite close to this condition. Their goal for optimization is just the balanced condition, but the result happens to be capacitive in the longitudinal direction and inductive in the transverse over a large bandwidth.

6.5 Impedance Surface Matched Feed Design

Let us take outset in the work of Wu and his colleagues and assume that we can successfully impose the extra design goal that the longitudinal reactance is small (see Figure 6.2). Then we will have a piece of waveguide or flared horn in which HE$_{11}$ and HE$_{21}$ propagate at nearly the same phase velocity.

First of all, in the classical matched feed structure, the mode launcher is placed at the beginning of the horn, before the flare. If the mode launcher is followed by a significant length of regular metallic waveguide, the phase difference between the fundamental and compensating mode will vary with frequency. This can be totally avoided with an impedance surface waveguide of this kind.

However, making the mode launcher in this type of waveguide is even more advantageous. When the phase velocities are nearly equal, the distributed directional coupler technology can be used to excite the higher order mode, as discussed in Chapter 5. In the impedance waveguide case, the two modes would exist in the same waveguide and not in separate ones as with the coaxial coupler, but the concept is the same. Mode launching would consist of small nonresonant inclusions, which enhance the operating bandwidth as in the case of the coaxial coupler. The mode launcher might then be followed by a flared section or incorporated into it.

Wu et al. [132–136] have demonstrated that this kind of metasurface structures are indeed realizable over significant bandwidths. The main reason for this is, that the elements do not have to be resonant.

6.5.1 Validation

Rudge and Adatia [6, 32] state that the HE_{21} mode in a corrugated waveguide can be used in matched feeds and it has been proven by several authors [17–19]. It will now be verified that the hybrid modes supported by the impedance waveguides presented in this chapter are also suitable for matched feed design. Figure 6.3 shows radiation patters of the HE_{11} and HE_{21} modes from an impedance waveguide with normalized reactances $x_z = -1$ and $x_\phi = 1$. The patterns are computed by first evaluating the transverse E- and H-fields of the hybrid modes from the formulas in Appendix B.2 and finding the equivalent magnetic and electric currents, respectively. The currents are numerically integrated to find the patterns by GRASP.

The HE_{11} mode radiates virtually no cross polarization and the pattern is almost perfectly Gaussian. The aperture efficiency, and therefore gain, is higher than would be the case for a soft surface HE_{11} mode, at the expense slightly higher side lobes. The HE_{21} mode exhibits the cross polarization lobes which we require to cancel out the cross polarization induced by the feed tilt. This is confirmed in Figure 6.4 where the secondary pattern of a standard reflector system is evaluated before and after the addition of HE_{21}. Cross polarization is reduced by 17 dB in this case.

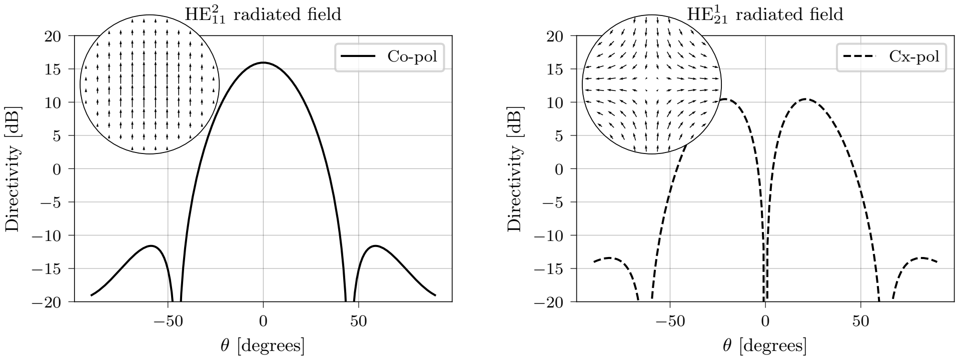

Figure 6.3: Radiation patterns of HE_{11} and HE_{21} hybrid modes from an impedance waveguide of radius $a = 25\,\mathrm{mm}$ with wall reactances $x_z = -1$ and $x_\phi = 1$. The cut shown is $\phi = 0°$ where the HE_{21} mode is purely cross polarized. The HE_{11} radiates almost no cross polarization in any plane. The patterns are evaluated at 13 GHz and calculated from numerical integration of the aperture E- and H-fields in GRASP.

6.6 Summary

In this chapter an investigation of the applicability of anisotropic impedance waveguides to matched feed design is presented. The essential goal of choosing other guiding

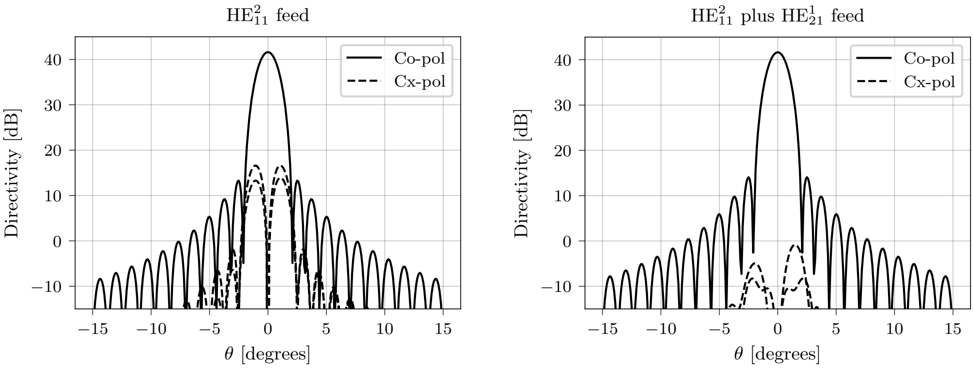

Figure 6.4: yz-offset reflector system with $f/D = 0.8$ illuminated by the hybrid modes of Figure 6.3. The left plot is of pure HE_{11} illumination, i.e. virtually zero cross polarization of the feed. The right plot shows how the feed tilt can be compensated by addition of $-18.5\,\mathrm{dB}$ HE_{21} in phase quadrature. The cross polarization is shown in both $\phi = 0°$ and $\phi = 45°$

structures than the PEC waveguide, is to eliminate the phase dispersion of the compensating mode relative to the fundamental one. To this end, it is desired that the difference in phase constant of the two modes is stable with frequency, or even better, that the phase constants are the same. It is found that the traditional soft surface waveguides and horns provide little improvement in this regard. However, other impedance surfaces exhibit much more promising characteristics with almost parallel dispersion lines and approaching equal phase constants. These surfaces are characterised by capacitive longitudinal reactances and inductive transverse reactances. Horn antennas designed, and tested, with these kind of surfaces have recently been published in the literature, though not for matched feed purposes.

CHAPTER 7

Conclusion

This study is concerned with identifying the reasons for and alleviating the bandwidth limitation of matched feed antennas for offset reflectors.

Matched feeds have seen some activity in the literature, however, none of the references provide a satisfactory account of all the aspects of the design process. For example, the so-called mode launchers of matched feeds are always presented without any motivation as to their design. Therefore, this work thoroughly describes the workings of these devices, such that basis can be made for improving them. Additionally, a new method is presented for determining the waveguide modes needed for matched feeds under varying geometrical setups. In the process, it is found that modes other than the previously employed ones, can be used.

Regarding the bandwidth limitations of existing matched feed antennas, two main culprits are identified: modal dispersion in waveguides and resonance effects of mode-launcher inclusions. Three strategies have been pursued to address these problems:

1. Optimization methods and limitation of waveguide horn length [P1].
2. Equalizing phase velocities by propagating higher order modes in a coaxial waveguide [P4].
3. Equalizing phase velocities by employing waveguides with engineered surface impedance [P3].

By careful design in several optimization steps, the first approach allowed us to achieve an unprecedented bandwidth for a dual-polarized matched feed. However, this approach does not solve the fundamental problem, only squeezes as much performance as possible out of the existing technology.

The second approach is based on the fact that while higher order modes in a single PEC waveguide will always have different cutoffs than the fundamental one, this is not true if the modes propagate in separate waveguides. It turns out that the dimensions of a coaxial waveguide surrounding a circular one can be tuned such that the TE_{21} mode has the same cutoff frequency as the TE_{11} mode in the circular guide, meaning that the two travel at the same speed for all frequencies. This property gets rid of the modal dispersion, but also enables the mode coupling to be distributed along the length of the waveguides.

The design of the coaxial coupler combines several elements: extensive use of the framework for mode launcher analysis, directional coupler design concepts, and again, optimization. With the presented method mode launchers working in dual polarizations over a 30 % bandwidth can be designed. Horn antennas which may be fitted to the coaxial coupler mode launcher have also been investigated. It proves that the concept can be used for dual polarized matched feeds, though the horn design is now the bottleneck for very wideband operation.

By the same reasoning as with the coaxial geometry, it is uncovered that impedance surface, or *metasurface*, horns are promising for matched feeds. An analysis of higher order waveguide modes in impedance waveguides shows that for a certain range of materials, HE_{11} and HE_{21} hybrid modes propagate at almost equal speeds in the waveguide. This means again, that modal dispersion is eliminated, and that coupling can be distributed as with the coaxial coupler. The impedance surface approach has the advantage over the coaxial coupler one that only a single waveguide region is needed, thus simplifying the horn design. Of course, the actual surface and its method of manufacture must be determined. By how much this complicates the design is still unknown, but promising results are published in the literature.

The matched feed designs in the literature have been almost exclusively single polarized. It seems that for real applications, reflector feeds are often required to be dual polarized. Using the framework for mode launcher analysis presented here, it is relatively straight forward to make a design which generates only the correct higher order modes for inputs of both polarizations. All designs presented in this study are therefore dual polarized[1].

This study has resulted in new insights into the technology referred to as matched feeds. These insights are used to provide novel methods to widen the achievable bandwidth, thus incrementing state-of-the-art. Many challenges still remain in this field. In my opinion, there are some very interesting paths to pursue further. Other horn topologies must be investigated in order to utilize the full bandwidth of the coaxial coupler and possibly a increase the directivity. The impedance surface horns for matched feeds need to be further matured by design of specific surfaces, directional coupler coefficients, and inclusions. The directional coupler framework for mode launcher synthesis is not limited to the coaxial or impedance surface waveguide, it can be readily applied to any guiding configuration. It would for example be interesting to apply distributed mode coupling along the length of a corrugated horn with hundreds of sub-resonance inclusions.

---

[1] Except the TM_{01} demonstrator design in Appendix A.

APPENDIX A

TM_{01} Matched Feed

In the following it shall be validated that the TM_{01} mode can be used in a circular matched feed instead of a TE_{21} mode. An example design is presented which, though relatively narrow band, substantially reduces cross polarization of an $f/D = 0.6$ reflector without generating any TE_{21} modes.

The feed is not intended to compete with other designs and shown here only as a demonstrator. Should a wideband matched feed be attempted, we would have to find an alternative to the augmented Potter horn topology. Naturally, the design is also single polarized, as only the TM_{01} mode is employed.

A.1 Design

The design is optimized for a single frequency of 5 GHz. The reflector system which the feed is meant for is summarized in Table A.1. It is a quite severely offset system with a focal length to diameter ratio of 0.6 and a feed tilt of nearly 60°.

	Symbol	Value
Frequency	-	5.0 GHz
Focal length	f	1.2 m
Aperture diameter	D	2.0 m
Clearance	D'	20 cm
f over D	f/D	0.6
Feed tilt	θ_f	57°

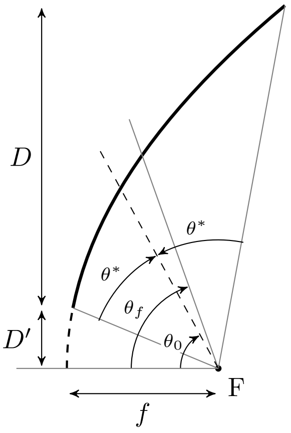

Table A.1: Parameters of the antenna measured in [3].

The design is carried out much like a classic matched feed design with TE_{21} modes. The differences are in the mode launcher, which we shall come back to, and in that the waveguide section following it does not support TE_{21}. The topology is shown in Figure A.1 and is very similar to the one shown in Figure 2.7. Below, the cutoff radii of the first few modes in a circular waveguide at 5 GHz are listed. The first section must propagate only TE$_{11}$, the second section only TE$_{11}$ and TM$_{01}$, and the final section must allow TM$_{11}$ for the Potter-horn effect.

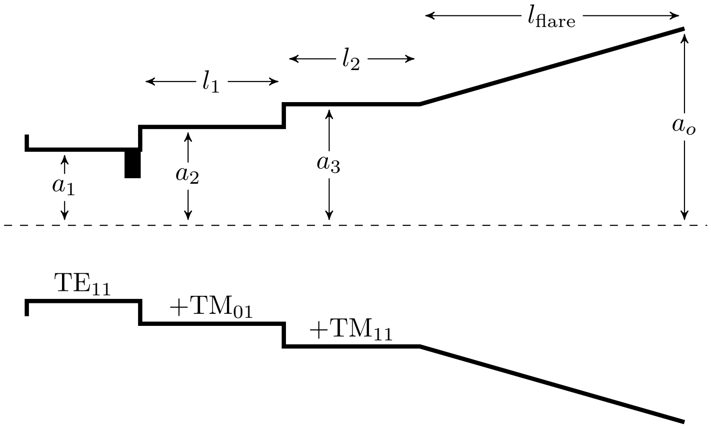

TE$_{11}$		TM$_{01}$		TE$_{21}$	TE$_{01}$/TM$_{11}$	
17.57	$< a_1 <$	22.95	$< a_2 <$	29.15	36.56	$< a_3$

Figure A.1: Topology of the TM$_{01}$ matched feed. Below it, the cutoff radii in mm of waveguide modes in a circular waveguide at 5 GHz are listed. The proper intervals of the horn sections are indicated.

A.1.1 Mode Launcher

The mode launcher is designed by inspection of Figure 4.6. TM$_{01}$ generation may be achieved by placing pins anywhere on either the top or bottom half of the waveguide. Placing pins in both halves would result in destructive interference. It is evident that other modes will be generated, but these will decay in the following waveguide section due to our choice of a_2. Four pins are placed symmetrically around $\phi = 90°$ so as to avoid any one pin having to be too long. The configuration is shown in Figure A.2(a).

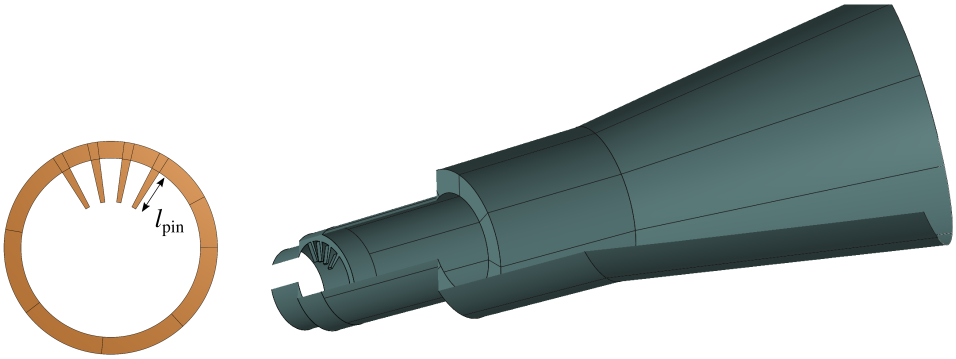

(a) Mode Launcher

(b) Full feed

Figure A.2: Finished design. (a): The TM$_{01}$ mode launcher seen from the front. The first pin is at $\phi = 60°$ and there is a 20° spacing between pins. (b) A rendering of the assembled matched feed.

A.1.2 Procedure

The design procedure employed here is quite simple. The following steps involving *engineering decisions*, manual adjustment, and numerical optimization are taken:

1. Consult Figure 3.4 to determine approximate TM$_{01}$ amount required: $V_{01}^{\mathrm{TM}} \approx 0.2$.
2. Fix a_1 and a_2 and adjust pin lengths (l_{pin}) until desired TM$_{01}$ is generated.
3. Optimize Potter horn part of the feed for low cross polarization and appropriate edge taper. Variables are a_3, l_2, l_{flare}, and a_o.
4. Assemble mode launcher and Potter horn. Adjust l_1 until TM$_{01}$ is approximately 90° ahead of TE$_{11}$ in the aperture.
5. Optimize reflector far field for low cross polarization with l_1 and pin length as variables.

Note that since TM$_{11}$ does not propagate in the section where the radius is a_2, we can adjust the TM$_{01}$ phasing length, l_1, without affecting the properties of the Potter horn. The design works without the last optimization, but can be significantly improved by including it. One reason is that the phase center of the horn is not exactly at the aperture.

The simulation method splits the horn into four parts: 1) mode launcher 2) the circular symmetric step (including waveguide sections before and after), 3) the horn flare, and 4) The transition to free space. Only the mode launcher part needs to be calculated with 3D MoM; the step is calculated with mode matching and the last two parts with Body of Revolution MoM. The parts are connected via waveguide ports and generalized scattering matrices. Therefore, only steps 2 and 5 in the above procedure require 3D calculations.

A.2 Results

The dimensions resulting from the above procedure are listed in Table A.2. Note that the radii are in the intervals as dictated in Figure A.1.

The reflector far-field pattern at the design frequency is shown in Figure A.3(a). The cross-polar lobes using a perfectly polarized Gaussian beam feed are shown for reference. The reduction in maximum cross polarization is 17 dB. The cross polarization level relative to peak as a function of frequency is shown to the right in Figure A.3(b). As expected, the design is relatively narrowband with a 10 dB reduction bandwidth of 2.2 %.

In order to validate that we have not just inadvertently made a regular matched feed, mode content in the aperture is evaluated. Figure A.4 shows the amount of TE$_{11}^{2}$, TE$_{21}^{1}$, and TM$_{01}$ modes in the aperture. The TE$_{21}$ mode is less than -55 dB at the design frequency and will hardly influence the pattern of the feed at all. The other TE$_{21}$ mode content is well below -100 dB and not shown here.

	[mm]
a_1	21.0
a_2	25.0
a_3	36.7
a_o	56.0
l_1	79.9
l_2	75.2
l_{flare}	147.5
l_{pin}	10.2

Table A.2: Final dimensions of the design.

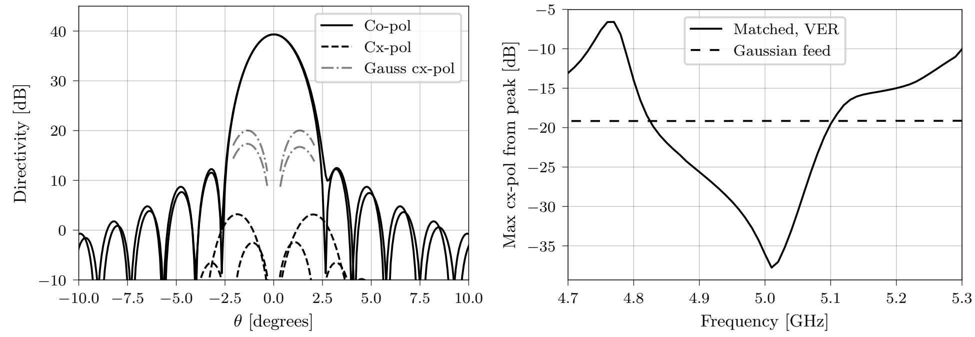

(a)

(b)

Figure A.3: Cross-polar performance of the TM_{01} matched feed. (a): Reflector radiation pattern in asymmetry and diagonal planes. Cross polarization of a Gaussian beam feed is indicated in grey. (b): Cross polarization relative to peak directivity as a function of frequency.

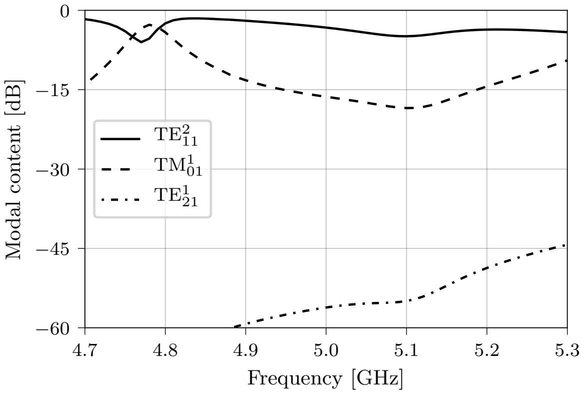

Figure A.4: Mode content in the aperture of the matched feed when excited by the TE_{11}^2 mode (y-polarized).

APPENDIX B

Waveguide Modal Analysis

This appendix holds some reference derivations and formulas regarding waveguides. The first part is concerned with general waveguides with general anisotropic impedance surfaces. Then we move on to circular waveguides of general surfaces before lastly specializing to PEC circular waveguides.

The methods presented in Section B.2 is the basis of the results in Chapter 6.

B.1 General Cylindrical Waveguides

A cylindrical waveguide does *not* mean a circular waveguide, but a waveguide whose (general) cross-section does not change along one direction. In the literature, the term cylindrical waveguide is often confused with a circular cylindrical waveguide. A rectangular waveguide is also a cylindrical waveguide, with a rectangular cross-section.

B.1.1 Decomposition in Transverse and Longitudinal Components

Maxwell's curl equations in a source free, simple medium read

$$\nabla \times \mathbf{E} = -j\omega\mu\mathbf{H} \tag{B.1a}$$

$$\nabla \times \mathbf{H} = j\omega\epsilon\mathbf{E}. \tag{B.1b}$$

Now let

$$\nabla = \nabla_t + \hat{\boldsymbol{z}}\frac{\partial}{\partial z} \tag{B.2}$$

$$\mathbf{E} = \mathbf{E}_t + \hat{\boldsymbol{z}}E_z \tag{B.3}$$

$$\mathbf{H} = \mathbf{H}_t + \hat{\boldsymbol{z}}H_z \tag{B.4}$$

which is inserted into (B.1) to yield

$$\begin{cases} (\nabla_t + \hat{\boldsymbol{z}}\frac{\partial}{\partial z}) \times (\mathbf{E}_t + \hat{\boldsymbol{z}}E_z) = -j\omega\mu(\mathbf{H}_t + \hat{\boldsymbol{z}}H_z) \\ (\nabla_t + \hat{\boldsymbol{z}}\frac{\partial}{\partial z}) \times (\mathbf{H}_t + \hat{\boldsymbol{z}}H_z) = j\omega\epsilon(\mathbf{E}_t + \hat{\boldsymbol{z}}E_z) \end{cases} \tag{B.5}$$

$$\Rightarrow \begin{cases} \nabla_t \times \mathbf{E}_t + \nabla_t \times \hat{\boldsymbol{z}}E_z + \frac{\partial}{\partial z}(\hat{\boldsymbol{z}} \times \mathbf{E}_t) = -j\omega\mu(\mathbf{H}_t + \hat{\boldsymbol{z}}H_z) \\ \nabla_t \times \mathbf{H}_t + \nabla_t \times \hat{\boldsymbol{z}}H_z + \frac{\partial}{\partial z}(\hat{\boldsymbol{z}} \times \mathbf{H}_t) = j\omega\epsilon(\mathbf{E}_t + \hat{\boldsymbol{z}}E_z) \end{cases} \tag{B.6}$$

Crossing with $\hat{\boldsymbol{z}}$, the longitudinal terms cancel, and we obtain

$$\Rightarrow \begin{cases} \dfrac{\partial \mathbf{E}_t}{\partial z} = j\omega\mu(\hat{\boldsymbol{z}} \times \mathbf{H}_t) + \nabla_t E_z \\ \dfrac{\partial \mathbf{H}_t}{\partial z} = -j\omega\epsilon(\hat{\boldsymbol{z}} \times \mathbf{E}_t) + \nabla_t H_z \end{cases} \tag{B.7}$$

We can go two ways from here. Let us start by obtaining equations in the transverse components. To this end, we find E_z and H_z from the standard form of Maxwell's equations (B.1), namely

$$\begin{aligned} -j\omega\mu H_z &= \frac{\partial E_y}{\partial x} - \frac{\partial E_x}{\partial y} \\ &= \nabla_t \cdot (\mathbf{E}_t \times \hat{\boldsymbol{z}}) \end{aligned} \tag{B.8a}$$

and

$$j\omega\epsilon E_z = \nabla_t \cdot (\mathbf{H}_t \times \hat{\boldsymbol{z}}). \tag{B.8b}$$

Inserting into (B.7) yields

$$\begin{cases} \dfrac{\partial \mathbf{E}_t}{\partial z} = j\omega\mu(\hat{\boldsymbol{z}} \times \mathbf{H}_t) + \dfrac{j}{\omega\epsilon}\nabla_t\nabla_t \cdot (\hat{\boldsymbol{z}} \times \mathbf{H}_t) \\ \dfrac{\partial \mathbf{H}_t}{\partial z} = -j\omega\epsilon(\hat{\boldsymbol{z}} \times \mathbf{E}_t) + \dfrac{j}{\omega\mu}\nabla_t\nabla_t \cdot (\mathbf{E}_t \times \hat{\boldsymbol{z}}) \end{cases} \tag{B.9}$$

or in dyadic form

$$\begin{cases} \dfrac{\partial \mathbf{E}_t}{\partial z} = j\omega\mu\left(\overline{\overline{I}} + \dfrac{1}{k^2}\nabla_t\nabla_t\right) \cdot (\hat{\boldsymbol{z}} \times \mathbf{H}_t) \\ \dfrac{\partial \mathbf{H}_t}{\partial z} = j\omega\epsilon\left(\overline{\overline{I}} + \dfrac{1}{k^2}\nabla_t\nabla_t\right) \cdot (\mathbf{E}_t \times \hat{\boldsymbol{z}}) \end{cases} \tag{B.10}$$

where $\overline{\overline{I}}$ is the unit dyadic. Equations (B.8) and (B.10) are equivalent to Maxwell's equations (B.1).

Wave Solutions in z

We now consider solutions which are travelling waves in the z-direction, thus

$$\begin{cases} \mathbf{E}(x,y,z) = \tilde{\mathbf{E}}(x,y)e^{\mp j\beta z}, \\ \mathbf{H}(x,y,z) = \tilde{\mathbf{H}}(x,y)e^{\mp j\beta z}, \end{cases} \tag{B.11}$$

and the functions $\tilde{\mathbf{E}}$ and $\tilde{\mathbf{H}}$ are only functions of the transverse coordinates. This assumption will enable us to find the transverse fields from the longitudinal ones. Consider again Equation (B.7). We take the derivative with respect to z of the first equation to obtain

$$\frac{\partial^2 \mathbf{E}_t}{\partial z^2} = j\omega\mu(\hat{\boldsymbol{z}} \times \frac{\partial \mathbf{H}_t}{\partial z}) + \frac{\partial}{\partial z}\nabla_t E_z. \tag{B.12}$$

We then insert $\frac{\partial \mathbf{H}_t}{\partial z}$ from the second equation, yielding

$$\frac{\partial^2 \mathbf{E}_t}{\partial z^2} = j\omega\mu\left(j\omega\epsilon \mathbf{E}_t + \hat{\boldsymbol{z}} \times \nabla_t H_z\right) + \frac{\partial}{\partial z}\nabla_t E_z \tag{B.13}$$

$$\Rightarrow \frac{\partial^2 \mathbf{E}_t}{\partial z^2} = -k^2\mathbf{E}_t + j\omega\mu\hat{\boldsymbol{z}} \times \nabla_t H_z + \frac{\partial}{\partial z}\nabla_t E_z. \tag{B.14}$$

We now use the assumption (B.11) to replace the z derivative with $\mp j\beta$:

$$\begin{aligned} -\beta^2 \mathbf{E}_t &= -k^2 \mathbf{E}_t + j\omega\mu \hat{\boldsymbol{z}} \times \nabla_t H_z \mp j\beta \nabla_t E_z \\ \Rightarrow \mathbf{E}_t &= \frac{j}{k_c^2} \left(\omega\mu \hat{\boldsymbol{z}} \times \nabla_t H_z \mp \beta \nabla_t E_z \right), \end{aligned} \tag{B.15a}$$

where we have used the defininition of the cutoff wavenumber $k_c^2 = k^2 - \beta^2$. A similar derivation for $\mathbf{H}_t$ yields

$$\mathbf{H}_t = \frac{j}{k_c^2} \left(\omega\epsilon \nabla_t E_z \times \hat{\boldsymbol{z}} \mp \beta \nabla_t H_z \right). \tag{B.15b}$$

Thus, we can determine just E_z and H_z from the scalar Helmholtz equation

$$\begin{cases} \nabla_t^2 E_z + k_c^2 E_z = 0 \\ \nabla_t^2 H_z + k_c^2 H_z = 0, \end{cases} \tag{B.16}$$

and find the transverse components from these. Then the boundary conditions are used to find relevant constants. In case of PEC walled guides, the boundary conditions can be met by purely TE or TM solutions, i.e. $E_z = 0$ or $H_z = 0$, respectively. For example, the boundary conditions for TM modes can be met by simply imposing that $E_z = 0$ on the guide wall.

For more general wall materials, hybrid modes may be required to satisfy boundary conditions. These are solutions where neither E_z or H_z are zero. This topic will be discussed further in the following section.

B.2 Circular Waveguides with Impedance Wall

Consider a cylindrical waveguide with circular cross section. The wall boundary is impenetrable, and thus, the electric surface current is given by

$$\mathbf{J}_{es} = \hat{\boldsymbol{n}} \times \mathbf{H} \tag{B.17}$$

where $\hat{\boldsymbol{n}} = -\hat{\boldsymbol{\rho}}$ for the circular waveguide in a usual cylindrical coordinate system. We let the material impose a linear relation between the current and the electric field, i.e. Ohm's law:

$$\mathbf{E}_t = \overline{\overline{Z}} \cdot \mathbf{J}_{es} \tag{B.18}$$

where the surface impedance, $\overline{\overline{Z}}$, is the dyadic

$$\overline{\overline{Z}} = \hat{\boldsymbol{z}}\hat{\boldsymbol{z}} Z_{zz} + \hat{\boldsymbol{\phi}}\hat{\boldsymbol{\phi}} Z_{\phi\phi} + \hat{\boldsymbol{\phi}}\hat{\boldsymbol{z}} Z_{\phi z} + \hat{\boldsymbol{z}}\hat{\boldsymbol{\phi}} Z_{z\phi}. \tag{B.19}$$

Thus, the material on the guide wall imposes the following condition on the field at the wall

$$\mathbf{E}_t = -\overline{\overline{Z}} \cdot \hat{\boldsymbol{\rho}} \times \mathbf{H}_t, \tag{B.20}$$

and if we let the cross terms be zero, $Z_{\phi z} = Z_{z\phi} = 0$, the boundary condition reduces to

$$-\frac{E_z}{H_\phi} = Z_{zz} = Z_z = R_z + jX_z \tag{B.21a}$$

$$\frac{E_\phi}{H_z} = Z_{\phi\phi} = Z_\phi = R_\phi + jX_\phi. \tag{B.21b}$$

In a PEC waveguide, both impedances Z_ϕ and Z_z are zero. For an isotropic wall surface, they are identical. In the more general anisotropic case, however, they can be different and complex. If the surface is lossless $R_z = R_\phi = 0$, and thus we shall often characterize a surface only by its reactances.

The scalar Helmholtz equation in cylindrical (transverse) coordinates

$$\nabla_t^2 \psi(\rho, \phi) + k_c^2 \psi(\rho, \phi) = 0, \tag{B.22}$$

has solutions of the form

$$\psi(\rho, \phi) \propto J_m(k_c \rho) \begin{matrix} \cos \\ \sin \end{matrix} m\phi \tag{B.23}$$

where ψ can be E_z or H_z. Thus, for a specific solution, i, we have

$$E_z(\rho, \phi) = j a_i J_m(k_c \rho) \begin{matrix} \cos \\ \sin \end{matrix} m\phi \tag{B.24}$$

$$H_z(\rho, \phi) = \pm j Y_0 \gamma a_i J_m(k_c \rho) \begin{matrix} \sin \\ \cos \end{matrix} m\phi, \tag{B.25}$$

from which it follows that

$$\gamma = Z_0 \frac{H_z(\rho, \phi)}{E_z(\rho, \phi - \frac{\pi}{2m})}, \tag{B.26}$$

the so-called *hybrid factor* which measures the ratio of longitudinal E- and H-fields. Z_0 and Y_0 are the free space impedance and admittance, respectively. The hybrid factor has slightly different definitions in the literature [99, 129, 130]. The one employed here is that of [129]. The factor j on both E_z and H_z is chosen to ensure that the *transverse* field components are real for the propagating lossless case (see Eq. (B.15)).

If the hybrid factor is zero, we have a pure TM solution, if it is infinite, we have a pure TE solution. Anything in between is a hybrid mode, with nonzero longitudinal components of both the electric and the magnetic field. If the hybrid factor is positive, we denote the solution a HE hybrid mode, and if negative, an EH hybrid mode [129]. In order to determine the constants γ and k_c, we find the transverse components from (B.15) and insert into the boundary conditions (B.21). The transverse gradient operator in cylindrical coordinates is

$$\nabla_t \psi = \hat{\boldsymbol{\rho}} \frac{\partial \psi}{\partial \rho} + \hat{\boldsymbol{\phi}} \frac{1}{\rho} \frac{\partial \psi}{\partial \phi} \tag{B.27}$$

and thus the transverse components of the field found from (B.15) are

$$E_\rho = \frac{j}{k_c^2} \left(-\omega\mu \frac{1}{\rho} \frac{\partial H_z}{\partial \phi} - \beta \frac{\partial E_z}{\partial \rho} \right) \tag{B.28}$$

$$E_\phi = \frac{j}{k_c^2} \left(\omega\mu \frac{\partial H_z}{\partial \rho} - \frac{\beta}{\rho} \frac{\partial E_z}{\partial \phi} \right) \tag{B.29}$$

$$H_\rho = \frac{j}{k_c^2} \left(\omega\epsilon \frac{1}{\rho} \frac{\partial E_z}{\partial \phi} - \beta \frac{\partial H_z}{\partial \rho} \right) \tag{B.30}$$

$$H_\phi = \frac{j}{k_c^2} \left(-\omega\epsilon \frac{\partial E_z}{\partial \rho} - \frac{\beta}{\rho} \frac{\partial H_z}{\partial \phi} \right) \tag{B.31}$$

where we have chosen to look only at waves travelling in the positive z-direction. The above expands to

$$E_\rho = \frac{a_i}{k_c^2}\left(\gamma\frac{mk}{\rho}J_m(k_c\rho) + \beta k_c J_m'(k_c\rho)\right) \begin{matrix}\cos\\ \sin\end{matrix}\; m\phi \tag{B.32a}$$

$$E_\phi = \mp\frac{a_i}{k_c^2}\left(\gamma k k_c J_m'(k_c\rho) + \frac{m\beta}{\rho}J_m(k_c\rho)\right) \begin{matrix}\sin\\ \cos\end{matrix}\; m\phi \tag{B.32b}$$

$$H_\rho = \pm\frac{a_i}{k_c^2}Y_0\left(\frac{mk}{\rho}J_m(k_c\rho) + \gamma\beta k_c J_m'(k_c\rho)\right) \begin{matrix}\sin\\ \cos\end{matrix}\; m\phi \tag{B.32c}$$

$$H_\phi = \frac{a_i}{k_c^2}Y_0\left(k k_c J_m'(k_c\rho) + \frac{\gamma m\beta}{\rho}J_m(k_c\rho)\right) \begin{matrix}\cos\\ \sin\end{matrix}\; m\phi. \tag{B.32d}$$

The field components are now inserted into the boundary conditions (B.21). This yields two equations with two unknowns, γ and k_c:

$$\gamma = -\frac{m\beta J_m(k_c a)}{k_c a\left[jk_c J_m(k_c a)z_\phi + kJ_m'(k_c a)\right]} \tag{B.33a}$$

$$\gamma = -k_c a\frac{jk_c J_m(k_c a) + z_z k J_m'(k_c a)}{m\beta z_z J_m(k_c a)}, \tag{B.33b}$$

where $z_z = Z_z/Z_0$ and $z_\phi = Z_\phi/Z_0$ are normalized surface impedances. By equating the two, γ is eliminated, and after some manipulations, we are left with a transcendental equation for k_c:

$$\begin{aligned} &jJ_m^2(k_c a)\left[z_z\frac{m^2}{(k_c a)^2}\left(\frac{k_c^2}{k^2}-1\right) - z_\phi\frac{k_c^2}{k^2}\right] \\ &\qquad + jJ_m'^2(k_c a)z_z - J_m(k_c a)J_m'(k_c a)\frac{k_c}{k}\left[z_z z_\phi + 1\right] = 0. \end{aligned} \tag{B.34}$$

To obtain modal solutions, the equation is solved numerically for the cutoff wavenumber, k_c, for each free space wavenumber, k.

By multiplying with k^2, we can obtain an alternate form, which is a simple quadratic equation in the wavenumber, k:

$$\begin{aligned} &k^2\left\{J_m'^2(k_c a) - J_m^2(k_c a)\frac{m^2 z_z}{(k_c a)^2}\right\} \\ &\quad + k\left\{jJ_m(k_c a)J_m'(k_c a)k_c\left[z_\phi + 1\right]\right\} \\ &\quad + k_c^2 J_m(k_c a)\left\{\frac{m^2 z_z}{(k_c a)^2} - z_\phi\right\} = 0, \end{aligned} \tag{B.35}$$

This equation can be solved exactly for a range of k_c values, yielding zero, one, or two real solutions for k. Thus, we do not need a numerical root finding algorithm as we do if we fix k_c and find k. However, problems arise in some situations. E.g. for the PEC or PMC walled guide, where the characteristic equation reduces to

$$J_m(k_c a)J_m'(k_c a) = 0, \tag{B.36}$$

which implies either that $J_m(k_c a) = 0$ or $J_m'(k_c a) = 0$, independently of k. I.e. pure TM and TE mode solutions, respectively. This situation must be handled separately if we solve for k. Once a solution set of k, k_c has been found, the hybrid factor can be evaluated from one of Equations (B.33).

B.2.1 The Balanced Hybrid Condition

Instead of equating, we can take the product of the two Equations (B.33) for the hybrid factor to obtain

$$\gamma^2 = \frac{z_z k J_m'(k_c a) + j k_c Jm(k_c a)}{z_z k J_m'(k_c a) + z_z z_\phi j k_c J_m(k_c a)}, \tag{B.37}$$

from which it is evident, that if $z_z z_\phi = 1$, then $\gamma = \pm 1$ independently of k and k_c — the so-called *balanced hybrid condition.* This is also true if $z_\phi = 0$ and z_z approaches infinity, which is the case with a corrugated surface at resonance.

Let $\gamma = +1$ in Equations (B.32), and at the same time let the phase constant, β, equal the free space wavenumber, k. Then E_ρ and E_ϕ will have the same ρ dependence, which we can denote

$$F(\rho) = \frac{a_i}{k_c^2}\left(\frac{mk}{\rho} J_m(k_c\rho) + k k_c J_m'(k_c\rho)\right). \tag{B.38}$$

The H-field components also have this ρ dependence, apart from a factor free space admittance, i.e.

$$E_\rho = F(\rho) \begin{array}{c}\cos\\ \cdot\\ \sin\end{array} m\phi \tag{B.39a}$$

$$E_\phi = \mp F(\rho) \begin{array}{c}\sin\\ \cos\end{array} m\phi \tag{B.39b}$$

$$H_\rho = \pm Y_0 F(\rho) \begin{array}{c}\sin\\ \cos\end{array} m\phi \tag{B.39c}$$

$$H_\phi = Y_0 F(\rho) \begin{array}{c}\cos\\ \sin\end{array} m\phi., \tag{B.39d}$$

which means that the field will have the same taper in all directions, and for $m = 1$, the field lines will be purely x- or y-directed:

$$\mathbf{E}_t = F(\rho) \begin{array}{c}\hat{\boldsymbol{x}}\\ \hat{\boldsymbol{y}}\end{array} \tag{B.40}$$

$$\mathbf{H}_t = \pm Y_0 F(\rho) \begin{array}{c}\hat{\boldsymbol{y}}\\ \hat{\boldsymbol{x}}\end{array}. \tag{B.41}$$

This is the desirable property of the balanced HE_1 mode which is often sought in corrugated horns. In radially corrugated horns, the phase constant, β, is not equal to k, but very parallel field lines can still be achieved over most of the aperture. In a hard horn or waveguide, β *can* be equal to k, and the field lines are in principle totally linear.

The opposite case, namely $\gamma = -1$, is also called a balanced condition. However, the EH modes in this case clearly do not exhibit the desirable property of the HE modes.

B.2.2 Numerical Implementation

In order to generate dispersion plots, we can solve either (B.34) for k_c or (B.35) for k. Solving the quadratic equation for k is definitely easier. However, we do not have control over which frequencies are covered in the resulting (k, k_c) pairs. We can only choose a range of k_c and hope for the best. When solving the transcendental Equation (B.34) instead, we have control over which k's we choose. However, robustly finding the k_c values which satisfy the equation — and thereby the boundary conditions — is quite tricky, especially for certain impedance values.

Solving a Quadratic Equation for k

We make a list of cutoff wavenumber values, k_c. The list consists of values from zero to the maximum desired k that we want to plot. Also purely imaginary values of k_c are included in the same interval. The imaginary values of k_c correspond to possible slow waves where the phase constant, $\beta = \sqrt{k^2 - k_c^2}$, is larger than k. For each k_c in the list, Equation (B.35) is solved for k. This results in zero, one, or two real solutions. Only real k values larger than the corresponding k_c value are usable, or for imaginary k_c, k values larger than zero. To illustrate this, a set of (k, k_c) pairs are plotted in Figure B.1(a), where only points above the black line are usable. Figure B.1(b) shows the corresponding dispersion diagram.

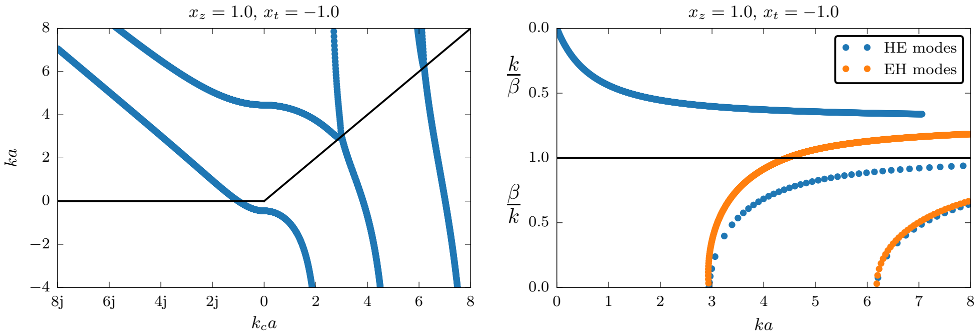

(a) (b)

Figure B.1: Waveguide with wall impedances $Z_z = Z_0 j$, $Z_\phi = -Z_0 j$. (a): k values found from a list of k_c values. Only points above the black line are usable. (b): Dispersion plot from accepted (k, k_c) pairs. Here the black line is the light line.

Solving Transcendental Equation for k_c

In this method, we solve Equation (B.34) directly using a numerical zero finding algorithm. The equation is solved for each k of interest, yielding a list of k_c's for which the equation is satisfied, corresponding to supported modes at that frequency. In order to find the zeros more robustly, zeros are first found in the analytical derivative of the characteristic equation. The zeros of the original equation must lie between zeros of the derivative. This helps for certain impedances where the characteristic equation has minima very close to the axis, where there can be zero, one, or two solutions, depending on whether it crosses the line. The dispersion characteristics of impedance waveguides used examined in Chapter 6 are calculated by this method.

B.3 Circular Waveguides with PEC wall

The following are some formulas pertaining a standard circular waveguide with PEC walls.

B.3.1 Fields in the Guide

As previously mentioned, the boundary conditions in a PEC waveguide can be satisfied by purely TE and TM modes. The tangential E-field for modes in a circular

PEC waveguide are given below. The fields are normalized such that they carry the same power as in [80].

$$\begin{aligned}\mathbf{e}_{mn}^{TM} =& \sqrt{\frac{\varepsilon_m}{\pi}}\frac{1}{|J_{m+1}(\chi_{mn})|}\left[-\hat{\boldsymbol{\rho}}\frac{J_m'\left(\frac{\chi_{mn}\rho}{a}\right)}{a}\begin{matrix}\cos\\ \sin\end{matrix}\ m\phi\right.\\ &\left.\pm\hat{\boldsymbol{\phi}}\frac{m}{\chi_{mn}}\frac{J_m\left(\frac{\chi_{mn}\rho}{a}\right)}{\rho}\begin{matrix}\sin\\ \cos\end{matrix}\ m\phi\right],\end{aligned} \tag{B.42a}$$

$$\begin{aligned}\mathbf{e}_{mn}^{TE} =& \sqrt{\frac{\varepsilon_m}{\pi}}\frac{1}{\sqrt{\chi_{mn}'^2-m^2}\,|J_m(\chi_{mn}')|}\left[\mp\hat{\boldsymbol{\rho}}m\frac{J_m\left(\frac{\chi_{mn}'\rho}{a}\right)}{\rho}\begin{matrix}\cos\\ \sin\end{matrix}\ m\phi\right.\\ &\left.+\hat{\boldsymbol{\phi}}\chi_{mn}'\frac{J_m'\left(\frac{\chi_{mn}'\rho}{a}\right)}{a}\begin{matrix}\sin\\ \cos\end{matrix}\ m\phi\right].\end{aligned} \tag{B.42b}$$

The constants ε_m take the values

$$\varepsilon_m = \begin{cases}1, & m=0\\ 2, & m\neq 0\end{cases}. \tag{B.43}$$

while χ_{mn} is the nth non-vanishing root of the mth order Bessel function, $J_m(\chi)$, and equivalently for χ_{mn}', but for the derivative of the Bessel function, $J_m'(\chi)$.

For $m > 0$, the full expansion in (B.42) contains two variants of each TE_{mn} and TM_{mn} mode, corresponding to the top and bottom choices. For instance, the fundamental TE_{11} mode exists in both an x-polarized and an y-polarized version. The modes corresponding to the top choice in (B.42) are denoted as the 1st set, whereas the modes corresponding to the bottom choice are denoted the 2nd set.

The cutoff wavenumber of a circular waveguide mode is

$$k_c = \frac{\chi}{a} \tag{B.44}$$

$$\tag{B.45}$$

where χ is either χ_{mn} or χ_{mn}' mentioned above. The phase constant follows as in the general waveguide case

$$\beta = \sqrt{k^2 - k_c^2} \tag{B.46}$$

in which k is the free space wavenumber. The cutoff frequency, f_c, is the frequency below which β is imaginary and the amplitude of the wave decays exponentially, i.e.

$$f_c = \frac{ck_c}{2\pi}. \tag{B.47}$$

where c is the speed of light. The first fifteen modes sorted by ascending cutoff wavenumber/frequency is listed in Table B.1. The first nine modes of the 1st and 2nd set are plotted in Figures B.2 and B.3, respectively.

B.3.2 Orthogonality

Orthogonality and normality of the modal basis functions can be expressed as

$$\int_S \mathbf{e}_i\cdot\mathbf{e}_j ds = \int_S \mathbf{h}_i\cdot\mathbf{h}_j ds = \begin{cases}0 & \text{for } j\neq i\\ 1 & \text{for } j = i\end{cases} \tag{B.48a}$$

$$\int_S \mathbf{e}_i\cdot\mathbf{h}_j ds = 0 \quad \forall\ i,j \tag{B.48b}$$

where S is the waveguide cross section and $\mathbf{h}$ are the corresponding modal H-fields to the normalized E-fields.

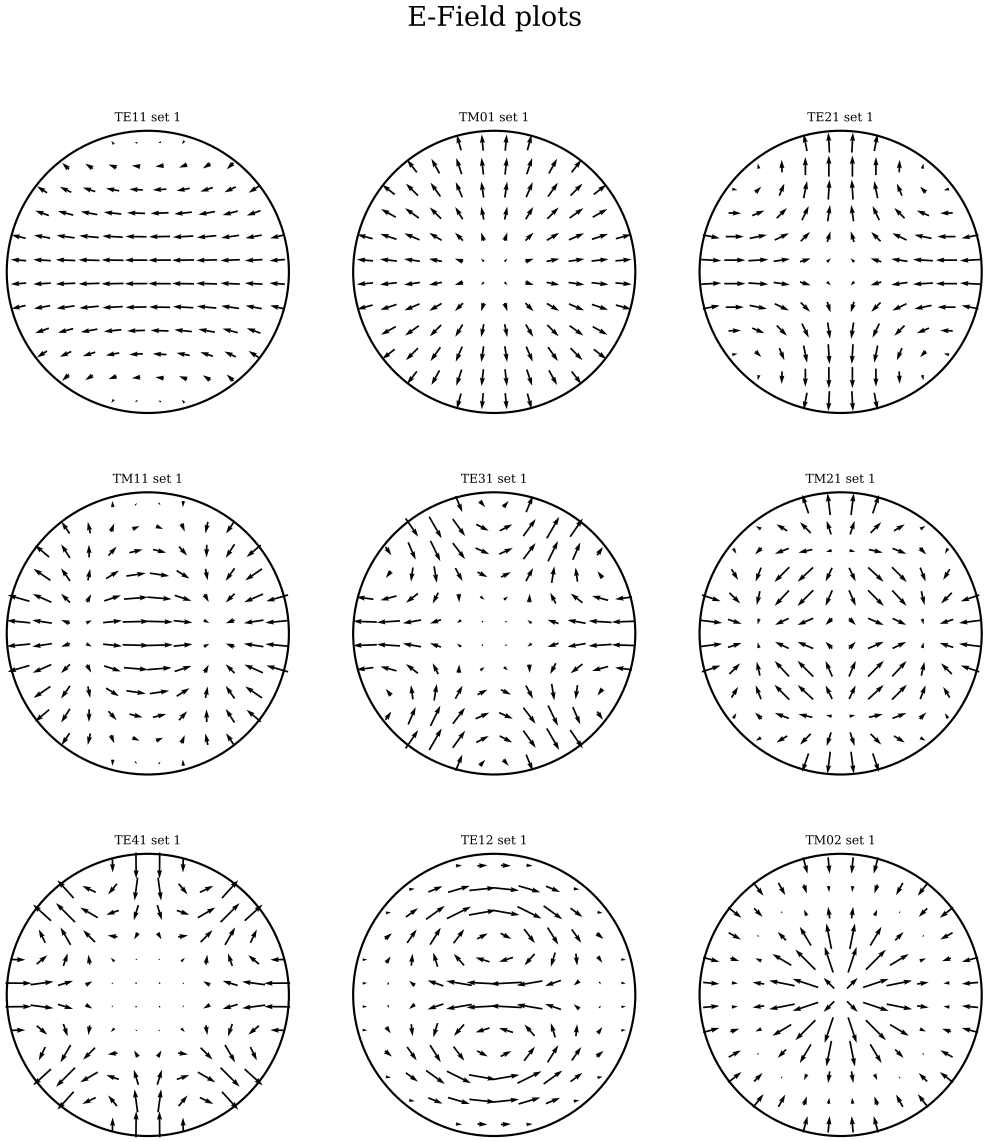

Figure B.2: The first 9 modes of the *first set* sorted by cutoff wavenumber (see Table B.1).

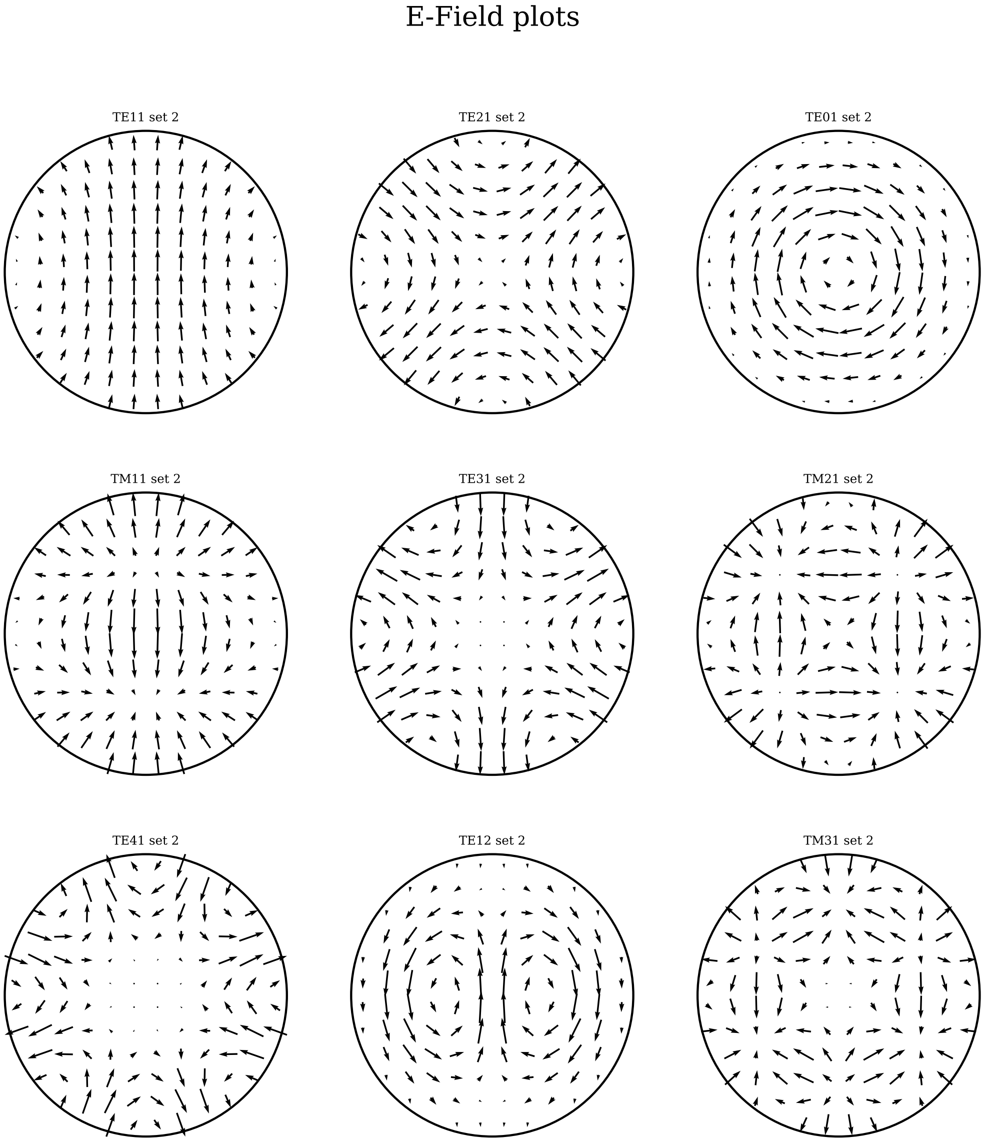

Figure B.3: The first 9 modes of the *second set* sorted by cutoff wavenumber (see Table B.1).

Mode	$\frac{k_c}{k_{c,\min}}$		
TE_{11}	1.000	TE_{12}	2.896
TM_{01}	1.306	TM_{02}	2.998
TE_{21}	1.659	TM_{31}	3.465
TE_{01}	2.081	TE_{51}	3.485
TM_{11}	2.081	TE_{22}	3.642
TE_{31}	2.282	TE_{02}	3.810
TM_{21}	2.789	TM_{12}	3.810
TE_{41}	2.888		

Table B.1: First 15 circular waveguide modes sorted by cutoff wavenumber/frequency. The wave numbers are normalized with respect to the smallest wavenumber, i.e. that of the fundamental mode.

B.3.3 Fields Radiated From Open Ended Waveguide

The fields radiated from a circular waveguide is calculated in [76] by analytically integrating the electric field of each mode in the waveguide aperture. The electric aperture field of a mode is assumed to be a sum of the incident wave electric field and a reflected part of the same mode:

$$E_t = (1+\Gamma)E_t^i, \tag{B.49}$$

where E_t is the total tangential E-field and E_t^i is that of the incident wave. The resultant far-fields are reproduced here, but with two lines, corresponding to the two degenerate versions of each mode, set 1 and set 2. Radiation from the TE modes becomes

$$\begin{aligned} E_\theta^{\mathrm{TE}} &= \mp j^{m+1}\frac{m\omega\mu}{2R}\left[1+\frac{\beta'_{mn}}{k}\cos\theta+\Gamma\left(1-\frac{\beta'_{mn}}{k}\cos\theta\right)\right] \\ &\qquad J_m(\chi'_{mn})\frac{J_m(ka\sin\theta)}{\sin\theta}\begin{matrix}\cos\\ \sin\end{matrix}\, m\phi\exp(-jkR) \end{aligned} \tag{B.50a}$$

$$\begin{aligned} E_\phi^{\mathrm{TE}} &= j^{m+1}\frac{ka\omega\mu}{2R}\left[\frac{\beta'_{mn}}{k}+\cos\theta-\Gamma\left(\frac{\beta'_{mn}}{k}-\cos\theta\right)\right] \\ &\qquad \frac{J_m(\chi'_{mn})J'_m(ka\sin\theta)}{1-\left(\frac{ka\sin\theta}{\chi'_{mn}}\right)^2}\begin{matrix}\sin\\ \cos\end{matrix}\, m\phi\exp(-jkR). \end{aligned} \tag{B.50b}$$

The upper and lower choices correspond to the 1st and 2nd set, respectively, as in Equation (B.42). And equivalently for TM modes:

$$\begin{aligned} E_\theta^{\mathrm{TM}} &= \pm j^{m+1}\frac{k\chi_{mn}}{2R\sin\theta}\left[\frac{\beta_{mn}}{k}+\cos\theta+\Gamma\left(\frac{\beta_{mn}}{k}-\cos\theta\right)\right] \\ &\qquad \frac{J_m(ka\sin\theta)J'_m(\chi_{mn})}{1-\left(\frac{\chi_{mn}}{ka\sin\theta}\right)^2}\begin{matrix}\cos\\ \sin\end{matrix}\, m\phi\exp(-jkR) \end{aligned} \tag{B.51a}$$

$$E_\phi^{\mathrm{TM}} = 0. \tag{B.51b}$$

For the calculations performed during the optimization in Section 3.2, it is assumed that there is no reflection at the waveguide aperture, namely

$$\Gamma = 0. \tag{B.52}$$

It may be noted that the radiated fields from waveguide modes of the same m-index and same set are not orthogonal as they are inside the waveguide. In practise, this means that the total field must be renormalized every time we evaluate the spillover efficiency in Section 3.2.

APPENDIX C

Papers

C.1 Paper 1

OPTIMIZATION PROCEDURE FOR WIDEBAND MATCHED FEED DESIGN

Michael Forum Palvig, Erik Jørgensen, Peter Meincke, and Olav Breinbjerg

Status: Presented April 2016.

Bibliography

[P1] M. F. Palvig, E. Jørgensen, P. Meincke, and O. Breinbjerg. “Optimization Procedure for Wideband Matched Feed Design”. In: *The 10th European Conference on Antennas and Propagation (EuCAP 2016).* Davos, Switzerland, Apr. 2016.

Optimization Procedure for Wideband Matched Feed Design

Michael Forum Palvig[1,2], Erik Jørgensen[2], Peter Meincke[2], Olav Breinbjerg[1]
[1]Department of Electrical Engineering, Electromagnetic Systems, Technical University of Denmark, Kgs. Lyngby, Denmark
[2]TICRA, Copenhagen, Denmark

***Abstract*—The inherently high cross polarization of prime focus offset reflector antennas can be compensated by launching higher order modes in the feed horn. Traditionally, the bandwidth of such systems is in the order of a few percent. We present a novel design procedure where the entire matched feed and reflector system can be efficiently optimized. This allows the design parameters of the matched feed to be directly related to the desired design goals in the secondary pattern over a specified band. Using this procedure, we present a design of a die-castable axially corrugated matched feed horn that provides an XPD improvement better than 7 dB over a 12% bandwidth for a reflector with an f/D of 0.5. An investigation of the mode requirement for an arbitrary circular aperture feed is also presented.**

***Index Terms*—matched feed, reflector antenna, horn antenna, optimization, antenna modelling.**

I. INTRODUCTION

Offset parabolic reflector antennas suffer from high cross polarization compared to their symmetric counterparts. On the other hand, they are very attractive in terms of avoiding feed and strut blockage. The cross polarization arises from tilting the otherwise perfectly polarized feed antenna away from the paraboloid apex. A solution to this was proposed by Rudge and Adatia in 1975 [1]. The idea is to use a non-perfectly polarized feed that has exactly the cross polarization that will cancel the one introduced by the asymmetry of the antenna system.

Rudge and Adatia examine the antenna in receiving mode of a plane wave from boresight. The focal region field in this situation was described some years earlier by Bem [2]. They find that this field can be approximately matched by the addition of the TE_{21} mode in a circular feed, the HE_{21} in a radially corrugated feed, or the TE_{11} mode in a rectangular feed. Their practical implementation is a Potter horn [3] with a TE_{21} mode launcher consisting of two pins inserted into the waveguide. There are many variations in the literature with pyramidal horns [4], corrugated horns [5], and feed arrays [6]. Mode launchers are usually some variation of either a pin/post in the waveguide or a slot/stub, but other concepts like exciting the higher order mode in the outer region of a coaxial horn [7] or a series of non-concentric irises [8] have also been published.

The challenge for designing a matched feed system is the bandwidth. The mode generation and mode propagation along a waveguide are dispersive phenomena and thus, performance of these feeds quickly deteriorate when the frequency moves away from the design frequency. To improve this, the full desired frequency band must be included in the design optimizations.

II. REQUIRED MODES FOR MATCHED CONDITION

As mentioned in the previous section, the fact that the required extra circular waveguide mode is TE_{21}, is usually justified from the focal region fields when a plane wave is incident on the reflector [1] (described in more detail in [9]). The method gives a good indication of the solution to the problem, but is not strictly rigorous. In principle, the procedure should be repeated for all angles of incidence within the main beam, and how should these different focal region fields be combined when designing the feed? Also, the focal field will have ringing effects due to the abrupt truncation of the reflector aperture field which cannot be reproduced with the feed.

In this paper, we validate the use TE_{21} for matched feeds by a more rigorous procedure. We let a circular aperture with a combination of waveguide modes illuminate the offset reflector. The mode coefficients, aperture size, and aperture pointing is then optimized to yield a satisfactory field distribution in the reflector aperture. Given that the definition of a satisfactory aperture field is judiciously chosen, this method will yield a *good* overall antenna. The figure of merit is chosen as

$$F = \eta_A \eta_s - K_{cr}\mathcal{E}_{cr}, \tag{1}$$

where η_A and η_s are the aperture and spillover efficiencies, respectively. K_{cr} is a constant weighing the importance of the *cross-polar aperture error*, $\mathcal{E}_{cr}$, defined as

$$\mathcal{E}_{cr} = \frac{\iint_A |E_{cr}|^2\, dA}{\iint_A (|E_{co}|^2 + |E_{cr}|^2) dA}, \tag{2}$$

with A being the projected aperture of the reflector. Maximizing the aperture and spillover efficiencies results in high gain, and minimising $\mathcal{E}_{cr}$ will enforce uniform polarization in the aperture and thus low cross polarization in the far-field. For a good antenna, a compromise between these goals must be made. Here, we maximize F for a chosen $K_{cr} = 10$, which is found experimentally to be a good compromise. The parameters to the optimization are complex excitation coefficients to a spectrum of radiating waveguide modes, as well as the aperture radius and tilt angle. The radiated field from a given mode is computed using numerically power normalized formulas from [10].

We let the antenna be offset in the vertical direction. Fig. 1 shows the optimized mode amplitudes as a function of f/D for the two polarizations. Superscripts denote the two degenerate modes for an m, n pair, i.e. TE_{11}^2 is a $90°$ rotated version of TE_{11}^1 and TE_{21}^2 is a $45°$ rotated version of TE_{21}^1. The regular co-polar part of the feed signal is seen as a combination of the fundamental TE_{11} mode and the TM_{11} mode as in the Potter horn. The required cross-polar part can be obtained by inclusion of TE_{21}, but can be improved by also including TM_{01} or TE_{01} for vertical and horizontal polarization, respectively. This fact is most often neglected. In fact, the TE_{21} mode can be left out, and TE_{01} and TM_{01} used instead. However, good results can also be obtained without the $m = 0$ modes, but more TE_{21} is then needed. In the following we shall focus on designing a matched feed based on TE_{21} generation, but a future investigation may show that feeds with TM_{01} and TE_{01} are just as good or better.

The drawback of the mode optimization technique is that it is hard to control where the optimization finds a maximum, and the maximum may not be the global maximum. For this reason, the curves in Fig. 1 are not smooth. However, for all f/D values, the plotted mode combination provides a satisfactory reflector aperture distribution with nearly parallel field lines.

III. REFLECTOR-FEED OPTIMIZATION

The GRASP software tool [11] offers highly accurate and efficient Physical Optics (PO) as well as Method of Moments (MoM) implementations. The latter is combined with the former in a domain decomposition technique [12] to jointly optimize feed-reflector systems. The interior of the feed itself can be split up into several *devices*. Generalized scattering matrices are computed for the waveguide ports of each device. Devices can then be cascaded to obtain a combined scattering matrix of the entire feed. Scattering matrices are computed using either 3D MoM, Body of Revolution (BoR) MoM, or Mode Matching techniques. The analysis method does not have to be the same for the different devices.

For radiation analysis, the interior scattering matrices of the horn are coupled to the exterior geometry using MoM. Rigorous coupling to the reflector is achieved through either PO or MoM/MLFMM. The final cascaded system can be used to calculate the field at any point given an arbitrary waveguide excitation.

When changing one variable of the antenna system, only the scattering matrices dependent on this variable need to be recomputed before cascading to obtain the entire antenna scattering matrix. This is very useful for optimization purposes and means that intermediary optimisation goals, like phase edge taper and beam width of the feed can be skipped, and the antenna system can be directly optimized based on the final far-field goals. By avoiding these indirect quantities, a better compromised design can be found over a larger bandwidth. These properties have been used in the matched feed design described in the following section.

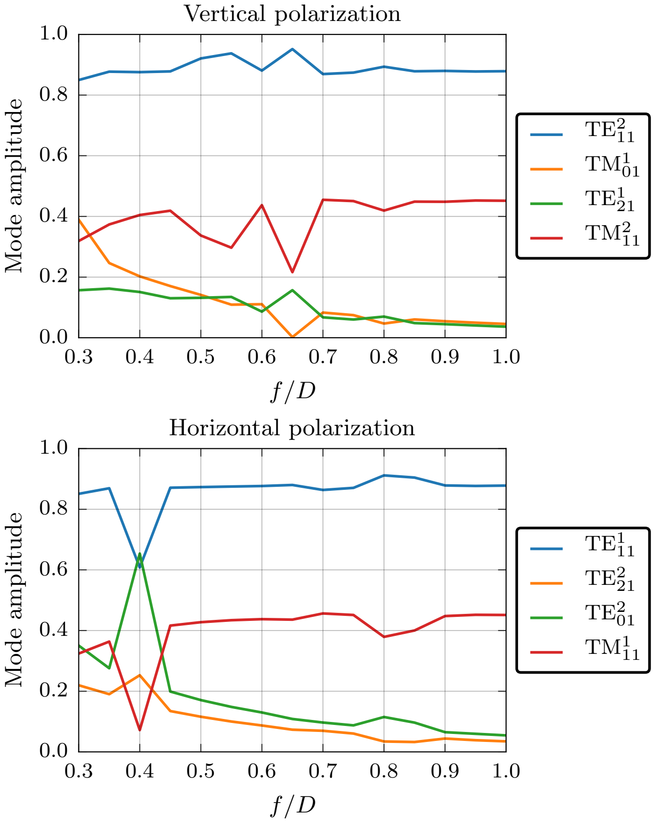

Fig. 1. Optimized mode content as a function of f/D. Superscripts enumerate the two degenerate field solutions for each mode type.

IV. AXIALLY CORRUGATED MATCHED FEED

Using the general mode guidelines of Section II and the tool described in Section III, a matched feed has been designed. The design is based on the axially corrugated horn. This feed type can be optimized to have good cross-polar performance over a reasonable bandwidth, and is much simpler to fabricate than the radially corrugated horn, as well as being shorter and lighter. The fact that the horn is short is also a desirable property when it comes to matched feeds or multimode feeds in general, because different modes have different phase velocities in the waveguide. The phase velocity of each mode is dependent on frequency and thus, the longer a waveguide or horn, the more sensitive the phase relationship between modes is to frequency.

The goal is to make a feed which reduces cross polarization for both linear polarizations in frequency band $27.5\,\mathrm{GHz}$ to $31\,\mathrm{GHz}$. This constitutes a relative bandwidth of $12\,\%$ which is considerable in the context of matched feeds. The feed will illuminate an $f = 0.25\,\mathrm{m}$ parabolic reflector with a $D = 0.5\,\mathrm{m}$ circular aperture diameter and an offset clearance of $D' = 0.05\,\mathrm{m}$.

The design will be carried out in the following four steps:

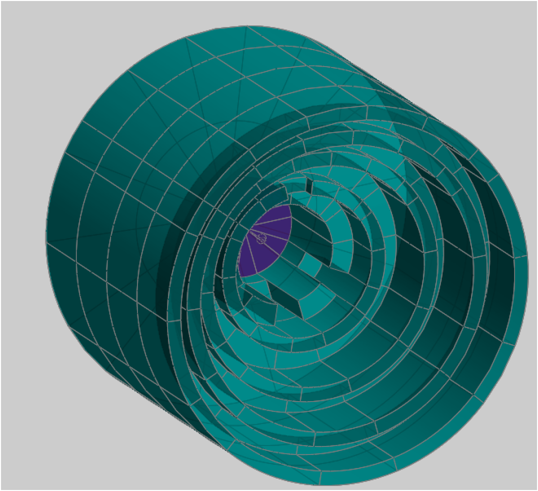

Fig. 2. Axially corrugated horn with modifications for matching. Radius of input waveguide is 3.5 mm and aperture radius is 12.3 mm.

1) A standard axially corrugated horn is optimized in CHAMP [13] to illuminate the given reflector with low feed cross polarization over the band.
2) The feed is imported into GRASP. Mode converting elements are added and scattering parameters are optimized over the band to approximately generate the amount of TE_{21} given in Fig. 1.
3) Mode converting elements are optimized, minimising the far-field maximum cross-polar level, while keeping the directivity intact.
4) All horn parameters are optimized.

A. Mode Conversion

In order to transfer some energy into the TE_{21} mode, a part of the geometry must be rotationally asymmetric. We have chosen to make asymmetries that preserve the ability to die-cast the horn. The chosen artefacts are cutouts, or chips, in the corrugation ridges as shown in Fig. 2. The innermost corrugation of the depicted horn has zero slot width/depth and thus collapses to a step. Likewise, the chips can be viewed as slots.

The middle chip or slot in each corrugation generates the proper TE_{21} from the horizontally polarized fundamental mode and the two slots on either side generate TE_{21} for the vertically polarized fundamental mode.

The principle of the horn and mode launcher is very similar to that of a Eutelsat patent [14].

B. Results

The cross-polar level for both linear polarizations is shown in Fig. 3 over the band. A cross-polar reduction better than 7 dB is achieved over the 12 % frequency bandwidth. A graphical representation of the feed and reflector is shown in Fig. 4. Pattern cuts for both polarizations at one frequency are shown in Fig. 5. The cuts are in the horizontal plane where the cross-polar level is largest in this case (but not necessarily in general). There are still many variations to the mode launcher that one might try in order to get a larger improvement and/or larger bandwidth.

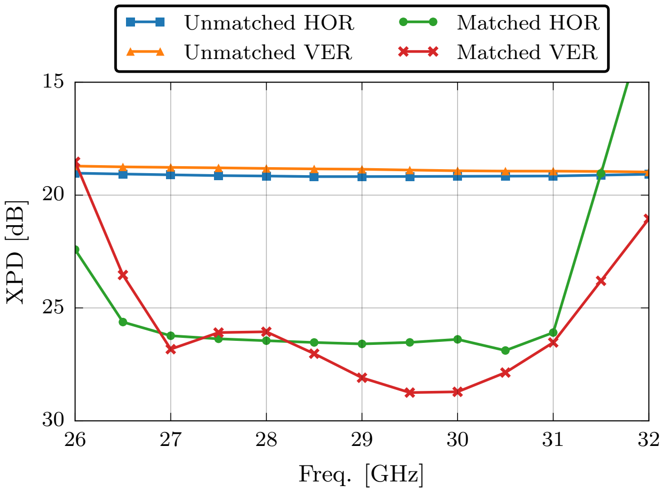

Fig. 3. Cross-polar discrimination (referenced to peak directivity) of the matched feed reflector system compared to unmatched as a function of frequency.

V. CONCLUSION

An alternative investigation of the waveguide modes required for matched feed operation has been presented. It is confirmed that the addition of the correct TE_{21} mode to an otherwise low cross polarization feed can provide the required compensation. However, it is also shown that TE_{01} and TM_{01} can be used alone or in conjunction with TE_{21}.

A versatile, efficient, and accurate design tool for combined reflector and feed optimization has been presented. This allows generalized scattering matrices computed with BoR-MoM, 3D MoM, or Mode matching to be accurately coupled to a PO or MoM/MLFMM solution of the reflector setup.

Finally, the tool has been used to design a matched feed based on an axially corrugated horn. The feed is modified by putting chips/slots in the corrugations of the horn. An XPD improvement better than 7 dB is achieved over the 12 % design frequency band.

REFERENCES

[1] A. W. Rudge and N. A. Adatia, “New class of primary-feed antennas for use with offset parabolic-reflector antennas,” *Electronics Letters*, vol. 11, no. 24, pp. 597–599, 1975.

[2] D. J. Bem, “Electric-field distribution in the focal region of an offset paraboloid,” *Proceedings of the Institution of Electrical Engineers*, vol. 116, no. 5, pp. 679–684, 1969.

[3] P. D. Potter, “A New Horn Antenna with Suppressed Sidelobes and Equal Beamwidths,” *Microwave Journal*, vol. 6, no. 6, pp. 71–78, 1963.

[4] S. B. Sharma, D. A. Pujara, S. B. Chakrabarty, and V. K. Singh, “Improving the Cross-Polar Performance of an Offset Parabolic Reflector Antenna Using a Rectangular Matched Feed,” *IEEE Antennas and Wireless Propagation Letters*, vol. 8, pp. 513–516, 2009.

[5] C. Yang, J. Yu, Y. Yao, X. Liu, and X. Chen, “Novel Corrugated Matched Feed for Cross-Polar Cancellation in Tri-Reflector Compact Range,” *IEEE Antennas and Wireless Propagation Letters*, vol. 13, pp. 1003–1006, 2014.

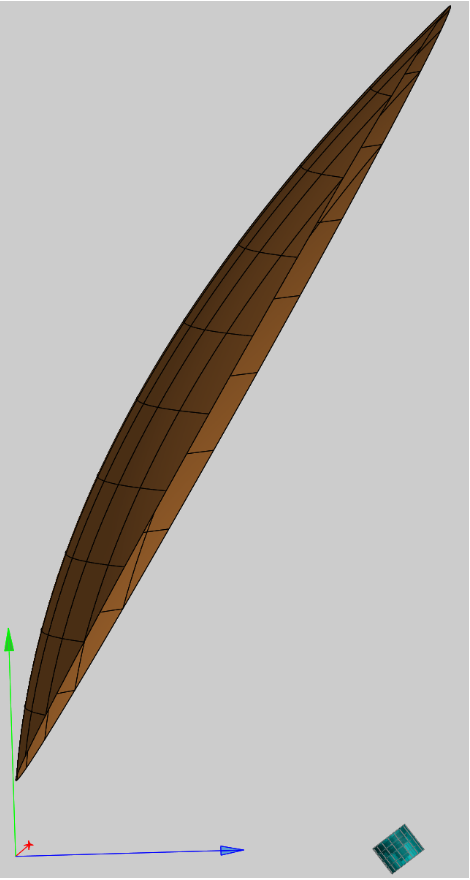

Fig. 4. Model of the entire antenna with $f/D = 0.5$.

- [6] S. M. Tun and P. J. B. Clarricoats, "Single offset reflector with a matched-feed array," in *IEEE Antennas and Propagation Society International Symposium*, 1984, pp. 486–489.
- [7] Z. A. Pour and L. Shafai, "A Ring Choke Excited Compact Dual-Mode Circular Waveguide Feed for Offset Reflector Antennas," *IEEE Transactions on Antennas and Propagation*, vol. 60, no. 6, pp. 3011–3015, 2012.
- [8] R. Dey, S. B. Chakrabarty, and R. Jyoti, "Broadband Conjugate Matched Feed Horn- A Novel Concept," *IEEE Antennas and Wireless Propagation Letters*, no. 99, pp. 1–1, 2015.
- [9] A. W. Rudge and N. A. Adatia, "Offset-parabolic-reflector antennas: a review," *Proceedings of the IEEE*, vol. 66, no. 12, pp. 1592–1618, 1978.
- [10] J. R. Risser, "Waveguide and Horn Feeds," in *Microwave Antenna Theory and Design*, ser. MIT Radiation Laboratory Series. McGraw-Hill, 1949, no. 12.
- [11] "GRASP Software," TICRA, Copenhagen, Denmark, *www.ticra.com*.
- [12] E. Jørgensen, P. Meincke, and M. Sabbadini, "Fast and accurate design tool for rotationally symmetric reflector antennas with 3d waveguide components and support structures," in *Proc. 34th ESA Antenna Workshop, Noordwijk, The Netherlands*, 2012.
- [13] "CHAMP Software," TICRA, Copenhagen, Denmark, *www.ticra.com*.
- [14] D. Tits, "Low cost high performance antanna for use in transmit/receive satellite terminals." Patent EP1 278 266B1, Sep., 2005.

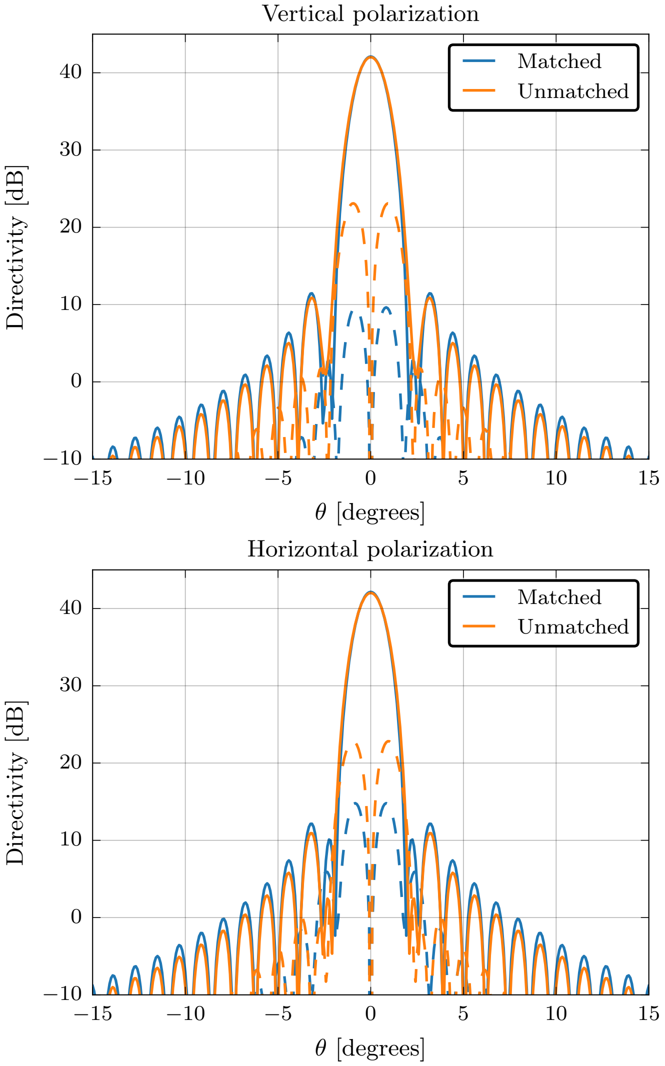

Fig. 5. Pattern cuts in the horizontal plane for the matched and unmatched antennas at 29.25 GHz. Solid lines and dashed lines are co- and cross-polar components, respectively.

C.2 Paper 2

Analytical Modelling of Waveguide Mode Launchers for Matched Feed Reflector Systems

Michael Forum Palvig, Erik Jørgensen, Peter Meincke, and Olav Breinbjerg

Status: Presented June 2016.

Bibliography

[P2] M. F. Palvig, O. Breinbjerg, P. Meincke, and E. Jørgensen. "Analytical Modelling of Waveguide Mode Launchers for Matched Feed Reflector Systems". In: *IEEE Antennas and Propagation Society International Symposium (AP-S 2016)*. Puerto Rico, June 2016.

Analytical Modelling of Waveguide Mode Launchers for Matched Feed Reflector Systems

Michael Forum Palvig[1,2] and Olav Breinbjerg[1]
[1]Department of Electrical Engineering
Technical University of Denmark
Kgs. Lyngby, Denmark
mpalvig@elektro.dtu.dk

Peter Meincke[2] and Erik Jørgensen[2]
[2]TICRA
Copenhagen, Denmark

***Abstract*—Matched feed horns aim to cancel cross polarization generated in offset reflector systems. An analytical method for predicting the mode spectrum generated by inclusions in such horns, e.g. stubs and pins, is presented. The theory is based on the reciprocity theorem with the inclusions represented by current sources. The model is supported by Method of Moments calculations in GRASP and very good agreement is seen. The model gives rise to many interesting observations and ideas for new or improved mode launchers for matched feeds.**

I. INTRODUCTION

Mode launchers are used in matched feeds for generating higher-order modes which create cross polarization cancelling that inherent to an offset reflector system. The invention was made by Rudge and Adatia [1] and has since received considerable attention in the literature (see e.g. [2], [3], [4]).

The mode launcher for matched feeds usually takes the form of pins attached to the wall of the waveguide or stubs/slots likewise along the wall. In circular symmetric horns, the mode launcher must exhibit non-circular symmetric geometry in order to excite the desired modes. Despite the mode launcher being a crucial part of the matched feed, there is very little literature explaining it's basic operation. Usually, the geometry of the mode launcher and the position of the inclusions are taken for granted and the motivation for the design is left out.

The exception is an analysis of radial pins using a Method of Moments approach with waveguide Green's functions [5]. In this paper, we develop a related, but simpler method for describing the operation of mode launchers. In essence, slots or stubs are modelled as magnetic current elements and pins are modelled as electric current elements. Using the reciprocity theorem and the orthogonality of the waveguide modes, it is possible to derive which modes are excited as well as the amplitude and phase relationships between them.

II. MODEL

Consider a waveguide with a source region containing electric and magnetic currents, $\mathbf{J}$ and $\mathbf{M}$. We do not assume a specific waveguide shape, only that we know an orthogonal eigenmode expansion of the fields. The fields from the current distribution can be found with the Green's functions associated with the waveguide shape, but since we are, in fact, not interested in the fields, we shall take the approach of [6, Sec. 4.10]. This method involves expanding the E- and H fields generated by the currents in waveguide eigenmodes and then successively using the reciprocity theorem with each mode of the expansion as the secondary field. Using field expansions as defined in [7] and including magnetic currents in the derivation, we arrive at the following expressions for mode coefficients generated by currents $\mathbf{J}$ and $\mathbf{M}$

$$C_i^{\pm} = \frac{Z_i}{2} \int_V \left(\mathbf{H}_i^{\mp} \cdot \mathbf{M} - \mathbf{E}_i^{\mp} \cdot \mathbf{J} \right) dV \tag{1}$$

where C_i^+ and C_i^- are mode coefficients of the i-th generated mode travelling in the positive and negative z-direction, respectively. $\mathbf{E}_i^{\pm}$ and $\mathbf{H}_i^{\pm}$ are unity excited E- and H-fields of the i-th mode travelling in the positive ($^+$) and negative ($^-$) z-direction. Z_i is the wave impedance of the i-th mode. Thus, the excitation coefficient of a specific mode traveling in one direction can be found simply by projecting the current onto the field of the same mode travelling in the opposite direction.

The second part of the model is the excitation of said currents which is dependent on the incident mode. The current on the pin or in the stub aperture is proportional to the projection of the incident mode fields onto the current orientation at the current position:

$$\mathbf{J} \propto (\mathbf{E}_{inc} \cdot \hat{\mathbf{c}})\hat{\mathbf{c}} \tag{2}$$

$$\mathbf{M} \propto (\mathbf{H}_{inc} \cdot \hat{\mathbf{c}})\hat{\mathbf{c}}, \tag{3}$$

where $\hat{\mathbf{c}}$ is a unit vector in the direction of the current (e.g. the orientation of the pin). This is an accurate model for electrically small inclusions.

III. APPLICATION

Using the above model we examine a longitudinal stub on a circular waveguide of radius $a = 6.3\,\mathrm{mm}$ at $30\,\mathrm{GHz}$. The waveguide is $20\,\mathrm{mm}$ long and the stub is located in the middle, as seen in Fig. 1. We model the stub as a single infinitesimal magnetic current filament located at the stub aperture, oriented in the z-direction.

We consider the two orthogonal fundamental modes as incident, namely TE_{11}^1 (x-polarized) and TE_{11}^2 (y-polarized). The ϕ-position of the stub is varied. An accurate Method of Moments (MoM) simulation of the waveguide device in GRASP [8] serves to validate the method. Fig. 2 shows the results from the model (solid line) and the MoM simulation (stars). Since the model does not predict the absolute excitation of the currents, the model results are scaled by a single complex constant. The excitation relationship between the modes is predicted by the simple model and is in very good agreement with the simulated results as can be seen in the figure.

Note that the excited modes also have two orthogonal versions (except for modes with azimuthal index $m = 0$). For a traditional matched feed with the reflector offset in the yz-plane, two TE$_{21}$ modes are needed, one for each polarization: TE$^2_{21}$ is needed for TE$^1_{11}$ operation (x-pol) and TE$^1_{21}$ is needed for TE$^2_{11}$ operation (y-pol) [9]. Thus, we want the purple curve in the top plot of Fig. 2 and the red curve in the bottom plot. It is easily deducible from the plots that this can be achieved by a stub at 90° and one at 35°. It is also straight forward to see (when looking at the phase plots) that placing an extra stub at 145° will cancel the unwanted TE$^1_{21}$ contribution for x-pol (top plot), but add constructively for y-pol (bottom plot). However, these two stubs will deduct from the desired TE$^2_{21}$ generation for x-pol. We can move them to 45° and 135° and avoid this effect or move them still further to 50° and 130° which, assuming identical stubs, is the exact point that will ensure equal generation of TE$^2_{21}$ for x-pol and TE$^1_{21}$ for y-pol.

Many other observations can be made by examining these kinds of plots. The model is approximate, but gives valuable insight into the workings of existing mode launchers and can provide ideas for improved mode launcher designs. The model can also enter into more complex optimization procedures, as it is extremely fast to evaluate. Similar simulations made with radial pins modelled as ρ-directed electric currents are omitted here due to shortage of space.

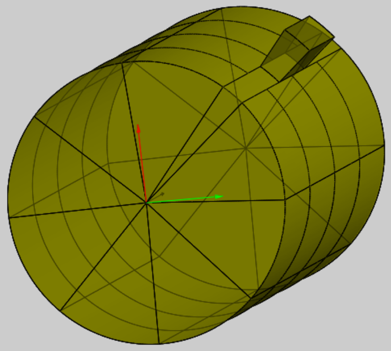

Fig. 1. MoM mesh of the mode launcher consisting of a longitudinal stub on a circular waveguide. In this picture the azimuthal position of the stub is $\phi = 45°$.

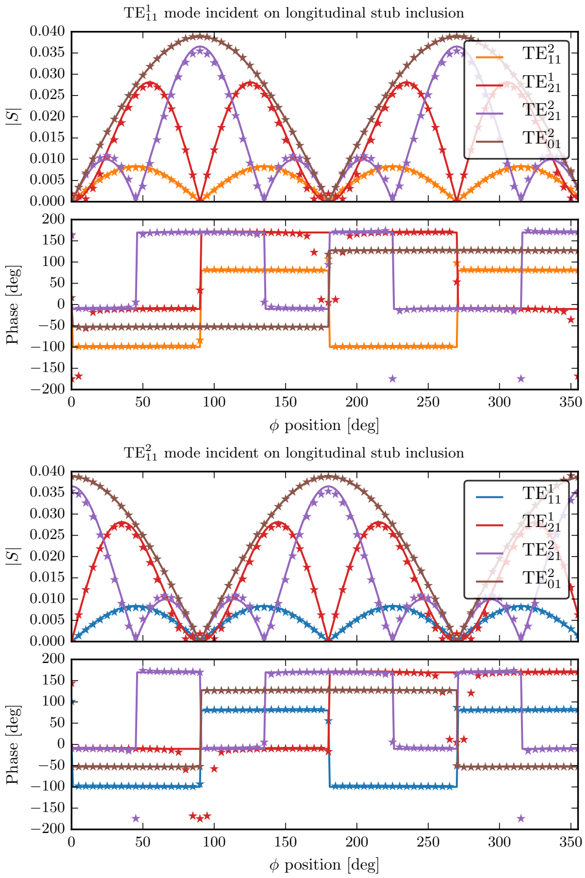

Fig. 2. Modes generated by longitudinal stub versus stub azimuthal position for x-polarized (top) and y-polarized (bottom) TE$_{11}$ incidence. Solid lines are calculations from the simple model and the stars are full wave MoM simulations from GRASP.

IV. CONCLUSION

A new model describing mode launcher operation for matched feeds is presented. It gives simple insight into previously presented designs and can form the basis of new and improved designs. An example with a longitudinal stub inclusion in a circular waveguide shows excellent agreement with full-wave simulations.

REFERENCES

[1] A. W. Rudge and N. A. Adatia, “New class of primary-feed antennas for use with offset parabolic-reflector antennas,” *Electronics Letters*, vol. 11, no. 24, pp. 597–599, 1975.

[2] B. K. Watson, A. W. Rudge, and N. A. Adatia, “Dual-Polarised Mode Generator for Cross-Polar Ccmpensation in Offset Parabolic Reflector Antennas,” *8th European Microwave Conference*, pp. 183–187, 1978.

[3] K. M. Prasad and L. Shafai, “Improving the symmetry of radiation patterns for offset reflectors illuminated by matched feeds,” *IEEE Transactions on Antennas and Propagation*, vol. 36, no. 1, pp. 141–144, 1988.

[4] K. Bahadori and Y. Rahmat-Samii, “Tri-Mode Horn Feeds Revisited: Cross-Pol Reduction in Compact Offset Reflector Antennas,” *IEEE Transactions on Antennas and Propagation*, vol. 57, no. 9, pp. 2771–2775, 2009.

[5] R. Dey, S. Chakrabarty, R. Jyoti, and T. Kurian, “Higher Order Mode Analysis of Dual-Post Discontinuity in a Circular Waveguide,” *IETE Journal of Research*, pp. 1–8, 2015.

[6] R. E. Collin, *Foundations for microwave engineering*. McGraw-Hill, 1992.

[7] N. Marcuvitz, *Waveguide handbook*. Peregrinus, 1986.

[8] “GRASP Software,” TICRA, Copenhagen, Denmark, *www.ticra.com*.

[9] M. F. Palvig, E. Jørgensen, P. Meincke, and O. Breinbjerg, “Optimization Procedure for Wideband Matched Feed Design,” in *To be presented at the 2016 European Conference on Antennas and Propagation*, 2016.

C.3 Paper 3

METASURFACE WAVEGUIDES APPLIED TO MATCHED FEEDS FOR REFLECTOR ANTENNAS

Michael Forum Palvig, Erik Jørgensen, Peter Meincke, and Olav Breinbjerg

Status: Presented March 2017.

Bibliography

[P3] M. F. Palvig, E. Jørgensen, P. Meincke, and O. Breinbjerg. “Metasurface Waveguides Applied to Matched Feeds for Reflector Antennas”. In: *The 11th European Conference on Antennas and Propagation (EUCAP 2017).* Paris, France, Mar. 2017, pp. 3636–3638.

Metasurface Waveguides Applied to Matched Feeds for Reflector Antennas

Michael Forum Palvig[1,2], Erik Jørgensen[2], Peter Meincke[2], Olav Breinbjerg[1]
[1]Department of Electrical Engineering, Electromagnetic Systems, Technical University of Denmark, Kgs. Lyngby, Denmark
[2]TICRA, Copenhagen, Denmark

***Abstract*—Waveguides with anisotropic surface impedance boundaries have been investigated for the purpose of matched feeds for offset reflectors. Matched feeds employ higher order waveguide modes to cancel out cross polarization introduced by the offset geometry. Since the higher order modes propagate at different speeds than the fundamental mode in conventional waveguides, it is challenging to meet phase relationship requirements over a large band. We have found that traditional corrugated waveguides are poorly suited for matched feed applications. However, other surfaces that satisfy the balanced hybrid condition, but have a small capacitive longitudinal reactance and large inductive azimuthal reactance show very promising properties: In a large band, HE$_{11}$ and HE$_{21}$ have similar propagation characteristics.**

***Index Terms*—metasurface, matched feed, offset reflector antenna.**

I. INTRODUCTION

Prime focus offset reflector antennas have many advantages, but suffer from high cross polarization [1]. It is a well known trade-off that a more compact system results in higher cross polarization. By using Bem's [2] analysis of the focal region field, Rudge and Adatia [3] proposed that the cross polarization be compensated by additional waveguide modes in the feed horn. For smooth walled circular horns, the TE$_{21}$ mode can compensate cross polarization if excited in phase quadrature with the fundamental mode, TE$_{11}$, though other modes can also be used [4]. For corrugated horns, the corresponding compensating mode is HE$_{21}$.

The corrugated horn represents a special case of an anisotropic impedance boundary waveguide. Here we shall investigate the propagation of higher order hybrid modes in more general waveguides with anisotropic impedance walls. Such surfaces may be implemented by periodic structures on the horn/waveguide wall, i.e. metasurfaces.

Wu et al. and Scarborough et al. have successfully demonstrated horns with metasurface walls [5], [6], [7], [8] which exhibit very good performance over a wide band. However, their focus was not matched feeds, but a good co-polarized feed and thus did need analysis of modes with higher order azimuthal index.

By considering dispersion characteristics of the hybrid modes HE$_{11}$ and HE$_{21}$ in circular cylindrical waveguides with anisotropic boundary conditions, we shall investigate if there are metasurface waveguides suitable for matched feed applications. First, a brief theory of modal solutions in impedance waveguides will be given, following the approach of e.g. [9] and [10].

II. THEORY

Consider a cylindrical waveguide with circular cross-section which extends along z. We assume solutions which are travelling waves in the positive z-direction with phase constant β, i.e. the field variation along z is $e^{-j\beta z}$, given a harmonic time factor of $e^{j\omega t}$. The longitudinal (z) components of the fields then satisfy the scalar Helmholtz equation. In a cylindrical coordinate system with its z-axis along the center of the waveguide, the longitudinal field components have solutions of the form

$$E_z(\rho,\phi,z) = E_0 J_m(k_c\rho) \begin{matrix}\cos\\ \sin\end{matrix}\, m\phi\; e^{-j\beta z} \tag{1a}$$

$$H_z(\rho,\phi,z) = \pm E_0 \frac{\gamma}{Z_0} J_m(k_c\rho) \begin{matrix}\sin\\ \cos\end{matrix}\, m\phi\; e^{-j\beta z}, \tag{1b}$$

from which it follows that the so-called *hybrid factor* [9] is

$$\gamma = Z_0 \frac{H_z(\rho,\phi,z)}{E_z(\rho,\phi-\frac{\pi}{2m},z)}, \tag{2}$$

which measures the ratio of longitudinal E- and H-fields for a solution. Z_0 is the free space impedance. The top and bottom choices of cos, sin, $+$, and $-$ correspond to two orthogonal solutions. The hybrid factor is zero and infinite for pure TM and TE modes, respectively. Any other value of γ is a hybrid mode: If the hybrid factor is positive, we denote the solution an HE hybrid mode, and if negative, an EH hybrid mode [9].

Given the simple z-variation of the field, the longitudinal components sufficiently characterize the field and the transverse components can be found from these:

$$\mathbf{E}_t = \frac{j}{k_c^2}\left(\omega\mu\hat{\mathbf{z}}\times\nabla_t H_z - \beta\nabla_t E_z\right) \tag{3a}$$

$$\mathbf{H}_t = \frac{j}{k_c^2}\left(\omega\epsilon\nabla_t E_z\times\hat{\mathbf{z}} - \beta\nabla_t H_z\right). \tag{3b}$$

We now impose boundary conditions in the form of normalized surface impedances at the wall of the waveguide

$$z_z = -\frac{E_z}{Z_0 H_\phi}, \quad z_\phi = \frac{E_\phi}{Z_0 H_z}. \tag{4}$$

The transverse field quantities are obtained from the longitudinal ones and evaluated on the boundary. The boundary conditions are then manipulated to obtain an equation which links the wavenumber, k, to the transverse wavenumber k_c — the characteristic equation:

$$jJ_m^2(k_ca)\left[z_z\frac{m^2}{(k_ca)^2}\left(\frac{k_c^2}{k^2}-1\right)-z_t\frac{k_c^2}{k^2}\right] + jJ_m'^2(k_ca)z_z - J_m(k_ca)J_m'(k_ca)\frac{k_c}{k}\left[z_zz_t+1\right]=0. \tag{5}$$

The characteristic equation is solved numerically for each k. For a given k, there may be several k_c which satisfy the equation, corresponding to different modal solutions.

III. DISPERSION ANALYSIS

Using the simple theory outlined in the previous section, we can investigate the modal solution of waveguides with different anisotropic wall impedances. A convenient way to analyze the modes is by dispersion diagrams. They provide a relation between the electrical radius of the waveguide (or frequency) and the phase constant of each mode. The phase constant is found from k and k_c as

$$\beta = \sqrt{k^2 - k_c^2}. \tag{6}$$

For a waveguide with PEC walls, the transverse wavenumber, k_c, is independent of k — this is not generally true for impedance surface waveguides.

For the purposes of this analysis, we shall concentrate on impedances which satisfy the *balanced hybrid condition* and thus support balanced hybrid modes. These are modes for which $|\gamma| = 1$. The balanced HE modes are desirable, as they approach totally parallel field lines when k and β are close. It can be shown that the balanced hybrid condition is fulfilled when

$$z_\phi = \frac{1}{z_z} \quad \text{or} \quad x_\phi = -\frac{1}{x_z}. \tag{7}$$

where x_z and x_ϕ are normalized reactances, i.e. for lossless surfaces $z_z = jx_z$ and $z_\phi = jx_\phi$. Under the balanced condition balanced EH modes are also present ($\gamma = -1$) in addition to the HE modes. These are usually not desirable and one would want to avoid exciting them.

In a classical matched feed design, the higher order mode is excited at the beginning of the horn and then propagates along with the primary mode in the rest of the horn. The phase relationship between the modes at the aperture of the horn is of vital importance. Thus, we want the phase constants of the two modes to have the same difference over the frequency band of interest, thereby making the phase difference at the aperture constant. This is impossible for smooth walled horns with the TE_{21} compensating mode.

Additionally, if the compensating mode is excited along a distributed section of the impedance waveguide, we know from directional coupler theory [11], that the two modes must have not only a constant difference in phase constant, but the *same* phase constant.

A. *Soft surface*

Fig. 1 shows the dispersion diagram of a waveguide with infinite longitudinal and zero azimuthal impedance — corresponding to a *soft* surface, e.g. a transversely corrugated surface at resonance. This surface satisfies the hybrid condition with both sides of Eq. (7) being zero. In a real corrugated waveguide, the surface impedance would change with frequency, resulting in different dispersion characteristics, but Fig. 1 shows results qualitatively similar to those at the aperture section of a corrugated horn. Evidently, the HE_{11} and HE_{21} modes have different dispersion characteristics. The two modes have varying difference in phase constant with frequency. Consequently, if they are allowed to propagate together for a length of waveguide, their mutual phase difference at the end of the section will change with frequency — which is exactly what should be avoided. This indicates that traditional corrugated horns have no advantage over smooth horns in the sense of matched feeds.

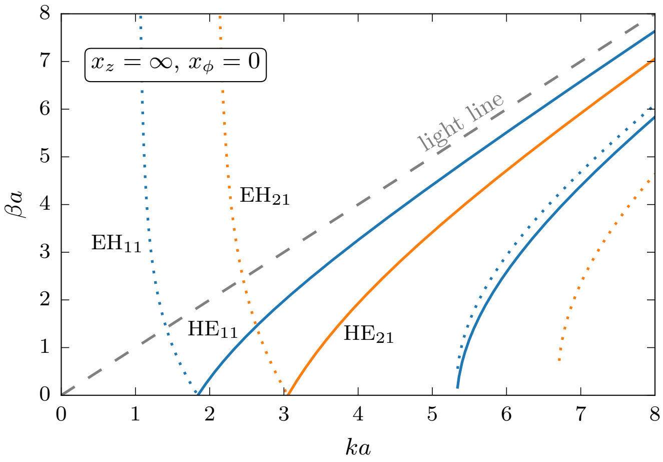

Fig. 1. Dispersion diagram for a circular waveguide with infinite longitudinal impedance, $x_z = \infty$ and zero azimuthal, $x_\phi = 0$. This corresponds to a corrugated surface where the corrugations are $\lambda/4$ deep. Blue curves represent $m = 1$ azimuthal variation and orange curves represent $m = 2$ variation. Full lines are HE modes and dotted lines are EH modes.

B. *Small Capacitive Longitudinal Impedance*

It turns out that impedance pairs where the longitudinal reactance, x_z, is negative (capacitive) and small, are more interesting for our purposes. We still require the balanced hybrid condition, Eq. (7), to be met. Fig. 2 shows examples of surfaces in this range with x_z equal to -1, -0.5, and -0.1, respectively. For $x_z = -1$, the HE_{11} and HE_{21} modes are much closer than in the ”corrugated” case of Fig. 1, and also have a more constant difference. Decreasing negative values of x_z moves the two phase constants even closer, and closer to that of free space. A surface of this type would be highly desirable for matched feed applications

IV. IMPLEMENTATION

The surface impedances in the previous section are idealized. An optimized surface for the matched feed purposes of

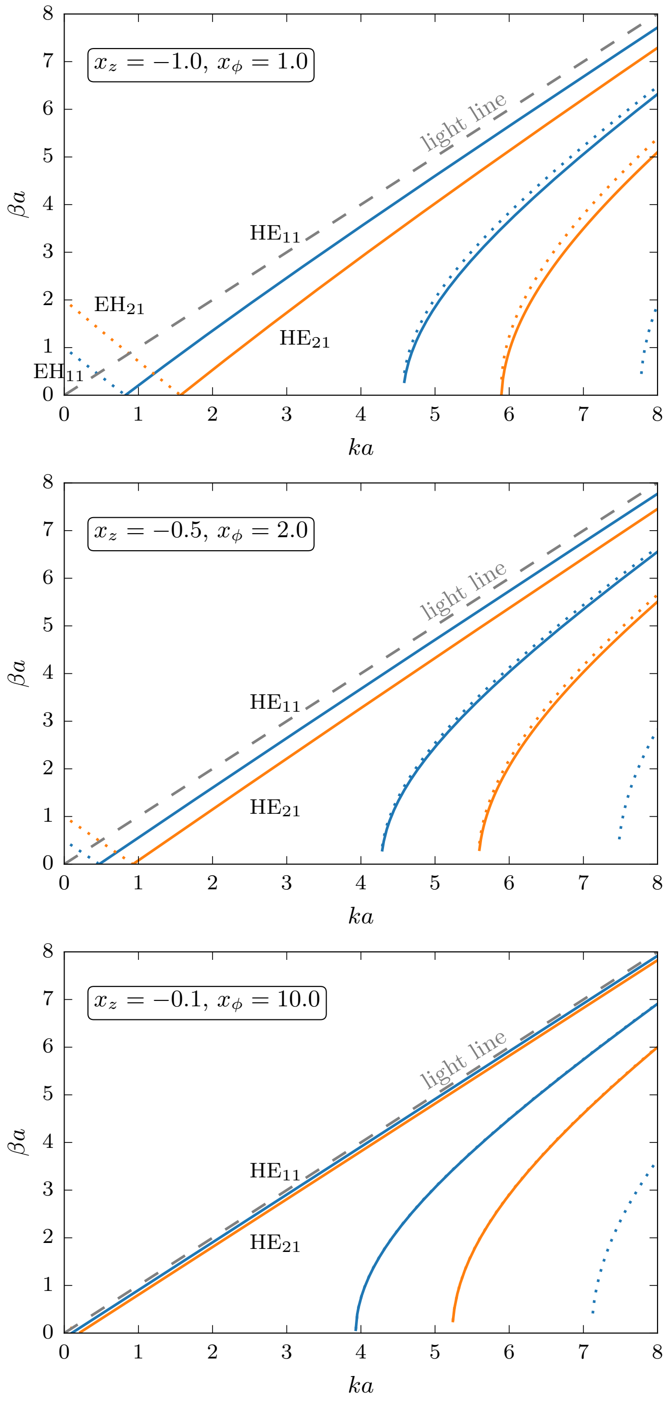

Fig. 2. Dispersion diagrams for a circular waveguide with three sets of surface reactances fulfilling the balanced hybrid condition: $x_z x_\phi = -1$. Blue curves represent $m = 1$ azimuthal variation and orange curves represent $m = 2$ variation. Full lines are HE modes and dotted lines are EH modes.

this paper, has not yet been found. However, looking in the literature, it does seem feasible. The horns designed by Wu et al. and Scarborough et al. [5], [6], [7], [8], feature impedances which are balanced and have a normalized longitudinal reactance of around $x_z = -1$. Again, their goal for optimization is not matched feeds, but the resulting surface happens to be promising for matched feed applications. The same is true for the surface designed in [12]. The surface designs might be even better suited if an optimization goal was added to possible make $|x_z|$ smaller.

V. CONCLUSION

We have made a study of circular cylindrical waveguides with anisotropic impedance walls for the possible application to offset reflector matched feed horns. The suitability of such waveguides relies on the dispersion characteristics of the primary HE_{11} mode and the HE_{21} mode used to compensate cross polarization. It is desirable that the phase constant of the two modes are close, or at least that the difference in phase constant does not change with frequency.

We can conclude that corrugated waveguides are unsuited to meet these requirements, but other balanced impedance surfaces are well suited. These surfaces are characterized by a capacitive (negative) reactance in the longitudinal direction and an inductive (positive) reactance in the azimuthal direction. Surfaces like this are shown in the literature to be realizable, and thus provide a promising platform for novel matched feed designs.

REFERENCES

[1] T.-S. Chu and R. H. Turrin, “Depolarization properties of offset reflector antennas,” *IEEE Transactions on Antennas and Propagation*, vol. Ap-21, no. 3, pp. 339–345, 1973.

[2] D. J. Bem, “Electric-field distribution in the focal region of an offset paraboloid,” *Proceedings of the Institution of Electrical Engineers*, vol. 116, no. 5, pp. 679–684, 1969.

[3] A. W. Rudge and N. A. Adatia, “New class of primary-feed antennas for use with offset parabolic-reflector antennas,” *Electronics Letters*, vol. 11, no. 24, pp. 597–599, 1975.

[4] M. Palvig, E. Jørgensen, P. Meincke, and O. Breinbjerg, “Optimization Procedure for Wideband Matched Feed Design,” in *The 10th European Conference on Antennas and Propagation (EuCAP 2016)*, Davos, Switzerland, Apr. 2016.

[5] Q. Wu, C. Scarborough, D. Werner, E. Lier, and X. Wang, “Design Synthesis of Metasurfaces for Broadband Hybrid-Mode Horn Antennas With Enhanced Radiation Pattern and Polarization Characteristics,” *IEEE Transactions on Antennas and Propagation*, vol. 60, no. 8, pp. 3594–3604, Aug. 2012.

[6] Q. Wu, C. Scarborough, B. Martin, R. Shaw, D. Werner, E. Lier, and X. Wang, “A Ku-Band Dual Polarization Hybrid-Mode Horn Antenna Enabled by Printed-Circuit-Board Metasurfaces,” *IEEE Transactions on Antennas and Propagation*, vol. 61, no. 3, pp. 1089–1098, Mar. 2013.

[7] Q. Wu, C. Scarborough, D. Werner, E. Lier, and R. Shaw, “Inhomogeneous Metasurfaces With Engineered Dispersion for Broadband Hybrid-Mode Horn Antennas,” *IEEE Transactions on Antennas and Propagation*, vol. 61, no. 10, pp. 4947–4956, Oct. 2013.

[8] C. Scarborough, Q. Wu, D. Werner, E. Lier, R. Shaw, and B. Martin, “Demonstration of an Octave-Bandwidth Negligible-Loss Metamaterial Horn Antenna for Satellite Applications,” *IEEE Transactions on Antennas and Propagation*, vol. 61, no. 3, pp. 1081–1088, Mar. 2013.

[9] B. M. Thomas and H. C. Minnett, “Modes of propagation in cylindrical waveguides with anisotropic walls,” *Proceedings of the Institution of Electrical Engineers*, vol. 125, no. 10, pp. 929–932, Oct. 1978.

[10] N. Raveu, B. Byrne, L. Claudepierre, and N. Capet, “Modal Theory for Waveguides With Anisotropic Surface Impedance Boundaries,” *IEEE Transactions on Microwave Theory and Techniques*, vol. 64, no. 4, pp. 1153–1162, Apr. 2016.

[11] S. E. Miller, “Coupled wave theory and waveguide applications,” *The Bell System Technical Journal*, vol. 33, no. 3, pp. 661–719, May 1954.

[12] N. Capet, B. Byrne, L. Claudepierre, and N. Raveu, “Metamaterial waveguide with reduced cross section,” in *2013 7th European Conference on Antennas and Propagation (EuCAP)*, Apr. 2013, pp. 2155–2157.

C.4 Paper 4

A DESIGN METHOD FOR MODE-SELECTIVE WAVEGUIDE COUPLERS IN DUAL-POLARIZED WIDEBAND MATCHED-FEED ANTENNAS

Michael Forum Palvig, Peter Meincke, Erik Jørgensen, and Olav Breinbjerg

Status: Accepted for publication November 2017. Published February 2018.

Bibliography

[P4] M. F. Palvig, P. Meincke, E. Jørgensen, and O. Breinbjerg. “A Design Method for Mode-Selective Waveguide Couplers in Dual-Polarized Wideband Matched-Feed Antennas”. In: *IEEE Transactions on Antennas and Propagation* 66.2 (Feb. 2018), pp. 990–995.

A Design Method for Mode-Selective Waveguide Couplers in Dual-Polarized Wideband Matched-Feed Antennas

Michael Forum Palvig, *Student Member, IEEE,* Peter Meincke, *Member, IEEE,* Erik Jørgensen, *Member, IEEE,*
Olav Breinbjerg, *Senior Member, IEEE*

***Abstract*—A novel type of multihole directional coupler is presented as well as a design method involving novel procedures. The device couples two orthogonal TE$_{11}$ modes in a circular waveguide into two orthogonal TE$_{21}$ modes with specified excitations in a surrounding coaxial waveguide, which has the circular waveguide as inner conductor. A simple, novel analytical procedure is used to determine azimuthal hole positions, such that each of the input modes couples to only the desired coaxial TE$_{21}$ mode. The method is applied to a specific coupler which is designed to couple $-14\,\mathrm{dB}$ to both higher-order coaxial modes in the band from $10\,\mathrm{GHz}$ to $14\,\mathrm{GHz}$. The suppression of undesired modes is generally better than $40\,\mathrm{dB}$. The coupler is intended for broadband, dual-polarized matched feeds, which are able to compensate the intrinsically high cross polarization of offset single reflector antenna systems.**

***Index Terms*—Directional Coupler, Reflector antenna feeds, Coaxial aperture antennas, Cross polarization**

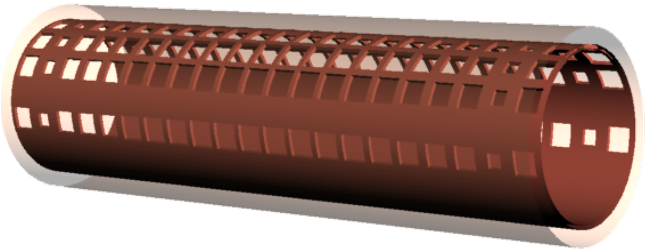

Fig. 1. Hole distribution in the coupler. The outer conductor of the coaxial part has been made transparent such that the holes are visible. The square hole sizes are from either end: 2.86, 1.77, 2.79, 2.74, 2.01, 3.09, 3.14, 3.16, 3.30, 3.33, and $3.27\,\mathrm{mm}$.

I. INTRODUCTION

Parabolic reflectors are the preferred choice for high gain antenna systems. Often, the reflector is chosen to be offset from the feed or subreflector in order to eliminate blockage. A drawback of the offset system is that the asymmetry of the configuration introduces high cross polarization. For dual reflector systems, this can be compensated by applying the Mizuguchi condition [1]. For a single reflector system, an alternative solution was proposed by Rudge and Adatia in 1975 [2]. It involves letting cross polarization from the feed antenna compensate the cross polarization introduced by the offset geometry. This is achieved by generating higher-order modes in a feed horn antenna that have specific amplitude and phase relationships with the fundamental mode. Such a feed is often called a *Matched Feed*. For a circular horn, the proposed higher-order mode was TE$_{21}$ in two orthogonal rotations for two operating polarizations.

Matched feeds have received considerable attention in recent years. Feed designs with circular [3]–[6], rectangular [7], [8], corrugated [9]–[11], and other geometries [12], [13] have been presented. The primary challenge of the matched-feed technique is to achieve a practically sufficient bandwidth for dual polarization applications, which is essential for the use of this technology in communication applications. This difficulty stems from the fact that the fundamental and higher-order modes have different cutoff frequencies, resulting in phase dispersion. The bandwidth can be defined as the frequency range within which the peak cross polarization is reduced by a certain amount, e.g. by $10\,\mathrm{dB}$ relative to the case with a purely co-polarized feed. Watson et al. [14] were first to introduce this bandwidth measure, achieving $4\,\%$ $10\,\mathrm{dB}$-bandwidth for both polarizations. By using an optimization procedure and trading maximum reduction for more bandwidth, the authors achieved a $7\,\mathrm{dB}$ reduction over a $12\,\%$ bandwidth for both polarizations [15]. Using a novel mode launching concept, Dey et al. [16] achieved a $10\,\mathrm{dB}$ reduction over a $10\,\%$ bandwidth for a single polarization.

A way to mitigate the phase dispersion problem is to somehow use higher-order modes that have the same or nearly the same cutoff frequency as the fundamental mode. This is not possible for conventional waveguide geometries, except if the waveguide walls are anisotropic impedance surfaces [17]. Jana and Bhattacharjee [13] presented an optimized waveguide cross section which brings the cutoffs closer together. Pour and Shafai [12] proposed coupling the higher-order modes to a coaxial waveguide surrounding the primary one. The higher-order modes are then radiated directly from the coaxial guide as in [18]. It turns out that the dimensions can be engineered such that the cutoff of the TE$_{21}$ mode in the coaxial waveguide is close to that of the TE$_{11}$ mode in the circular waveguide. In [12] the bandwidth is limited because of the resonance of a single coupling hole and the design is single polarized.

O. Breinbjerg is with the Department of Electrical Engineering, Electromagnetic Systems, Technical University of Denmark, DK-2800 Kgs. Lyngby, Denmark. (email: ob@elektro.dtu.dk)

E. Jørgensen, and P. Meincke are with TICRA Engineering Consultants, DK-1119 Copenhagen K, Denmark. (email: ticra@ticra.com)

M. F. Palvig is affiliated with both of the above institutions. (email: mpalvig@elektro.dtu.dk or mfp@ticra.com)

The present work is based on the concept in [12], but is extended to a multi-hole design in order to support dual polarizations and avoid resonances of individual holes. The device is designed as a distributed directional waveguide coupler, which has not previously been done for matched-feed mode launchers. The presented design method concerns the mode coupler itself, not the full antenna. The theoretical basis of coupling between waveguides through small holes was laid by Bethe [19] in 1944. Later, Miller [20] described the theory of distributed couplers with tapered coupling functions to enhance directivity and discrimination of undesired modes. This theory was utilized in [21], [22] to create mode selective directional couplers, coupling specific higher-order modes from a circular waveguide into rectangular ones. This work follows the same methodology, but is extended to account for unequal cutoff of input and output modes, and for the fact that the two output modes are not isolated in rectangular waveguides, but must coexist in the same coaxial waveguide. The latter challenge is overcome by a simple analytical method for determining an azimuthal hole distribution (in addition to the longitudinal one) which enables coupling from two orthogonal input modes to two orthogonal output modes, without cross coupling the wrong modes. To the authors' knowledge, this type of directional coupler and elements of the design method are not previously published in the literature.

The paper is organized as follows: In Section II, we shall briefly rederive the *loose coupling* theory of Miller [20] followed by determination of optimal coupling coefficients in Section III. Then we will address the optimal selection of the azimuthal distribution of coupling holes in Section IV. Then, by simulation experiments, Section V will cover optimal hole shape and simple, but effective mapping from coupling coefficients to hole sizes. Finally, the resulting design will be analyzed by full-wave simulation in Section VI.

II. LOOSE COUPLING THEORY

Loose coupling theory, as opposed to *tight coupling* theory, assumes that the wave in the driven line is unpertubed by the coupling [20]. For matched feeds, we are interested in coupling only a small amount of the power to the coaxial waveguide, and a tight coupling analysis can thus be omitted. The theory is quite intuitive and can be written up by inspection. For the use in subsequent sections, we briefly rederive loose coupling for couplers with discrete coupling points. Note that the definitions differ slightly from [20].

Consider a wave incident on a transmission line, the *input line*. The wave is coupled to another line, the *output line*, at discrete coupling points over a section of length L, see Fig. 2. The phase constant in the input line is β_{in} and the phase constant in the output line is β_{out}. If the lines are modes in smooth walled waveguides, the phase constant β of each line is found from the cutoff frequency as

$$\beta = \frac{2\pi}{c}\sqrt{f^2 - f_c^2}, \tag{1}$$

in which c is the speed of light, f is the frequency, and f_c is the cutoff frequency. At each coupling point, the complex coupling coefficient, a_m, determines the amplitude and phase of the coupled wave relative to the input wave at the coupling location. The input and output line can represent modes in different waveguides or two modes in the same waveguide.

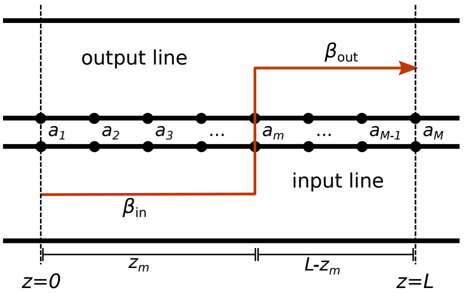

Fig. 2. Loose coupling with discrete coupling points.

The contribution to the coupled wave in the forward direction at $z = L$ from a single hole at $z = z_m$, as depicted in Fig. 2, can be expressed as

$$\begin{aligned} I_{fm} &= e^{-j\beta_{\text{in}} z_m} a_m e^{-j\beta_{\text{out}}(L - z_m)} \\ &= a_m e^{-j\beta_{\text{out}} L} e^{-j z_m(\beta_{\text{in}} - \beta_{\text{out}})}, \end{aligned} \tag{2}$$

in which a timefactor of $e^{j\omega t}$ is used. Summing over all coupling points yields the total forward coupled wave

$$I_f = e^{-j\beta_{\text{out}} L} \sum_{m=1}^{M} a_m e^{-j z_m(\beta_{in} - \beta_{\text{out}})}. \tag{3}$$

Similarly, the contribution of the hole to the coupled wave in the backward direction at $z = 0$ in the output line is

$$\begin{aligned} I_{bm} &= e^{-j\beta_{\text{in}} z_m} a_m e^{-j\beta_{\text{out}} z_m} \\ &= a_m e^{-j z_m(\beta_{\text{in}} + \beta_{\text{out}})} \end{aligned} \tag{4}$$

and the total backward coupled wave thus

$$I_b = \sum_{m=1}^{M} a_m e^{-j z_m(\beta_{\text{in}} + \beta_{\text{out}})}. \tag{5}$$

Note that both the backward and forward coupled waves can be evaluated from the function

$$F(\theta) = \sum_{m=1}^{M} a_m e^{-j z_m \theta} \tag{6}$$

where $\theta = \beta_{\text{in}} - \beta_{\text{out}}$ and $\theta = \beta_{\text{in}} + \beta_{\text{out}}$ for forward and backward coupling, respectively. It is seen that $F(\theta)$ is simply a Fourier transform of the coupling distribution in the spectral variable θ, transforming the coupling coefficients to the θ-*domain*. If the coupling coefficients, a_m, are symmetric and all have the phase $\angle a$, it can be shown that the phase difference between the output and input wave at the end of the coupler is

$$\Delta\phi = \angle a + \frac{L}{2}\left(\beta_{\text{in}} - \beta_{\text{out}}\right). \tag{7}$$

If the cutoffs of the input and desired coupled wave are identical, the phase constants are the same, and θ for the forward direction is zero for all frequencies. This condition is sought in most traditional directional couplers. Then the function F is designed to have the desired coupling value at

$\theta = 0$ and a lower value in θ-ranges of undesired modes, backward and forward [20]. In our case, the cutoff of the desired mode in the coaxial waveguide is close to that of the input mode, but may not be exactly equal, so we cannot assume that θ is zero.

III. DESIGN OF OPTIMAL DIRECTIONAL COUPLER

We will find the *optimal* coefficients, a_m, given certain criteria. The length of the coupler and number of coupling points are first to be determined. This choice corresponds to choosing filter length and sampling frequency of a digital Finite Impulse Response (FIR) filter. Among other things, it determines the steepness of the filter roll-off in the spectral domain. For the present design there are additional considerations to take into account: 1) we want the coupler as short as possible, 2) holes must not overlap, and 3) coefficient values must be within a feasible range. Balancing these goals, we arrive at a coupler length of $80\,\mathrm{mm}$ with 21 holes. The length of the coupler is measured from the center of the first hole to the center of the last, and the remaining holes are equally distributed in between.

We consider a circular waveguide surrounded by a coaxial waveguide such that the circular waveguide constitutes the inner conductor of the coaxial one. The principal dimensions are listed in Table I. We are interested in coupling orthogonal TE_{11} modes in the circular guide to orthogonal TE_{21} modes in the coaxial guide as shown in Fig. 3. The outer radius is chosen to approximately fulfill $a_{\mathrm{outer}} = 1.173 a_{\mathrm{circ}} - a_{\mathrm{inner}}$, which ensures that the cutoff of TE_{21} in the coaxial guide is nearly equal to the cutoff of TE_{11} in the circular guide [23, p. 70,77] (see Table I).

For the present design, the power of the desired coupled mode compared to the input power should be $-14\,\mathrm{dB}$, which is approximately the amount needed to compensate the cross polarization in an offset reflector system with a focal length to diameter ratio (f/D) of 0.6. The frequency band of operation is $10\,\mathrm{GHz}$ to $14\,\mathrm{GHz}$, i.e. a fractional bandwidth (FBW) of $33\,\%$.

The θ-values for the forward and backward coupling of each mode can now be found from the above. Mapping the operating frequency range to θ-values results in Fig. 4. A range of θ-values are identified as undesired, which we will denote the *stopband* in the θ-domain. The *passband* given by the green line is comparatively narrow owing to the closeness in cutoff between input and desired coupled modes (see Table I).

TABLE I
PRINCIPAL DIMENSIONS AND CUTOFF FREQUENCIES OF THE COUPLER

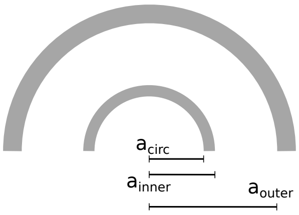

a_{circ}	$10.0\,\mathrm{mm}$
a_{inner}	$10.5\,\mathrm{mm}$
a_{outer}	$12.5\,\mathrm{mm}$
Coupler length	$80\,\mathrm{mm}$
N° coupling points	21
Circ TE_{11} cutoff	$8.8\,\mathrm{GHz}$
Coax TE_{21} cutoff	$8.3\,\mathrm{GHz}$
Coax TE_{31} cutoff	$12.5\,\mathrm{GHz}$
Circ TE_{21} cutoff	$14.6\,\mathrm{GHz}$

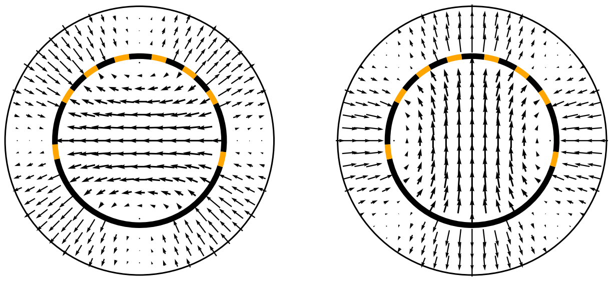

(a) (b)

Fig. 3. Modal E-fields of the incident circular and desired coaxial modes for the two polarizations: (a) TE_{11}^1 to TE_{21}^2 and (b) TE_{11}^2 to TE_{21}^1. The coupling holes are indicated in orange and their angular positions in degrees are $\phi = \{30.9°, 53.8°, 76.7°, 102.1°, 125.0°, 147.9°, 187.6°, 347.4°\}$.

The coupling function (6) is equivalent to the frequency response of a FIR filter with filter coefficients a_m. The coupler can thus be designed as a FIR filter, defining stop- and passbands in the spectral θ-domain. Optimal coefficients can be determined by standard techniques for FIR filter design. The coefficients in Fig. 5 are found from the SciPy [24] implementation of [25], which minimizes the maximum deviation from the desired coupling in each band. The coupling holes will all be electrically small and reactive, yielding coupling coefficients with constant phase, $\angle a$, close to $90°$. This phase relationship is desirable for matched feed design. From Eq. (6), the resulting θ-response is shown in Fig. 6. Pass- and stopbands are indicated in green and red, respectively.

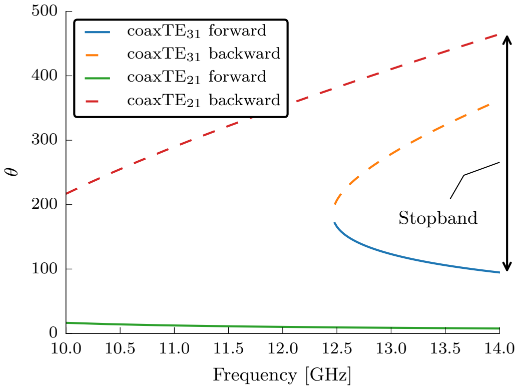

Fig. 4. θ-values evaluated over the frequency band of interest in order to find pass- and stop bands in the θ-domain.

IV. AZIMUTHAL HOLE DISTRIBUTION

As explained in the previous section, the distribution of holes in the longitudinal direction can suppress the generation of undesired modes with different phase constants than the desired, but it cannot distinguish modes with the same phase constant. Since we require that each polarization of TE_{11} couples only to the correct TE_{21} mode, unwanted TE_{21} couplings must be suppressed in another way. We denote two orthogonal versions of the circular modes with superscripts 1 and 2: TE_{11}^1 should couple to TE_{21}^2, but not to TE_{21}^1 and vice versa as depicted in Fig. 3. The suppression is achieved by placing

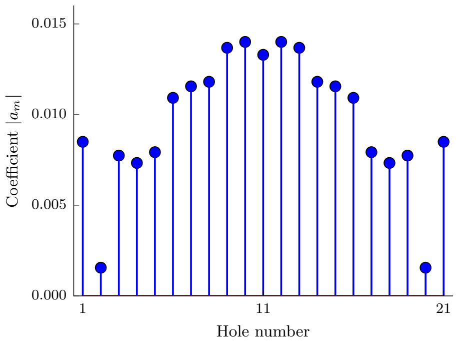

Fig. 5. Optimal coupling coefficients minimizing the maximum deviation from the desired coupling in both bands, i.e. $-14\,\mathrm{dB}$ in the passband and $-\infty\,\mathrm{dB}$ in the stopband. All coefficients have the same phase.

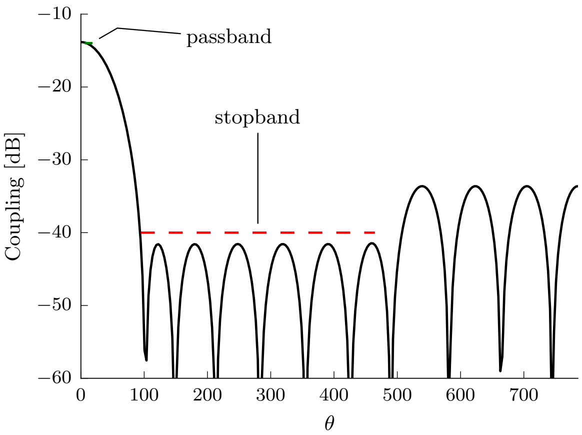

Fig. 6. θ-response of the coupling coefficients. The theta ranges of desired and undesired modes are indicated by *passband* and *stopband*, respectively.

several holes around the circumference at each coupling point along z.

The coupling from one mode to another through a waveguide wall can be modelled by representing the hole with an electric dipole normal to the wall and a magnetic dipole parallel to the wall [19]. The dipoles are excited proportional to the respective input fields: normal E-field and tangential H-field. The proportionality constants, the *polarizabilities* of the hole, depend on the hole shape and size. The dipoles radiate and excite modes in the output waveguide. The strength of each excited mode is proportional to that mode's field projected onto the dipoles [26, Sec. 4.10].

From these considerations, we can determine the effect of moving a coupling hole around the circumference of the circular waveguide wall. For circular and coaxial waveguide modes, the azimuthal (ϕ-) variation of the fields is given by sine and cosine functions of the ϕ variable times the azimuthal (m-) index of the modes. The ϕ-variation of a mode coupling is a product of the field variation for the input and output mode. The resulting ϕ-dependence of the desired and the most critical undesired couplings are listed in Table II.

TABLE II
SUMMARY OF DESIRED AND UNDESIRED MODE COUPLINGS

Coupling	ϕ-dependence
Desired	
$\mathrm{TE}_{11}^{1} \rightarrow \mathrm{TE}_{21}^{2}$	$\cos\phi \sin 2\phi$
$\mathrm{TE}_{11}^{2} \rightarrow \mathrm{TE}_{21}^{1}$	$\sin\phi \cos 2\phi$
Undesired	
$\mathrm{TE}_{11}^{1} \rightarrow \mathrm{TE}_{21}^{1}$	$\cos\phi \cos 2\phi$
$\mathrm{TE}_{11}^{2} \rightarrow \mathrm{TE}_{21}^{2}$	$\sin\phi \sin 2\phi$
$\mathrm{TE}_{11}^{x} \rightarrow \mathrm{TE}_{31}^{x}$	$\cos\phi \cos 3\phi$ $\cos\phi \sin 3\phi$ $\sin\phi \sin 3\phi$ $\sin\phi \cos 3\phi$

With this information, we can select a number of hole positions, such that the combined contributions from all holes will cancel out undesired couplings [27]. Additionally, the two desired couplings should be of approximately the same strength and the hole positions must be separated a certain distance such that they do not overlap for a certain hole size.

The process of choosing hole positions is automated with an optimization procedure. A local minimax optimizer (fminimax of Matlab) is used to minimize undesired couplings while satisfying constraints. Since the objective functions are computationally very light, the global best solution is sought simply by trying many starting guesses at random.

The resulting configuration is the 8 hole distribution indicated with orange in Fig. 3. This configuration suppresses undesired TE_{21} couplings by approximately $30\,\mathrm{dB}$ compared to desired ones. Undesired TE_{31} couplings are suppressed by $22\,\mathrm{dB}$, but these can be further suppressed by the arrangement of holes in the longitudinal direction as described in Sec. III. The coupler consists of 21 *slices* of equal thickness corresponding to the 21 coupling points. Each coupling point, or slice, will have 8 equally sized holes with the optimized ϕ-distribution, but the hole size will change from slice to slice in correspondence with the coefficients in Fig. 5.

V. MAPPING COEFFICIENTS TO HOLE SIZES

The amount of coupling into each hole can be estimated by Bethe theory [19] or by improved methods [28], [29]. However, we shall take a shortcut and use a simpler, but very effective method. Since the coupling generally has a cubic relationship with the size of the hole [19], we just make a few simulation experiments with different hole sizes and fit a cubic spline to the data. In this way, effects like wall thickness and aperture shape are automatically taken into account. The simulations are carried out with a higher-order method of moments solver from TICRA [30]. Generalized scattering parameters between four waveguide ports are extracted: one circular and one coaxial at each end of the slice. The results are in excellent agreement with another commercial tool [31] (not shown here).

The holes are chosen to be square, in effect, there is a contribution to the coupling from both a longitudinal and an azimuthal equivalent magnetic dipole. This reduces the frequency dependence of the isolated hole, since the longitudinal coupling is inversely proportional to frequency and the azimuthal coupling is proportional to frequency [32].

Using the azimuthal hole distribution illustrated in Fig. 3, we simulate a single slice of the waveguide structure. The results are shown in Fig. 7. Six hole sizes are simulated and cubic splines are fitted to the data. Note that as a consequence of the optimized azimuthal hole distribution, the two desired couplings are nearly equal and the undesired TE$_{21}$ couplings are suppressed. The data shown in Fig. 7 is averaged over the frequency range of interest: 10 GHz to 14 GHz.

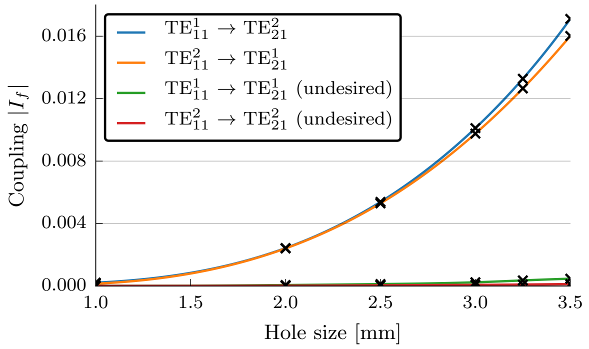

Fig. 7. Interpolation of the amount of desired coupling as a function of hole size. Based on six experiments indicated by black markers. The data for each hole size is averaged over a frequency range from 10 GHz to 14 GHz. This data is used to map coupling coefficients to hole sizes. The undesired TE$_{21}$ couplings are also shown, the suppression is better than 30 dB for the hole sizes used.

Using the interpolating function, all the coefficients of Fig. 5 are mapped to hole sizes. A coupler device with the resulting hole distribution is rendered in Fig. 1. In case there are any negative coupling coefficients, these can be implemented by negating the ϕ-positions of the holes in the corresponding slice. This results in coupling of the opposite sign of both the desired coupling components (a consequence of the single sine factor in these couplings, Table II).

VI. Coupler Performance

The performance of the coupler is evaluated by the same computation method as the single slice. Again, a coaxial and circular waveguide port is placed at each end of the coupler. The coaxial port at the back of the coupler will be terminated in a practical design, but is included in the simulation to ensure that very little power is coupled in the backward direction. As mentioned we are interested in having a constant coupling from TE$^1_{11}$ to TE$^2_{21}$ and from TE$^2_{11}$ to TE$^1_{21}$. All other possible couplings are desired to be low.

Several couplings (scattering parameters) are plotted in Fig. 8 as a function of frequency. The goal level of -14 dB for the two desired couplings is indicated by a horizontal dashed black line. The realized coupling for both polarizations are within 2 dB of the desired over the entire band and within 0.5 dB of each other.

Undesired couplings are all the TE$_{21}$ couplings in the backward direction, undesired TE$_{21}$ couplings in the forward direction, and all TE$_{31}$ couplings (see Table II). The level of the undesired couplings is below -40 dB in the design band 10 GHz to 14 GHz, except for one of the TE$_{31}$ couplings. This coupling increases at higher frequencies to a level of about -36 dB at 14 GHz, which is still sufficient suppression for our application. All couplings to the backward port in the coaxial waveguide are low, and we can thus justify that terminating it will not affect performance. Also, the reflection at the input circular waveguide is of general interest, and is better than -35 dB in the design band for both polarizations.

The reason for the increased TE$_{31}$ coupling shown in green in Fig. 8, can be explained by the θ-domain (Figs. 6 and 4): the θ-values of the TE$_{31}$ couplings come close to the passband at higher frequencies. From Fig. 6, it is evident that the filter response only just drops off quickly enough from passband to stopband. The filter design is based on phase constants of modes in the simple, unperforated waveguides. The many holes are likely to disturb the cutoff frequencies and phase constants of the modes in both the circular and coaxial guide, thus shifting the bands in the θ-domain. This is most likely the reason for slightly higher TE$_{31}$ coupling at the end of the band.

The relative phase of desired modes to the input mode is shown in the bottom part Fig. 8. The realized phase is close to the expected result from Eq. (7), which is obtained assuming $\angle a = \pm 90°$. Choosing different waveguide dimensions can bring the expected — and realized — relative phases closer to $\pm 90°$. However, lower values can be desirable to balance the opposite effect, if a subsequent horn section is added to the coupler.

The coupler presented here was designed with very little computational effort, from filter theory and analytical hole coupling theory. Only full wave simulation of a single slice was used in the design to establish the mapping from coefficients to hole sizes. Nevertheless, the resulting coupler performs well and as expected. Due to the nonresonant nature of coupling holes, the design is insensitive to manufacturing tolerances; this is supported by preliminary simulation experiments (not shown here).

VII. Conclusion

A design method for a directional coupler coupling orthogonal TE$_{11}$ modes from a circular waveguide into orthogonal TE$_{21}$ modes in a coaxial waveguide surrounding the circular one, is presented. The method of mode selective directional couplers needed to be extended to allow coupling of specific degenerate modes into the same waveguide, where the coupled modes do not have the exact same cutoff as the source modes.

Optimal finite impulse response filter (FIR) techniques have been used in the determination of hole distribution in the longitudinal direction. This allows for discrimination of undesired modes which travel in the backward direction or have a different cutoff than desired modes.

Undesired TE$_{21}$ modes which have the same cutoff as desired modes, cannot be suppressed by directional coupler theory. A novel method which optimizes the azimuthal distribution of the holes ensures that only the correct TE$_{21}$ mode from each TE$_{11}$ mode is coupled and that they both couple in equal amount.

The method is applied to a specific design which exhibits good performance over the band (33 % FBW). Only a single

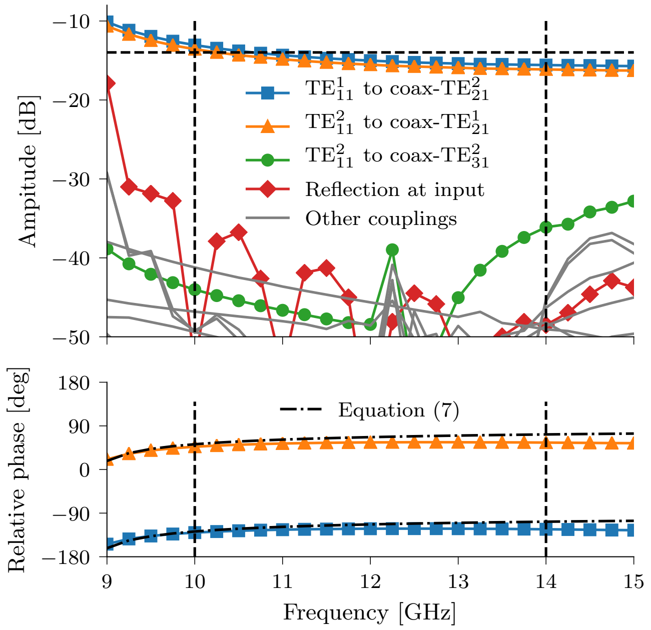

Fig. 8. Coupling from the two input modes in the circular waveguide to several modes in the coaxial guide. The two desired couplings are colored as well as the most critical undesired coupling. In addition, the maximum reflection at the input circular port is plotted in red. The Horizontal dashed line indicates the desired coupling level -14 dB. Vertical dashed lines delimit the frequency range of interest. The phases of desired modes are plotted relative to the phase of TE_{11} propagation through the circular waveguide.

higher-order mode couples more than -40 dB at the higher end of the band, but not to a critical degree. The two desired couplings have the same strength to within 0.5 dB over the entire band. The coupler is intended to be placed before a matched-feed horn antenna, feeding an offset reflector. The higher-order TE_{21} modes will allow suppression of cross polarization over a wide bandwidth in dual polarized operation.

REFERENCES

[1] A. W. Rudge and N. A. Adatia, “Offset-Parabolic-Reflector Antennas: A Review,” *Proceedings of the IEEE*, vol. 66, no. 12, pp. 1592–1618, Dec. 1978.

[2] ——, “New class of primary-feed antennas for use with offset parabolic-reflector antennas,” *Electronics Letters*, vol. 11, no. 24, pp. 597–599, Nov. 1975.

[3] K. Bahadori and Y. Rahmat-Samii, “Back-to-Back Reflector Antennas With Reduced Moment of Inertia for Spacecraft Spinning Platforms,” *IEEE Transactions on Antennas and Propagation*, vol. 55, no. 10, pp. 2654–2661, Oct. 2007.

[4] ——, “Tri-Mode Horn Feeds Revisited: Cross-Pol Reduction in Compact Offset Reflector Antennas,” *IEEE Transactions on Antennas and Propagation*, vol. 57, no. 9, pp. 2771–2775, Sep. 2009.

[5] Z. Pour and L. Shafai, “A Novel Dual-Mode Dual-Polarized Circular Waveguide Feed Excited by Concentrically Shorted Ring Patches,” *IEEE Transactions on Antennas and Propagation*, vol. 61, no. 10, pp. 4917–4925, Oct. 2013.

[6] ——, “Analytical Models of Dual-Polarized Primary Matched Feeds for Offset Reflector Antennas with Low Cross Polarization Properties at both Asymmetry and Diagonal Planes,” *IEEE Transactions on Antennas and Propagation*, vol. 64, no. 5, pp. 1627–1633, May 2016.

[7] R. Jana and R. Bhattacharjee, “Matched feed design employing TE01 and TM11 modes in a smooth walled rectangular waveguide for cross-polar reduction in offset reflector antenna systems,” *AEU - International Journal of Electronics and Communications*, vol. 69, no. 6, pp. 873–877, Jan. 2015.

[8] D. Pujara and S. B. Chakrabarty, “Cancellation of High Cross-polarization of an Offset Parabolic Reflector Antenna using a Rectangular Matched Feed,” *IETE Journal of Research*, vol. 58, no. 4, pp. 317–321, Jul. 2012.

[9] S. B. Sharma, D. Pujara, S. B. Chakrabarty, and R. Dey, “Cross-Polarization Cancellation in an Offset Parabolic Reflector Antenna Using a Corrugated Matched Feed,” *IEEE Antennas and Wireless Propagation Letters*, vol. 8, pp. 861–864, Jul. 2009.

[10] C. Yang, J. Yu, Y. Yao, X. Liu, and X. Chen, “Novel Corrugated Matched Feed for Cross-Polar Cancellation in Tri-Reflector Compact Range,” *IEEE Antennas and Wireless Propagation Letters*, vol. 13, pp. 1003–1006, May 2014.

[11] R. Dey, “Wideband Corrugated Conjugate Matched Feed Horn,” *Electromagnetics*, vol. 37, no. 3, pp. 150–161, Apr. 2017.

[12] Z. A. Pour and L. Shafai, “A Ring Choke Excited Compact Dual-Mode Circular Waveguide Feed for Offset Reflector Antennas,” *IEEE Transactions on Antennas and Propagation*, vol. 60, no. 6, pp. 3011–3015, Jun. 2012.

[13] R. Jana and R. Bhattacharjee, “A Novel Matched Feed Structure for Achieving Wide Cross-polar Bandwidth for an Offset Parabolic Reflector Antenna System,” *IEEE Antennas and Wireless Propagation Letters*, vol. 14, pp. 1590–1593, Mar. 2015.

[14] B. K. Watson, A. W. Rudge, and N. A. Adatia, “Dual-Polarised Mode Generator for Cross-Polar Compensation in Offset Parabolic Reflector Antennas,” *8th European Microwave Conference*, pp. 183–187, Sep. 1978.

[15] M. F. Palvig, E. Jørgensen, P. Meincke, and O. Breinbjerg, “Optimization Procedure for Wideband Matched Feed Design,” in *The 10th European Conference on Antennas and Propagation (EuCAP 2016)*, Davos, Switzerland, Apr. 2016.

[16] R. Dey, S. B. Chakrabarty, and R. Jyoti, “Broadband Conjugate Matched Feed Horn- A Novel Concept,” *IEEE Antennas and Wireless Propagation Letters*, vol. 15, pp. 496–499, Jul. 2015.

[17] M. F. Palvig, E. Jørgensen, P. Meincke, and O. Breinbjerg, “Metasurface Waveguides Applied to Matched Feeds for Reflector Antennas,” in *The 11th European Conference on Antennas and Propagation (EUCAP 2017)*, Paris, France, Mar. 2017, pp. 3636–3638.

[18] G. Koch, “Coaxial Feeds for High Aperture Efficiency and Low Spillover of Paraboloidal Reflector Antennas,” *IEEE Transactions on Antennas and Propagation*, vol. 21, no. 2, pp. 164–169, Mar. 1973.

[19] H. A. Bethe, “Theory of Diffraction by Small Holes,” *Physical Review*, vol. 66, no. 7-8, pp. 163–182, Oct. 1944.

[20] S. E. Miller, “Coupled Wave Theory and Waveguide Applications,” *The Bell System Technical Journal*, vol. 33, no. 3, pp. 661–719, May 1954.

[21] Y. H. Choung, K. R. Goudey, and L. G. Bryans, “Theory and Design of a Ku-Band TE21-Mode Coupler,” *IEEE Transactions on Microwave Theory and Techniques*, vol. 30, no. 11, pp. 1862–1866, Nov. 1982.

[22] Y. H. Choung, “Wideband TM01-mode travelling wave coupler,” *IEE Proceedings - Microwaves, Antennas and Propagation*, vol. 144, no. 5, pp. 315–320, Oct. 1997.

[23] N. Marcuvitz, *Waveguide handbook*. Peregrinus, 1951.

[24] E. Jones, T. Oliphant, P. Peterson *et al.*, “SciPy: Open source scientific tools for Python,” 2001–.

[25] J. McClellan and T. Parks, “A Unified Approach to the Design of Optimum FIR Linear-Phase Digital Filters,” *IEEE Transactions on Circuit Theory*, vol. 20, no. 6, pp. 697–701, Nov. 1973.

[26] R. E. Collin, *Foundations for Microwave Engineering*. McGraw-Hill, 1966.

[27] M. F. Palvig, O. Breinbjerg, P. Meincke, and E. Jørgensen, “Analytical Modelling of Waveguide Mode Launchers for Matched Feed Reflector Systems,” in *IEEE Antennas and Propagation Society International Symposium (AP-S 2016)*, Puerto Rico, Jun. 2016.

[28] S. B. Cohn, “Microwave Coupling by Large Apertures,” *Proceedings of the IRE*, vol. 40, no. 6, pp. 696–699, Jun. 1952.

[29] R. Levy, “Improved Single and Multiaperature Waveguide Coupling Theory, Including Explanation of Mutual Interactions,” *IEEE Transactions on Microwave Theory and Techniques*, vol. 28, no. 4, pp. 331–338, Apr. 1980.

[30] “GRASP Software,” TICRA, Copenhagen, Denmark, *www.ticra.com*.

[31] “HFSS 17.1 Software,” ANSYS, Inc., Canonsburg, PA, USA, *www.ansys.com*.

[32] H. J. Riblet and T. S. Saad, “A New Type of Waveguide Directional Coupler,” *Proceedings of the IRE*, vol. 36, no. 1, pp. 61–64, Jan. 1948.

Bibliography

[1] T. M. Braun. *Satellite Communications Payload and System.* John Wiley & Sons, 2012.

[2] J. W. M. Baars. *The Paraboloidal Reflector Antenna in Radio Astronomy and Communication: Theory and Practice.* Astrophysics and Space Science Library. Springer New York, 2007.

[3] T.-S. Chu and R. H. Turrin. “Depolarization Properties of Offset Reflector Antennas”. In: *IEEE Transactions on Antennas and Propagation* 21.3 (1973), pp. 339–345.

[4] Y. Mizuguchi, M. Akagawa, and H. Yokoi. “Offset Gregorian Antenna”. In: *Electronics and Communications in Japan* 61.3 (1978), pp. 58–66.

[5] C. Dragone. “Conformal Mapping and Complex Coordinates in Cassegrainian and Gregorian Reflector Antennas”. In: *The Bell System Technical Journal* 60.10 (Dec. 1981), pp. 2397–2420.

[6] A. W. Rudge and N. A. Adatia. “New class of primary-feed antennas for use with offset parabolic-reflector antennas”. In: *Electronics Letters* 11.24 (Nov. 1975), pp. 597–599.

[7] J. Jacobsen. “On the Cross Polarization of Asymmetric Reflector Antennas for Satellite Applications”. In: *IEEE Transactions on Antennas and Propagation* 25.2 (1977), pp. 276–283.

[8] B. K. Watson, A. W. Rudge, and N. A. Adatia. “Dual-Polarised Mode Generator for Cross-Polar Compensation in Offset Parabolic Reflector Antennas”. In: *8th European Microwave Conference* (Sept. 1978), pp. 183–187.

[9] O. Aboul-Atta and L. Shafai. “Performance of offset parabolic reflectors illuminated by matched feeds”. In: *Electrical Engineering Journal, Canadian* 4.3 (July 1979), pp. 26–32.

[10] K. M. Prasad and L. Shafai. “Improving the Symmetry of Radiation Patterns for Offset Reflectors Illuminated by Matched Feeds”. In: *IEEE Transactions on Antennas and Propagation* 36.1 (1988), pp. 141–144.

[11] K. Bahadori and Y. Rahmat-Samii. “Back-to-Back Reflector Antennas With Reduced Moment of Inertia for Spacecraft Spinning Platforms”. In: *IEEE Transactions on Antennas and Propagation* 55.10 (Oct. 2007), pp. 2654–2661.

[12] K. Bahadori and Y. Rahmat-Samii. “Tri-Mode Horn Feeds Revisited: Cross-Pol Reduction in Compact Offset Reflector Antennas”. In: *IEEE Transactions on Antennas and Propagation* 57.9 (Sept. 2009), pp. 2771–2775.

[13] Z. Pour and L. Shafai. “A Novel Dual-Mode Dual-Polarized Circular Waveguide Feed Excited by Concentrically Shorted Ring Patches”. In: *IEEE Transactions on Antennas and Propagation* 61.10 (Oct. 2013), pp. 4917–4925.

[14] Z. Pour and L. Shafai. “Analytical Models of Dual-Polarized Primary Matched Feeds for Offset Reflector Antennas with Low Cross Polarization Properties at both Asymmetry and Diagonal Planes”. In: *IEEE Transactions on Antennas and Propagation* 64.5 (May 2016), pp. 1627–1633.

[15] R. Jana and R. Bhattacharjee. “Matched feed design employing TE01 and TM11 modes in a smooth walled rectangular waveguide for cross-polar reduction in offset reflector antenna systems”. In: *AEU - International Journal of Electronics and Communications* 69.6 (Jan. 2015), pp. 873–877.

[16] D. Pujara and S. B. Chakrabarty. “Cancellation of High Cross-polarization of an Offset Parabolic Reflector Antenna using a Rectangular Matched Feed”. In: *IETE Journal of Research* 58.4 (July 2012), pp. 317–321.

[17] S. B. Sharma, D. Pujara, S. B. Chakrabarty, and R. Dey. “Cross-Polarization Cancellation in an Offset Parabolic Reflector Antenna Using a Corrugated Matched Feed”. In: *IEEE Antennas and Wireless Propagation Letters* 8 (July 2009), pp. 861–864.

[18] C. Yang, J. Yu, Y. Yao, X. Liu, and X. Chen. “Novel Corrugated Matched Feed for Cross-Polar Cancellation in Tri-Reflector Compact Range”. In: *IEEE Antennas and Wireless Propagation Letters* 13 (May 2014), pp. 1003–1006.

[19] R. Dey. “Wideband Corrugated Conjugate Matched Feed Horn”. In: *Electromagnetics* 37.3 (Apr. 2017), pp. 150–161.

[20] “Low cost high performance antanna for use in transmit/receive satellite terminals.” EP1278266B1. D. Tits. Sept. 2005.

[21] “Cross-polar compensating feed horn and method of manufacture”. US Patent 7,755,557. N. McGonigle, C. Mitchelson, D. Geen, and G. Agnew. July 2010.

[22] Z. A. Pour and L. Shafai. “A Ring Choke Excited Compact Dual-Mode Circular Waveguide Feed for Offset Reflector Antennas”. In: *IEEE Transactions on Antennas and Propagation* 60.6 (June 2012), pp. 3011–3015.

[23] R. Jana and R. Bhattacharjee. “A Novel Matched Feed Structure for Achieving Wide Cross-polar Bandwidth for an Offset Parabolic Reflector Antenna System”. In: *IEEE Antennas and Wireless Propagation Letters* 14 (Mar. 2015), pp. 1590–1593.

[24] R. Dey, S. B. Chakrabarty, and R. Jyoti. “Broadband Conjugate Matched Feed Horn- A Novel Concept”. In: *IEEE Antennas and Wireless Propagation Letters* 15 (July 2015), pp. 496–499.

[25] *Intelsat Earth Station Standards (IESS) 208: Antenna and wideband RF performance characteristics of Ku–band earth stations accessing the Intelsat space segment for standard services*. 2006. URL: `http://www.intelsat.com/tools-resources/library/iess-documents/`.

[26] *Eutelsat Systems Operation Guidelines (ESOG) 120: Antenna and VSAT type Approval/Characterization*. 2016. URL: `http://www.eutelsat.com/en/support/earth-stations/esog.html`.

[27] *SES Earth Station Performance Requirements*. 2006. URL: `https://www.ses.com/our-coverage/technical-data`.

[28] N. Adatia, B. Watson, and S. Ghosh. “Dual polarized elliptical beam antenna for satellite application”. In: *1981 Antennas and Propagation Society International Symposium*. Vol. 19. June 1981, pp. 488–491.

[29] A. C. Ludwig. “The Definition of Cross Polarization”. In: *IEEE Transactions on Antennas and Propagation* 21.1 (1973), pp. 116–119.

[30] *GRASP Software*. TICRA, Copenhagen, Denmark, *www.ticra.com*.

[31] N. A. Adatia and A. W. Rudge. “Beam squint in circularly polarised offset-reflector antennas”. In: *Electronics Letters* 11.21 (Oct. 1975), pp. 513–515.

[32] A. W. Rudge and N. A. Adatia. "Offset-Parabolic-Reflector Antennas: A Review". In: *Proceedings of the IEEE* 66.12 (Dec. 1978), pp. 1592–1618.

[33] Rudge. "Multiple-Beam Antennas: Offset Reflectors with Offset Feeds". In: *IEEE Transactions on Antennas and Propagation* 23.3 (1975), pp. 317–322.

[34] A. W. Rudge and N. A. Adatia. "Matched-Feeds for Offset Parabolic Reflector Antennas". In: *8th European Microwave Conference* (1976), pp. 143–147.

[35] P. D. Potter. "A New Horn Antenna with Suppressed Sidelobes and Equal Beamwidths". In: *Microwave Journal* 6.6 (1963), pp. 71–78.

[36] S. B. Sharma, D. A. Pujara, S. B. Chakrabarty, and V. K. Singh. "Removal of beam squinting effects in a circularly polarized offset parabolic reflector antenna using a matched feed". In: *Progress in Electromagnetics Research Letters* 7 (2009), pp. 105–114.

[37] D. J. Bem. "Electric-field distribution in the focal region of an offset paraboloid". In: *Proceedings of the Institution of Electrical Engineers* 116.5 (1969), pp. 679–684.

[38] A. W. Rudge and N. A. Adatia. "Primary feeds for boresight-jitter compensation of offset-reflector radar antennas". In: *RADAR 1977* (1977).

[39] "Improved Primary Feeds for Offset Reflector Antennas". 1 525 514 (The Patent Office, London). A. W. Rudge and N. A. Adatia. Sept. 1978.

[40] A. A. Zaghloul and L. Shafai. "Performance of offset paraboloid reflectors with offset matched feeds". In: *Canadian Electrical Engineering Journal* 5.3 (1980), pp. 12–15.

[41] S. M. Tun and P. J. B. Clarricoats. "Single offset reflector with a matched-feed array". In: *IEEE Antennas and Propagation Society International Symposium.* 1984, pp. 486–489.

[42] L. J. Foged, R. Braun, G. Pinchuk, M. Boumans, and P. O. Iversen. "Dual Polarized Wideband Feed with Cross-Polarization Reduction and Compensation Proprieties for Compact Antenna Test Range". In: *AMTA 36th Annual Meeting & Symposium.* 2014, pp. 57–62.

[43] L. J. Foged, A. Riccardi, and A. Giacomini. "Numerical Investigation of Cross Polar Reduction CATR Feed in Dual Linar Polarisation". In: *2016 IEEE International Symposium on Antennas and Propagation (APSURSI).* June 2016, pp. 1621–1622.

[44] A. Zamanifekri and A. Smolders. "Beam Squint Compensation in Circularly Polarized Offset Reflector Antennas Using a Sequentially Rotated Focal-Plane Array". In: *IEEE Antennas and Wireless Propagation Letters* 14 (2015), pp. 815–818.

[45] V. Jamnejad-Dailami and Y. Rahmat-Samii. "Some Important Geometrical Features of Conic-Section-Generated Offset Refelector Antennas". In: *IEEE Transactions on Antennas and Propagation* 28.6 (Nov. 1980), pp. 952–957.

[46] S. Silver. *Microwave Antenna Theory and Design.* Microwave Antenna Theory and Design 12. McGraw-Hill, 1949.

[47] K. Shee and W. Smith. "Optimizing Multimode Horn Feed Arrays for Offset Reflector Antennas Using a Constrained Minimization Algorithm to Reduce Cross Polarization". In: *IEEE Transactions on Antennas and Propagation* 45.12 (Dec. 1997), pp. 1883–1885.

[48] K. Bahadori and Y. Rahmat-Samii. “A Tri-mode Horn Feed for Gravitationally Balanced Back-to-Back Reflector Antennas”. In: *IEEE Antennas and Propagation Society International Symposium.* July 2006, pp. 4397–4400.

[49] D. Pujara, S. Chakrabarty, R. Dey, I. Agnihotri, and S. Sharma. “Tri-Mode Horn Array Fed Multiple-Beam Offset Reflector Antenna with Low Cross-Polarization and Improved Side Lobes”. In: *International Conference on Recent Advances in Microwave Theory and Applications, 2008. MICROWAVE 2008.* Nov. 2008, pp. 8–11.

[50] S. Sharma, D. Pujara, S. Chakrabarty, and V. Singh. “Performance Comparison of a Matched Feed Horn with a Potter Feed Horn for an Offset Parabolic Reflector”. In: *IEEE Antennas and Propagation Society International Symposium.* July 2008, pp. 1–4.

[51] D. Pujara, S. Sharma, S. Chakrabarty, R. Dey, and V. Singh. “Design of a Novel Corrugated Matched Feed for an Offset Parabolic Reflector Antenna”. In: *IEEE Antennas and Propagation Society International Symposium.* June 2009, pp. 1–4.

[52] D. A. Pujara, S. B. Sharma, and S. B. Chakrabarty. “Improving the Beam Efficiency of an Offset Parabolic Reflector Antenna for Spaceborne Radiometric Applications”. In: *Progress In Electromagnetics Research C* 10 (2009), pp. 143–150.

[53] S. B. Sharma, D. A. Pujara, S. B. Chakrabarty, and V. K. Singh. “Improving the Cross-Polar Performance of an Offset Parabolic Reflector Antenna Using a Rectangular Matched Feed”. In: *IEEE Antennas and Wireless Propagation Letters* 8 (2009), pp. 513–516.

[54] S. Sharma, D. Pujara, S. Chakrabarty, R. Dey, and V. Singh. “Design and development of a conjugate matched feed for an offset parabolic reflector antenna”. In: *IET Microwaves, Antennas Propagation* 4.11 (Nov. 2010), pp. 1782–1788.

[55] S. B. Sharma, D. Pujara, and S. B. Chakrabarty. “Design and development of a dual-mode corrugated horn for an offset reflector antenna”. In: *Microwave and Optical Technology Letters* 52.1 (2010), pp. 113–116.

[56] R. Dey, S. B. Chakrabarty, and R. Jyoti. “Analysis and Application of Triple-Post Discontinuity in Circular Waveguide”. In: *Electromagnetics* 36.2 (Feb. 17, 2016), pp. 67–77.

[57] S. Sharma, V. Singh, R. Dey, and S. Chakrabarty. “Analysis of a Post Discontinuity in an Oversized Circular Waveguide”. In: *IEEE Transactions on Microwave Theory and Techniques* 57.8 (Aug. 2009), pp. 1989–1995.

[58] R. Dey, S. Chakrabarty, R. Jyoti, and T. Kurian. “Higher Order Mode Analysis of Dual-Post Discontinuity in a Circular Waveguide”. In: *IETE Journal of Research* (2015), pp. 1–8.

[59] Z. Pour and L. Shafai. “A Novel Dual Mode Circular Waveguide Horn Antenna”. In: *2010 14th International Symposium on Antenna Technology and Applied Electromagnetics the American Electromagnetics Conference (ANTEM-AMEREM).* July 2010, pp. 1–4.

[60] Z. Pour and L. Shafai. “Investigation of Asymmetric Phase Errors of an Optimized Dual-Mode Primary Feed on the Cross Polarization of Offset Reflector Antennas”. In: *IEEE Antennas and Wireless Propagation Letters* 9 (2010), pp. 872–875.

[61] Z. A. Pour and L. Shafai. “A Novel Impedance Matched Mode Generator for Excitation of the TE21 Mode in Compact Dual-Mode Circular Waveguide Feeds”. In: *IEEE Antennas and Wireless Propagation Letters* 10 (2011), pp. 427–430.

[62] Z. A. Pour and L. Shafai. “A Simplified Feed Model for Investigating the Cross Polarization Reduction in Circular- and Elliptical-Rim Offset Reflector Antennas”. In: *IEEE Transactions on Antennas and Propagation* 60.3 (Mar. 2012), pp. 1261–1268.

[63] Z. A. Pour. “Investigation of parabolic reflector antennas as single- and multi-phase centre virtual antennas”. PhD thesis. Jan. 13, 2012. URL: `https://mspace.lib.umanitoba.ca/handle/1993/5080`.

[64] Z. Pour and L. Shafai. “Improved Cross-Polarization Performance of a Multi-Phase-Center Parabolic Reflector Antenna”. In: *IEEE Antennas and Wireless Propagation Letters* 13 (2014), pp. 540–543.

[65] Z. A. Pour and L. Shafai. “Beam Squint Correction in Offset Reflector Antennas with Circularly-Polarized Tapered Primary Feeds”. In: *Antennas and Propagation & USNC/URSI National Radio Science Meeting, 2015 IEEE International Symposium on*. IEEE, 2015, pp. 2189–2190.

[66] C. Yang, J. Yu, Y. Yao, X. Liu, and X. Chen. “Analysis of Focal Region Field of the Offset Tri-Reflector for Compact Antenna Test Range”. In: *2014 IEEE Antennas and Propagation Society International Symposium (APSURSI)*. July 2014, pp. 1483–1484.

[67] C. Yang, J. Yu, Y. Yao, X. Liu, L. Xu, and X. Chen. “Corrugated Matched Horn with Low Side-Lobes for High Performance Offset Reflector Systems”. In: *Antennas and Propagation & USNC/URSI National Radio Science Meeting, 2015 IEEE International Symposium on*. IEEE, 2015, pp. 1058–1059.

[68] R. Jana and R. Bhattacharjee. “A Tri-mode Low Cross-Polarized Circular Matched Feed for Offset Reflector Antenna System”. In: *2015 Twenty First National Conference on Communications (NCC)*. Feb. 2015, pp. 1–6.

[69] P. Anoop and R. Bhattacharjee. “Investigation on Crosspolar Performance of a Coaxial Fed Dual Mode Matched Rectangular Feed Horn with Step Discontinuity”. In: *2014 Twentieth National Conference on Communications (NCC)*. Feb. 2014, pp. 1–6.

[70] R. Jana and R. Bhattacharjee. “Analysis of Scattering Parameters of a Stepped Cylindrical Horn Containing Inner Posts Using MM and 2-D FEM”. In: *2014 Twentieth National Conference on Communications (NCC)*. Feb. 2014, pp. 1–6.

[71] R. Jana and R. Bhattacharjee. “A Hybrid Numerical Technique to Investigate the Performances of Offset Reflector and Matched Feed”. In: *2015 Ieee Applied Electromagnetics Conference, Aemc 2015*. 2015, p. 7509180.

[72] R. Jana. “Analysis and Design of Matched Feeds for Offset Parabolic Reflector Antennas using Analytical and Numerical Techniques”. PhD thesis. Jan. 2016. URL: `http://gyan.iitg.ernet.in/handle/123456789/795`.

[73] A. Valentino and P. Toulios. “Fields in the Focal Region of Offset Parabolic Antennas”. In: *IEEE Transactions on Antennas and Propagation* 24.6 (Nov. 1976), pp. 859–865.

[74] R. E. Collin. *Antennas and Radiowave Propagation*. McGraw-Hill, 1985.

[75] J. J. More, D. C. Sorensen, B. S. Garbow, and K. E. Hillstrom. “The MINPACK Project”. In: *Sources and Dev of Math Software* (1984), pp. 88–111.

[76] J. R. Risser. “Waveguide and Horn Feeds”. In: *Microwave Antenna Theory and Design*. MIT Radiation Laboratory Series 12. John Wiley & Sons, 1949.

[77] A. Wexler. “Solution of waveguide discontinuities by modal analysis”. In: *Microwave Theory and Techniques, IEEE Transactions on* 15.9 (1967), pp. 508–517.

[78] R. E. Collin. *Foundations for Microwave Engineering*. McGraw-Hill, 1966.

[79] D. M. Pozar. *Microwave engineering*. Third. John Wiley, 2005.

[80] N. Marcuvitz. *Waveguide handbook*. IEE Electromagnetic Waves Series 21. Peregrinus, 1951.

[81] T. H. Chang, C. F. Yu, and C. T. Fan. “Polarization-controllable TE21 mode converter”. In: *Review of Scientific Instruments* 76.7 (2005), p. 074703.

[82] D. A. Constable, X. S. Fampris, K. Ronald, W. He, C. G. Whyte, and C. W. Robertson. “A novel cylindrical TE21 mode converter”. In: *Review of Scientific Instruments* 81.9 (2010), p. 094702.

[83] C.-F. Yu and T.-H. Chang. “High-Performance Circular TE01-Mode Converter”. In: *IEEE Transactions on Microwave Theory and Techniques* 53.12 (Dec. 2005), pp. 3794–3798.

[84] Y. H. Choung, K. R. Goudey, and L. G. Bryans. “Theory and Design of a Ku-Band TE21-Mode Coupler”. In: *IEEE Transactions on Microwave Theory and Techniques* 30.11 (Nov. 1982), pp. 1862–1866.

[85] Y. H. Choung. “Wideband TM01-mode travelling wave coupler”. In: *IEE Proceedings - Microwaves, Antennas and Propagation* 144.5 (Oct. 1997), pp. 315–320.

[86] S. E. Miller. “Coupled Wave Theory and Waveguide Applications”. In: *The Bell System Technical Journal* 33.3 (May 1954), pp. 661–719.

[87] J. McClellan and T. Parks. “A Unified Approach to the Design of Optimum FIR Linear-Phase Digital Filters”. In: *IEEE Transactions on Circuit Theory* 20.6 (Nov. 1973), pp. 697–701.

[88] J. McClellan, T. Parks, and L. Rabiner. “A Computer Program for Designing Optimum FIR Linear Phase Digital Filters”. In: *IEEE Transactions on Audio and Electroacoustics* 21.6 (Dec. 1973), pp. 506–526.

[89] E. Jones, T. Oliphant, P. Peterson, et al. *SciPy: Open source scientific tools for Python*. 2001–. URL: `http://www.scipy.org/`.

[90] H. A. Bethe. “Theory of Diffraction by Small Holes”. In: *Physical Review* 66.7 (Oct. 1944), pp. 163–182.

[91] S. B. Cohn. “Microwave Coupling by Large Apertures”. In: *Proceedings of the IRE* 40.6 (June 1952), pp. 696–699.

[92] R. Levy. “Improved Single and Multiaperature Waveguide Coupling Theory, Including Explanation of Mutual Interactions”. In: *IEEE Transactions on Microwave Theory and Techniques* 28.4 (Apr. 1980), pp. 331–338.

[93] H. J. Riblet and T. S. Saad. “A New Type of Waveguide Directional Coupler”. In: *Proceedings of the IRE* 36.1 (Jan. 1948), pp. 61–64.

[94] *HFSS 17.1 Software*. ANSYS, Inc., Canonsburg, PA, USA, *www.ansys.com*.

[95] C. Granet, G. L. James, and A. R. Forsyth. “Aperture Antennas: Waveguides and Horns”. In: *Modern Antenna Handbook*. John Wiley & Sons, 2008.

[96] T. Bird, G. James, and S. Skinner. "Input mismatch of TE11 mode coaxial waveguide feeds". In: *IEEE Transactions on Antennas and Propagation* 34.8 (Aug. 1986), pp. 1030–1033.

[97] T. Bird. "TE11 mode Excitation of Flanged Circular Coaxial Waveguides with an Extended Center Conductor". In: *IEEE Transactions on Antennas and Propagation* 35.12 (Dec. 1987), pp. 1358–1366.

[98] C. Granet and G. James. "Design of Corrugated Horns: A Primer". In: *IEEE Antennas and Propagation Magazine* 47.2 (2005), pp. 76–84.

[99] P. J. Clarricoats and A. Olver. *Corrugated horns for microwave antennas.* 1984.

[100] G. Figlia, D. Savini, D. Forigo, K. V. T. Klooster, and T. Berceli. "Coaxial waveguide discontinuities as matching elements for coaxial horns". In: *Proceedings of the Colloquium on Microwave Communication* (1986), pp. 349–350.

[101] G. L. James. "Admittance of Irises in Coaxial and Circular Waveguides for TE11-Mode Excitation". In: *IEEE Transactions on Microwave Theory and Techniques* 35.4 (Apr. 1987), pp. 430–434.

[102] A. D. Olver, P. J. B. Clarricoats, A. A. Kishk, and L. Shafai. *Microwave horns and feeds.* 1994.

[103] G. Koch. "Coaxial Feeds for High Aperture Efficiency and Low Spillover of Paraboloidal Reflector Antennas". In: *IEEE Transactions on Antennas and Propagation* 21.2 (Mar. 1973), pp. 164–169.

[104] J. Teniente, I. Gómez-López, R. Caballero-Nagore, G. Crespo-López, and A. Martínez-Agoües. "Quad band X/Ka horn antenna and feed chain designs". In: *2017 11th European Conference on Antennas and Propagation (EUCAP).* Mar. 2017, pp. 3432–3436.

[105] C. Granet, G. L. James, R. Bolton, and G. Moorey. "A Smooth-Walled Spline-Profile Horn as an Alternative to the Corrugated Horn for Wide Band Millimeter-Wave Applications". In: *IEEE Transactions on Antennas and Propagation* 52.3 (Mar. 2004), pp. 848–854.

[106] Q. Zhang, C. W. Yuan, and L. Liu. "A Coaxial Corrugated Dual-Band Horn Feed". In: *IEEE Antennas and Wireless Propagation Letters* 8 (Dec. 2009), pp. 1357–1359.

[107] H. Minnett and B. Thomas. "A Method of Synthesizing Radiation Patterns with Axial Symmetry". In: *IEEE Transactions on Antennas and Propagation* 14.5 (Sept. 1966), pp. 654–656.

[108] P. J. B. Clarricoats and M. I. Sobhy. "Propagation behaviour of periodically loaded waveguides containing dielectric and ferrimagnetic materials". In: *Proceedings of the Institution of Electrical Engineers* 115.5 (May 1968), pp. 652–661.

[109] G. H. Bryant. "Propagation in corrugated waveguides". In: *Proceedings of the Institution of Electrical Engineers* 116.2 (Feb. 1969), pp. 203–213.

[110] P. J. B. Clarricoats and P. K. Saha. "Theoretical analysis of cylindrical hybrid modes in a corrugated horn". In: *Electronics Letters* 5.9 (May 1969), pp. 187–189.

[111] M. J. Al-Hakkak and Y. T. Lo. "Circular waveguides with anisotropic walls". In: *Electronics Letters* 6.24 (Nov. 1970), pp. 786–789.

[112] P. Clarricoats and P. Saha. “Propagation and radiation behaviour of corrugated feeds. Part 2: Corrugated-conical-horn feed”. In: *Proceedings of the Institution of Electrical Engineers* 118.9 (Sept. 1971), pp. 1177–1186.

[113] R. B. Dybdal, L. Peters, and W. H. Peake. “Rectangular Waveguides with Impedance Walls”. In: *IEEE Transactions on Microwave Theory and Techniques* 19.1 (Jan. 1971), pp. 2–8.

[114] L. Shafai and J. E. Hansen. “Matrix formulation of corrugated feeds by using impedance boundary conditions”. In: *Electronics Letters* 13.11 (May 1977), pp. 310–311.

[115] G. L. James. “Surface reactance of corrugated planes”. In: *Electronics Letters* 15.23 (Nov. 1979), pp. 751–753.

[116] G. L. James. “Propagation and Radiation Properties of Corrugated Cylindrical Coaxial Waveguides”. In: *IEEE Transactions on Antennas and Propagation* 31.3 (May 1983), pp. 477–483.

[117] P.-S. Kildal. “Artificially Soft and Hard Surfaces in Electromagnetics”. In: *IEEE Transactions on Antennas and Propagation* 38.10 (Oct. 1990), pp. 1537–1544.

[118] S. Skobelev and P. .-.-S. Kildal. “Mode-Matching Modeling of a Hard Conical Quasi-TEM Horn Realized by an EBG Structure with Strips and Vias”. In: *IEEE Transactions on Antennas and Propagation* 53.1 (Jan. 2005), pp. 139–143.

[119] E. Lier. “Review of Soft and Hard Horn Antennas, Including Metamaterial-Based Hybrid-Mode Horns”. In: *IEEE Antennas and Propagation Magazine* 52.2 (Apr. 2010), pp. 31–39.

[120] A. Mohsen and M. a. K. Hamid. “Wave Propagation in a Circular Waveguide with an Absorbing Wall”. In: *Journal of Applied Physics* 41.1 (Jan. 1, 1970), pp. 433–434.

[121] C. Dragone. “High-Frequency Behavior of Waveguides with Finite Surface Impedances”. In: *The Bell System Technical Journal* 60.1 (Jan. 1981), pp. 89–116.

[122] Unger. “Waveguides with anisotropic impedance walls”. In: (1964).

[123] J. R. Wait. “A fundamental difficulty in the analysis of cylindrical waveguides with impedance walls”. In: *Electronics Letters* 3.2 (Feb. 1967), pp. 87–88.

[124] P. Bernardi. “Electromagnetic Waves Guided by the Most General Anisotropic Impedance Wall”. In: *Il Nuovo Cimento B Series 10* 43.2 (1966), pp. 338–346.

[125] J. B. Andersen. “Propagation in the General, Rectangular Waveguide”. In: *Microwave Conference, 1975. 5th European.* Sept. 1975, pp. 595–599.

[126] A. Z. Elsherbeni and M. Hamid. “Hybrid modes in a circular waveguide with an impedance wall”. In: *Journal of Applied Physics* 62.6 (Sept. 15, 1987), pp. 2572–2573.

[127] A. Z. Elsherbeni, J. Stanier, and M. Hamid. “Eigenvalues of propagating waves in a circular waveguide with an impedance wall”. In: *Antennas and Propagation IEE Proceedings H - Microwaves* 135.1 (Feb. 1988), pp. 23–26.

[128] S. Mahmoud. *Electromagnetic waveguides: Theory and applications.* IEE Electromagnetic Waves Series 32. Peregrinus, 1991.

[129] B. M. Thomas and H. C. Minnett. “Modes of propagation in cylindrical waveguides with anisotropic walls”. In: *Proceedings of the Institution of Electrical Engineers* 125.10 (Oct. 1978), pp. 929–932.

[130] N. Raveu, B. Byrne, L. Claudepierre, and N. Capet. “Modal Theory for Waveguides With Anisotropic Surface Impedance Boundaries”. In: *IEEE Transactions on Microwave Theory and Techniques* 64.4 (Apr. 2016), pp. 1153–1162.

[131] E. Lier and R. Shaw. “Design and simulation of metamaterial-based hybrid-mode horn antennas”. In: *Electronics Letters* 44.25 (Dec. 2008), pp. 1444–1445.

[132] Q. Wu, C. Scarborough, D. Werner, E. Lier, and X. Wang. “Design Synthesis of Metasurfaces for Broadband Hybrid-Mode Horn Antennas With Enhanced Radiation Pattern and Polarization Characteristics”. In: *IEEE Transactions on Antennas and Propagation* 60.8 (Aug. 2012), pp. 3594–3604.

[133] Q. Wu et al. “A Ku-Band Dual Polarization Hybrid-Mode Horn Antenna Enabled by Printed-Circuit-Board Metasurfaces”. In: *IEEE Transactions on Antennas and Propagation* 61.3 (Mar. 2013), pp. 1089–1098.

[134] Q. Wu, C. Scarborough, D. Werner, E. Lier, and R. Shaw. “Inhomogeneous Metasurfaces With Engineered Dispersion for Broadband Hybrid-Mode Horn Antennas”. In: *IEEE Transactions on Antennas and Propagation* 61.10 (Oct. 2013), pp. 4947–4956.

[135] C. Scarborough, Q. Wu, D. Werner, E. Lier, R. Shaw, and B. Martin. “Demonstration of an Octave-Bandwidth Negligible-Loss Metamaterial Horn Antenna for Satellite Applications”. In: *IEEE Transactions on Antennas and Propagation* 61.3 (Mar. 2013), pp. 1081–1088.

[136] E. Lier, D. H. Werner, C. P. Scarborough, Q. Wu, and J. A. Bossard. “An octave-bandwidth negligible-loss radiofrequency metamaterial”. In: *Nature Materials* 10.3 (Mar. 2011), pp. 216–222.

[137] N. Capet, B. Byrne, L. Claudepierre, and N. Raveu. “Metamaterial waveguide with reduced cross section”. In: *2013 7th European Conference on Antennas and Propagation (EuCAP)*. Apr. 2013, pp. 2155–2157.

[138] P. S. Kildal. “Definition of artificially soft and hard surfaces for electromagnetic waves”. In: *Electronics Letters* 24.3 (Feb. 1988), pp. 168–170.

www.elektro.dtu.dk

Department of Electrical Engineering

Electromagnetic Systems Group
Technical University of Denmark
Ørsteds Plads
Building 348
DK-2800 Kgs. Lyngby
Denmark
Tel: (+45) 45 25 38 00
Fax: (+45) 45 93 16 34
Email: info@elektro.dtu.dk